

Calculation Methods for Compressible Turbulent Boundary Layers—1976



National Aeronautics and
Space Administration

NASA SP-422

Calculation Methods for Compressible Turbulent Boundary Layers—1976

Dennis M. Bushnell
Aubrey M. Cary, Jr.
and Julius E. Harris

Prepared by
NASA Langley Research Center



Scientific and Technical Information Office
National Aeronautics and
Space Administration

1977

PREFACE

Calculation procedures for nonreacting compressible two- and three-dimensional turbulent boundary layers are reviewed. A summary of integral, transformation, and correlation methods, as well as finite-difference solutions of the complete boundary-layer equations is included. Alternative numerical solution procedures are examined, and both mean field and mean turbulence field closure models are considered. A discussion of physics and related calculation problems peculiar to compressible turbulent boundary layers is included. A listing of available solution procedures (finite-difference, finite-element, and weighted-residual methods) is provided. Detailed consideration is given to influence of compressibility, low Reynolds number, wall blowing, and pressure gradient upon mean field closure constants.

The information contained in this publication was presented at the 1976 Von Kármán Institute for Fluid Dynamics Lecture Series "Compressible Turbulent Boundary Layers," March 1-5, 1976, Rhode-St.-Genèse, Belgium.

CONTENTS

PREFACE	iii
INTRODUCTION	1
SYMBOLS	1
MAJOR GENERAL REFERENCES	5
EQUATIONS AND CLOSURE METHODS	6
Governing Differential Equations	6
Closure Methods	7
FLOW PHENOMENA PECULIAR TO CALCULATION OF COMPRESSIBLE TURBULENT	
BOUNDARY LAYERS	9
Normal Pressure Gradient	9
Influence of Compressibility and Density Fluctuation Terms	10
Comparison of Mean Static Temperature and Turbulent Kinetic	
Energy	11
Precursor Transition Effect	12
Large p' Levels	13
Definition of Boundary-Layer Thickness	13
Energy Loss Via Acoustic Waves	14
TRADITIONAL PREDICTION METHODS	14
Transformations	15
Correlation Methods	17
Integral Methods	23
NUMERICAL SOLUTION PROCEDURES	27
Solution Techniques	27
Systems of Independent Variables	29
MEAN FIELD CLOSURE	31
Wall Damping Constant	33
Prandtl Wall Constant	35
Outer or Wake Constant	35
Turbulent Prandtl Number	37
Intermittency Normal to the Wall	38
APPLICATIONS OF MEAN FIELD CLOSURE METHODS	38
The Case of the Nozzle Wall Turbulent Boundary Layer	38
Influence of Wall Blowing Upon Skin Friction	40
Transitional Flow Calculations	40
Additional "Nontypical" Applications of Mean Field Closure	
Methods	41
NONEQUILIBRIUM AND MEAN TURBULENT FIELD CLOSURE	44
Physical Problem	44
Equations and Modeling for Compressible Nonequilibrium Flows	45

Single-Equation Models	46
Two-Equation (and More) Models for Compressible Flows	46
CALCULATION OF THREE-DIMENSIONAL COMPRESSIBLE TURBULENT BOUNDARY	
LAYERS	
Status	47
Boundary-Layer Equations	48
Coordinate Systems and Transformations	51
Turbulence Modeling	54
Numerical Solution Procedures	57
Status of Three-Dimensional Boundary-Layer Computational Techniques	66
RÉSUMÉ	67
Compressibility Influence on Turbulent Boundary-Layer Shear Stress	67
Computational Capability of Existing Procedures	68
Important Unresolved Issues	68
APPENDIX - SUMMARY OF CALCULATION PROCEDURES FOR NONSIMILAR TWO- AND THREE-DIMENSIONAL COMPRESSIBLE TURBULENT BOUNDARY LAYERS (FINITE DIFFERENCE, FINITE ELEMENT, AND MASS-WEIGHTED RESIDUAL METHODS)	
	69
REFERENCES	79
FIGURES	104

INTRODUCTION

The design of missiles, manned and unmanned entry vehicles, and transportation systems capable of speeds in the transonic and supersonic regimes requires detailed information on such boundary-layer quantities as skin friction, aerodynamic heating, and viscous displacement thickness and mass flow. Typical components requiring such design information include nacelles, control surfaces, turbomachinery blading, nozzles, airfoils and fuselage, inlets, and combustors. Detailed boundary-layer predictions are also needed for the design of facilities used in experimental investigations.

The various stages of design demand boundary-layer information in increasing detail. For this reason and also because flow complexity varies considerably (depending upon the design and component), a hierarchy of calculation procedures has been developed over the years, ranging from simple, "back of the envelope" methods to complex, numerical approaches which require use of the largest digital computers. In the present paper this entire gamut of methods is reviewed, with emphasis on the more complete procedures which solve numerically the partial-differential equations governing boundary-layer motion and on the influence of conditions usually encountered in practice (such as pressure gradient, mass injection, and low Reynolds number) upon the necessary closure "constants" used in representing the turbulent shear. Also included is a detailed discussion of some physics and resultant calculation problems which are peculiar to compressible turbulent boundary layers. The basic purpose of this volume is to provide a ready reference and introduction to the various procedures currently available for calculation of compressible turbulent boundary layers. Therefore, also included is a listing of available methods of the more complete type and some discussion of the various alternate numerical procedures which can be used for solving the nonlinear partial-differential equations governing fluid motion in compressible turbulent boundary layers. This review does not include detailed consideration of time-dependent boundary layers, relaminarization, and heterogeneous or chemically reacting flows.

SYMBOLS

A	Van Driest damping factor (eq. (41))
A^+	$= Au_T/\nu$
a	speed of sound
a_1	$= \overline{u'v'}/2e$
C_f	skin friction coefficient, $\tau_w/\frac{1}{2}\rho_e u_e^2$
$C_{f,0}$	skin friction coefficient without wall blowing
c	wing chord

c_p specific heat at constant pressure
 d unit length
 e turbulent kinetic energy, $\frac{1}{2}(\overline{u'^2} + \overline{v'^2} + \overline{w'^2})$
 F mass flow parameter, $\rho_w v_w / \rho_e u_e$
 $F_C, F_{R_x}, F_{R_\theta}$ functions from Spalding and Chi (ref. 81)
 $G = u_2 / u_{2,e}$
 H total enthalpy, $h + \frac{u^2}{2}$; also form factor, $\frac{\delta^*}{\theta}$
 $\tilde{H} = u_3 / u_{1,e}$ (eq. (95))
 $H_i^* = \delta_i^* / \theta_i$
 h static enthalpy
 h_1, h_2, h_3 metric coefficients
 K Prandtl constant
 \hat{K} factor for variable grid spacing, $\Delta \eta_{n+1} / \Delta \eta_n$
 L reference length; also dissipation length scale (fig. 48)
 l mixing length
 M Mach number
 \dot{m} mass flow
 N_{Nu} Nusselt number, $(N_{St})(N_{Pr})(R_{e,x})$
 N_{Pr} molecular Prandtl number
 $N_{Pr,T}$ total turbulent Prandtl number, ϵ / κ_T
 $N_{Pr,t}$ static turbulent Prandtl number, ϵ / κ_t
 N_{St} Stanton number, $\dot{q}_w / \rho_e u_e c_p (T_{aw} - T_w)$
 p pressure
 p^+ pressure gradient parameter, $(\nu u_e / u_\tau^3)(du_e/dx)$
 \dot{q} wall heat transfer rate

R	Reynolds number, $\rho u/\mu$; also universal gas constant
r_c	transverse radius of curvature
r_N	nose radius
T	temperature
u,v,w	velocity components in x-, y-, and z-directions
u_i	general velocity notation ($i = 1, 2, 3$)
u^+	$= u/u_\tau$
u^*	Van Driest's generalized velocity
u_τ	friction velocity, $(\tau_w/\rho_w)^{1/2}$
V	total velocity vector
x,y,z	Cartesian coordinates
x_i	curvilinear coordinates ($i = 1, 2, 3$)
y^+	$= yu_\tau/\nu$
α	Clauser constant; also angle of attack
β_K	pressure gradient parameter, $(\delta_i^*/\tau_w)(dp/dx)$
Γ	intermittency function
Γ_x	streamwise intermittency function
Γ_y	normal intermittency function
γ	ratio of specific heats
δ	boundary-layer thickness
δ^*	displacement thickness, $\int_0^\delta \left(1 - \frac{\rho u}{\rho_e u_e}\right) dy$
δ^+	$= \delta u_\tau/\nu_w$
ϵ	dynamic eddy viscosity
ζ	transformed normal coordinate, Crocco (eq. (91))
η	transformed normal coordinate, Levy-Lees (eq. (32)); also transformed transverse coordinate for Crocco variables (see fig. 53)

Θ	$= T/T_e$
θ	momentum thickness, $\int_0^\delta \frac{\rho u}{\rho_e u_e} \left(1 - \frac{u}{u_e}\right) dy$
κ_T	$= \frac{\overline{v'H'}}{\partial \bar{H}/\partial y}$
κ_t	$= \frac{\overline{v'h'}}{\partial h/\partial y}$
μ	molecular viscosity
ν	kinematic viscosity
ξ	transformed streamwise coordinate (eq. (31)); also x_1 -coordinate for Crocco variables
ρ	density
σ	kinematic eddy viscosity (eq. (40))
τ	shear stress
Φ	shear function (eq. (92))
ϕ	spreading angle (fig. 5)
φ	circumferential angle
ψ	stream function
ω	vorticity

Subscripts:

aw	adiabatic wall
bl	boundary layer
cr	critical value
e	local edge of boundary layer
eff	effective value
i	incompressible
i, j, k	indices
L	reference length

max	maximum value
n	index integer
o	stagnation value
p	region of peak $\overline{v'^2}$
t	total
tr	transition value
vo	based on virtual origin location
x	based on distance coordinate x
x_i	coordinate direction (i = 1, 2, 3)
w	wall value
θ	based on momentum thickness
∞	free stream

A prime denotes a fluctuating quantity.

A bar indicates a mean quantity.

MAJOR GENERAL REFERENCES

The major reference books pertinent to the calculation of compressible turbulent boundary layers were mainly written in two distinct time frames: late fifties to early sixties (refs. 1 to 5) and late sixties to early seventies (refs. 6 to 12). Of these works, the ones most useful in the preparation of the present volume on calculation methods included references 2, 5, 8, 9, and 12. Several review and background articles are also available (e.g., refs. 13 to 25). All of these were quite valuable, especially the papers of Reynolds (refs. 19 and 20) and Bradshaw (ref. 22). Another category of general references is conference proceedings (e.g., refs. 26 to 30). These are excellent sources, particularly for comparisons between data and theory (especially refs. 28 and 30). Reference 26 contains many of the fundamental concepts, such as the Morkovin hypothesis, which are the foundation for the current generation of compressible calculation procedures. A final category of general references includes reviews of available data (e.g., refs. 11 and 31 to 37), which are especially important for evaluation of test cases suitable to "calibrate" the various turbulence closure constants.

EQUATIONS AND CLOSURE METHODS

Governing Differential Equations

The basic differential equations governing compressible turbulent boundary-layer flow are (1) a statement of the conservation of mass, (2) momentum equations obtained from the Navier-Stokes equations, and (3) an expression for the conservation of energy. Also needed for solution is an equation of state (ideal gas assumed herein) and equations for molecular transport properties.

Given this set of equations it is conceptually possible to integrate forward in time on a computer and, given sufficient grid resolution, obtain the turbulent motions "exactly" with very little empiricism. However, as noted in reference 12 and elsewhere, the computer capacity currently available falls several orders of magnitude short of the capability needed for such a solution. Therefore, one must resort to the usual Reynolds averaging, where the flow is represented by a time mean and an instantaneous fluctuation; for example,

$$u = \bar{u} + u' \quad v = \bar{v} + v'$$

where the following averaging rules apply:

$$\overline{\bar{u} v'} = 0 \quad \overline{u' v'} \neq 0$$

To simplify the problem for ease of solution, with very little loss of accuracy (ref. 38), order of magnitude arguments are made (usually referred to as the boundary-layer assumptions); that is,

$$x \gg y \quad u \gg v \quad \frac{\partial}{\partial x} \ll \frac{\partial}{\partial y}$$

The resultant set of governing equations in surface curvilinear coordinates for the steady, two-dimensional boundary-layer flow ($\delta/r_c \ll 1$) of a compressible ideal gas (in the turbulent state) are

Conservation of mass:

$$\frac{\partial(\bar{\rho}u)}{\partial x} + \frac{\partial(\bar{\rho}v)}{\partial y} = 0 \tag{1}$$

Longitudinal momentum:

$$\bar{\rho}u \frac{\partial \bar{u}}{\partial x} + \bar{\rho}v \frac{\partial \bar{u}}{\partial y} = - \frac{\partial \bar{p}}{\partial x} + \frac{\partial}{\partial y} \left[\mu \frac{\partial \bar{u}}{\partial y} - \overline{(\rho v)' u'} \right] \tag{2}$$

Normal momentum:

$$\frac{\partial \bar{p}}{\partial y} = - \frac{\partial}{\partial y} \left[\overline{(\rho v)' v'} \right] \tag{3}$$

Conservation of energy:

$$\overline{\rho u} \frac{\partial \bar{H}}{\partial x} + \overline{\rho v} \frac{\partial \bar{H}}{\partial y} = \frac{\partial}{\partial y} \left\{ \frac{\mu}{N_{Pr}} \left[\frac{\partial \bar{H}}{\partial y} + (N_{Pr} - 1) \frac{\partial \bar{u}^2}{2 \partial y} \right] - \overline{(\rho v)'h'} - \bar{u} \left[\overline{(\rho v)'u'} \right] \right\} \quad (4)$$

Detailed discussion and derivation of these equations are available in references 2, 12, 39, 40, and 41. The equations are also given in references 42 and 43, in terms of mass-weighted dependent variables.

There are two points to be made concerning these basic equations (eqs. (1) to (4)). First of all, in the averaging process the usual new unknowns have appeared (shown underlined) which account for the turbulent fluxes of momentum and energy. The specification of these quantities, in terms of known parameters, comprises the major difficulty in the calculation of compressible turbulent boundary layers and is usually termed the "closure problem." The other point concerns the term $\overline{\rho v}$. Expanded out, this term is

$$\overline{\rho v} = \bar{\rho} \bar{v} + \overline{\rho'v'} \quad (5)$$

Since $\overline{\rho'v'}$ appears in the equations with normal or y-derivatives, the term is not negligible and must be accounted for. Fortunately, $\overline{\rho'v'}$ always appears with $\bar{\rho} \bar{v}$, and therefore, a new definition of v can be used

$$\tilde{v} = \bar{v} + \frac{\overline{\rho'v'}}{\bar{\rho}} \quad (6)$$

(which is actually a mass-weighted variable), and the influence of $\overline{\rho'v'}$ can be included implicitly in the solution. This approach is satisfactory as long as the actual \bar{v} value is not required. If \bar{v} values must be computed, some model of $\overline{\rho'v'}$ is obviously necessary. This inclusion of $\overline{\rho'v'}$ is an important issue. If the $\overline{\rho v}$ term were not handled in the manner shown in equations (2) and (4), then two Reynolds stress terms appear: $\bar{u} \overline{\rho'v'}$ and $\bar{\rho} \overline{u'v'}$. Morkovin, in reference 44, shows that $\bar{u} \overline{\rho'v'}/\bar{\rho} \overline{u'v'}$ (or the ratio of the compressibility term to the usual low-speed Reynolds stress term) can be of the order of 0.6 to 1.0 for a supersonic boundary layer, and therefore $\overline{\rho'v'}$ would have to be accurately modeled (an extremely difficult task).

Closure Methods

In the present paper the usual breakdown of closure procedures (e.g., ref. 45) into (1) simple or zeroth-order methods, (2) first-order or mean field closure methods, and (3) second-order or mean turbulence field closure methods is followed.

The zeroth-order case consists of two major subcategories: integral approaches and empirical laws, such as C_f correlations. In the most general of these approaches, the integral methods, equations (1) to (4) are formally integrated in the normal or y-direction. As a result of this procedure the unknown turbulent flux terms disappear, but their influence is still present in that profiles must be supplied (assumed, obtained from data, etc.), and these profiles are influenced to a great extent by the turbulence induced fluxes. There-

fore, the simple or zeroth-order procedures are characterized by a requirement for substantial amounts of empiricism.

In the mean field closure approaches the partial-differential equations are solved directly (eqs. (1) to (4)) and the turbulent flux terms are related to mean flow quantities. This approach is nearly correct (and indeed quite exact) for slowly varying flows and over a wide variety of boundary conditions. At the present time this closure approach is tending to supplant the integral approaches in industrial application, primarily as a result of a greater reliability (accuracy of prediction) over a wide range of conditions and routine use of high-speed computers. This increased capability is purchased at the expense of considerably increased computer time (compared with the best of the integral methods).

In mean turbulent field closure, the differential equations (derived from the Navier-Stokes equations, as described in a later section) governing the turbulence flux terms are solved. These new equations involve additional unknowns, but the mean profiles generally are relatively insensitive to the precise details of the modeling in these second-order equations. This approach has actually had limited application to the compressible boundary-layer case (primarily as a result of the success of the mean field methods) and is really needed only in cases where the flow undergoes a sudden change in boundary condition or experiences a large gradient (a situation generally termed nonequilibrium).

The usual range of application of each of these three closure approaches is indicated schematically as follows:

EQUILIBRIUM	NEAR EQUILIBRIUM	NONEQUILIBRIUM
<ul style="list-style-type: none"> • ZERO OR EQUILIBRIUM GRADIENTS OF PRESSURE, WALL TEMPERATURE, AND WALL INJECTION 	<ul style="list-style-type: none"> • MODERATE DEPARTURES FROM ZERO OR EQUILIBRIUM GRADIENTS 	<ul style="list-style-type: none"> • SUDDEN APPLICATION OR REMOVAL OF LARGE GRADIENTS IN WALL TEMPERATURE, PRESSURE, WALL INJECTION
<ul style="list-style-type: none"> • HIGH REYNOLDS NUMBER 	<ul style="list-style-type: none"> • LOW REYNOLDS NUMBER 	<ul style="list-style-type: none"> • TRANSITIONAL FLOWS
ZEROTH ORDER METHODS		
MEAN FIELD METHODS		
MEAN TURBULENCE FIELD METHODS (WITH LENGTH SCALE EQUATION)		

In the present review an operational definition of equilibrium is used, taken from reference 46: [equilibrium refers] "to a layer that has completely settled down after a discontinuity and is developing with its new boundary conditions with no 'memory' of the discontinuity." Succeeding portions of the present report cover these three closure approaches in considerable detail, especially the mean field approaches.

FLOW PHENOMENA PECULIAR TO CALCULATION OF COMPRESSIBLE

TURBULENT BOUNDARY LAYERS

Calculation procedures for compressible turbulent boundary layers are based, to a great extent, upon techniques, modeling constants, etc., developed originally for the low-speed case. This section discusses many of the significant differences and new or altered physics which occur in the compressible case, as compared with the low-speed situation. The discussion is intended to aid in evaluating the applicability of low-speed results to the compressible (particularly high Mach number) case and to indicate possible pitfalls and sources of inaccuracy in the calculation of compressible turbulent boundary layers.

Normal Pressure Gradient

Shown in figure 1 are typical static-pressure distributions measured across high Mach number turbulent boundary layers (two cases are shown, helium (ref. 47) and nitrogen (ref. 48)). In both cases the boundary layer involved was on a nozzle wall with only a small local longitudinal pressure gradient, although there are significant free-stream static-pressure variations due to uncanceled Mach waves. (See ref. 48.) Two points are obvious from this figure: the static pressure is not constant across these high Mach number turbulent boundary layers ($\partial p/\partial y \approx 0$ for $M \rightarrow 0$), and the wall pressure value is greater than the edge value by approximately 50 percent for these cases ($M_\infty \approx 20$).

A possible origin of at least a portion of this nonconstant $p(y)$ can be readily seen from a simple examination of equation (3) (normal momentum equation)

$$\frac{\partial \bar{p}}{\partial y} \approx - \frac{\partial}{\partial y} (\bar{\rho} \overline{v'^2}) \quad (7)$$

or

$$\bar{p} + \bar{\rho} \overline{v'^2} \approx \text{Constant} \quad (8)$$

Evaluating this expression between the region of peak $\overline{v'^2}$ ($y/\delta = 0(0.1)$ and $p_p \approx p_e$ from fig. 2) and the wall, one obtains

$$\bar{p}_w \approx p_e + f \rho_e u_e^2 \frac{v_p'^2}{u_e^2} \quad (9)$$

where $\bar{\rho}_p \approx f \rho_e$ or

$$\frac{\bar{p}_w}{\bar{p}_e} \approx 1 + f \gamma M_e^2 \frac{v_p'^2}{u_e^2} \quad (10)$$

Limited data (e.g., ref. 49) indicate that the nondimensional velocity fluctuation levels in boundary layers are not significantly influenced by Mach number,

and therefore a reasonable value for $\sqrt{v_p'^2/u_e^2}$ of 0.06 was used (from low-speed data). Using $f = 0.2$ and $\gamma = 1.4$, equation (10) becomes (to correct order of magnitude)

$$\frac{\bar{p}_w}{\bar{p}_e} = 1 + (10^{-3}) M_e^2 \quad (11)$$

and indicates a possible dominant influence of Mach number upon the nonconstant $p(y)$ phenomenon, although the influence may not be as strong as M^2 due to f being a function of M . Shown in figure 2 (from ref. 50) is a comparison between this simple prediction (eq. (11)) and most of the available data. The relatively good agreement between the present simple expression (eq. (11)) and the available data (fig. 2) may indicate that at least some of the nonconstant $p(y)$ effect is caused by the turbulence field. This is probably aggravated at high Mach number by the fact that the dynamic pressure associated with the turbulent fluctuations becomes a significant fraction of the static pressure level at high Mach number. Research by Finley (ref. 51) indicates that most of the $p_w > p_e$ problem is due primarily to inviscid disturbances whose detailed influence is modified by the turbulence effect just described.

Calculation experience indicates that the large \bar{p} changes associated with static temperature variations for high Mach number boundary layers (a change in density by a factor of approximately 100 for $M \approx 20$, $T_w \rightarrow T_t$, and $\gamma = 5/3$) greatly override the $p_w/p_e > 1$ effect and therefore, while interesting, the $p_w/p_e > 1$ effect is not currently considered first order for calculating high Mach number boundary-layer flows.

Influence of Compressibility and Density Fluctuation Terms

There are no definitive, detailed measurements of the complete second-order correlations in a highly compressible flow (including p' and ρ' terms) with which to assess, in a straightforward manner, the influence of compressibility and density fluctuation terms upon closure models used in the calculation of compressible turbulent boundary layers. There is evidently a true Mach number effect on turbulence structure for free flows (ref. 52), at least for the free shear layer case at high Reynolds number with a sustained Mach number difference across the shear layer. However, no important compressibility (p' , ρ') influence has ever been isolated for the boundary-layer case (except for $\overline{\rho'v'}$; see discussion following eq. (6)). Detailed consideration of this area is beyond the scope of the present paper; the purpose here is merely to warn the reader that the following arguments concerning the relative absence of noticeable compressibility effects are deductive. There does not yet exist a definitive set of measurements to completely lay to rest the question of possible compressibility effects upon turbulence structure, although Morkovin's arguments (ref. 26, pp. 367-380), which were based upon hot-wire data up to $M \approx 5$ where p' effects were neglected, have proved thus far to be correct.

Fluctuating Mach number.— One method of evaluating the possible influence of compressibility upon turbulence structure is to examine the magnitude of the fluctuating Mach number M' ; that is,

$$M' \approx \frac{u'}{\bar{a}} - \frac{\bar{M}a'}{\bar{a}} \quad (12)$$

For the case of maximum ρ' (i.e., $T_w \rightarrow T_{t,e}$ and $T_t(y) \approx \text{Constant}$) near the edge of the sublayer

$$\frac{u'}{\bar{a}} = \frac{u'}{u_e} M_e \sqrt{\frac{T_e}{T}} \quad (13)$$

and for $\gamma = 1.4$

$$\frac{u'}{\bar{a}} \approx \frac{u'}{u_e} \frac{M_e}{\sqrt{\frac{1 + M_e^2}{5}}} \quad (14)$$

which is only of the order of 0.2 for high M_e and $u'/u_e \approx 0.1$. Therefore the main term in equation (12) is the second one ($\bar{M}a'/\bar{a}$), which, for $a'/\bar{a} = O(0.1)$, can be of the order of 1 or greater for high M_e . Therefore, for the high hypersonic case the fluctuating Mach number can be of the order of 1 and compressibility effects may become important for accurate turbulence modeling.

Presence of ρ' terms in Reynolds stress expression. - In equation (2) the complete Reynolds stress term is $(\rho v)'u'$. Expanding this term (ref. 13) one obtains

$$(\rho v)'u' = \bar{\rho} \overline{u'v'} + \bar{v} \overline{\rho'u'} + \overline{\rho'u'v'} \quad (15)$$

Using the usual order of magnitude arguments, $\bar{v} \ll \bar{\rho}$ and $\rho' \ll \bar{\rho}$,

$$(\rho v)'u' \approx \bar{\rho} \overline{u'v'} \quad (16)$$

within an accuracy of approximately 20 percent. Calculation experience (e.g., ref. 53) indicates that the ρ' terms in the Reynolds stress equation (eq. (15)) are only important for the case where ϵ/μ is relatively small ($\epsilon/\mu < 100$). Therefore, for the calculation of compressible turbulent boundary layers the Reynolds stress term generally assumes the same form as the low-speed case ($\bar{\rho} \overline{u'v'}$). This does not imply, however, that $\overline{u'v'}$ can be modeled in the same manner (or has similar values) as in the low-speed case.

Comparison of Mean Static Temperature and Turbulent Kinetic Energy

As will now be shown, there is a possibility that, for high Mach numbers, the static temperature can be of the same order of magnitude as the temperature equivalence of the energy associated with the turbulent velocity fluctuations. The basic problem is most easily seen by beginning with the expression for instantaneous total enthalpy

$$H = c_p T_t = c_p T + \frac{u^2}{2} + \frac{v^2}{2} + \frac{w^2}{2} \quad (17)$$

The use of Reynolds time averaging (and recognizing that $\bar{w} = 0$ for two-dimensional boundary layers) yields

$$c_p \bar{T}_t = c_p \bar{T} + \frac{\bar{u}^2}{2} + \frac{\overline{u'^2}}{2} + \frac{\bar{v}^2}{2} + \frac{\overline{v'^2}}{2} + \frac{\overline{w'^2}}{2} \quad (18)$$

or

$$\bar{T} = \underbrace{\bar{T}_t}_{\text{I}} - \underbrace{\frac{\bar{u}^2}{2c_p}}_{\text{II}} - \underbrace{\left(\frac{\overline{u'^2}}{2c_p} + \frac{\overline{v'^2}}{2c_p} + \frac{\overline{w'^2}}{2c_p} + \frac{\bar{v}^2}{2c_p} \right)}_{\text{III}} \quad (19)$$

In order to determine the static temperature from a boundary-layer solution, some form of equation (19) is generally employed, using terms I and II only. Term III has been almost universally neglected. For $M_e \approx 22$, $T_w \rightarrow \bar{T}_{t,e}$, and $\bar{M}_{\text{local}} \approx 10$ (i.e., at $y/\delta \approx 0.5$) in air, the usual terms (I and II) yield $\bar{T}/\bar{T}_t \approx 0.0476$. Assuming $u'/u_e \approx 0.05$, the additional (high M) term (III) yields a value of approximately 0.0075, or approximately 16 percent of the value of terms I and II combined. Similar comparisons over the Mach number range are shown in figure 3.

What this discussion indicates is that for very high Mach numbers, $\bar{T}_t \approx \bar{u}^2/2c_p$ and \bar{T}_{static} can become of the same order as the temperature equivalence of the energy associated with the turbulent motions. Since the intensity of the turbulence is not generally known to within an accuracy of approximately 20 to 30 percent and \bar{T}_{static} can depend upon the square of the intensity (eq. (19)), the accuracy of the computed mean density field for extremely high Mach number turbulent boundary layers could be quite poor.

Precursor Transition Effect

The precursor transition effect is characterized by the existence of large-scale disturbances (and subsequent breakdown into turbulence) in the outer region of compressible boundary layers far upstream of the nominal wall transition point. (See fig. 4 for typical schlieren photographs of this behavior.) This phenomenon is quite commonly observed (e.g., refs. 54 to 56). The spreading rates and possible structure of these disturbances were examined in reference 57 (see fig. 5, taken from ref. 57), while an attempt to model their influence in a mean field closure procedure is reported in reference 58. The major impact of this phenomenon upon the calculation of turbulent boundary layers is that at the nominal wall transition location, the outer portion of the profile is already transitional and turbulent in nature (see fig. 6, taken from ref. 58), and therefore, the usual procedure of starting the calculation at the beginning of the wall transition location with a laminar profile cannot be followed.

A simple method of including this phenomenon is to start the calculation upstream of the wall transition location (with a laminar-like profile) where the transition bursts first initiate. (See ref. 59.) Figure 7 shows a possible further manifestation of this effect - an increase in surface heating upstream of the nominal wall transition point as usually defined (taken from ref. 60). As a

result of the outward movement of the critical layer with Mach number (fig. 8 (from ref. 61) for near adiabatic conditions), this precursor effect occurs further upstream and becomes more important as Mach number increases. Unless a measured starting profile is available, accurate compressible-boundary-layer calculations, at least for the low to moderate Reynolds number range, should include some consideration of this precursor influence. (See also ref. 32.) Experimental evidence indicates that the magnitude of the precursor transition effect may be influenced by T_w/T_e , the effect perhaps becoming less pronounced at lower values of T_w/T_e .

Large p' Levels

The usual assumption in second-order closure approaches is that most pressure fluctuation terms, especially the so-called pressure-dilatation terms (ref. 52) can be neglected. The reasons for this assumption are threefold: (1) The limited data for low speeds indicate that these terms are indeed small; (2) since M' is usually small, the influence of compressibility (which is primarily represented in the second-order approaches by the p' terms) must be small; (3) there is an absence of data concerning the actual magnitude of these terms. Although no data for the terms themselves exist, there is limited data for p' itself, which will now be examined.

Figure 9 indicates the level of rms wall-pressure fluctuations (normalized by the external mean static pressure) as a function of Mach number (from ref. 47). These data indicate that for moderate hypersonic Mach numbers ($M \approx 8$ to 12) the wall-pressure fluctuation levels approach 10 percent, which is a fluctuation level typical of the longitudinal velocity field. In fact, data from reference 62 at $M_e = 9.4$ indicate that the turbulence is dominated by high-frequency pressure fluctuations.

The distribution of p' with distance away from the wall is shown in figure 10 (from ref. 62). These data indicate that p' levels are large, not only at the wall, but across the sensibly turbulent portion of the boundary layer. The p' intensity diminishes only in the outer (intermittent) portion of the flow. Therefore, the p' levels for hypersonic turbulent boundary layers can evidently be large; this calls for a close, careful examination of second-order closure schemes for the high M case (and also for separated flows, where p' levels are large even at low Mach number). Of especial importance are p' terms such as $p'(\partial u_i / \partial x_i)$. (See also ref. 63.)

Definition of Boundary-Layer Thickness

Difficulty in defining the boundary-layer thickness occurs because of large differences between δ_{pitot} and δ_{velocity} for high M boundary layers. A typical result for $M \approx 20$ (from ref. 47) is shown in figure 11, where the nominal δ_{velocity} is approximately 50 percent of δ_{density} (or δ_{pitot}). The pitot edge is easier to measure but there are two fundamental questions: with a relative absence of mean shear above δ_{velocity} , what is the turbulence shear stress (and turbulence eddy) content in this region, and what thickness does one use to scale conventional mean field closure models (such as mixing length) for

the high M case? These questions also involve the fact, as previously discussed, that the density becomes difficult to determine accurately for high M because it is a small difference between two large numbers. These questions are still open, but limited information (for instance, ref. 64) indicates that δ_{velocity} should be used as the scaling function.

Energy Loss Via Acoustic Waves

This subject has received little attention since the original work of Laufer (ref. 26, pp. 381-393). The physical problem arises because of the increasing intensity of turbulent boundary-layer sound radiation with increasing Mach number. For large enough radiated sound levels the amount of energy carried by these waves can be appreciable and represents a new energy dissipation mechanism in high Mach number compressible flows.

In reference 26 Laufer computed that for $M_e \approx 5$, the energy radiated away is approximately 1 percent of the work done by turbulent shear and therefore is negligible. However, if Laufer's equations hold for the case with $M_e = 20$, $T_w/T_t \rightarrow 1$, and $\gamma = 5/3$, the same calculation yields radiated energy of 25 percent which is no longer negligible. For the nozzle wall boundary layers or for boundary layers measured on wind-tunnel models which have turbulent boundary layers, the flow probably reaches an equilibrium state involving a balance between the absorption of acoustic energy radiated by the turbulent flows which surround the local flow and the acoustic energy radiated by the local flow itself, that is, a balance between gain and loss as far as acoustic energy is concerned. This balance probably results in a lower net loss and thus may tend to obscure (in ground facilities) the true importance of this energy radiation effect. Only measurements in a "quiet tunnel" (ref. 65) or on a flight vehicle can clarify the true influence of energy loss via acoustic waves.

There are other problems peculiar to the calculation of compressible turbulent boundary layers such as (1) persistence and importance of wall temperature history effects, (2) increasing predominance of low Reynolds number amplification, and (3) variable edge entropy, but these topics are more conveniently discussed in connection with the mean field closure methods. It should be noted that the nondimensional burst period for compressible flows is approximately the same as that for low-speed flows (ref. 66).

TRADITIONAL PREDICTION METHODS

Methods for calculating turbulent, compressible boundary-layer development have been a topic of extensive research for many years. Until the advent of the high-speed computer, most of this research effort was concerned with prediction methods which could be applied by using only hand calculations or very simple machine computations. Even now, work is continuing on these easily calculable methods because of their inherent accuracy (due to extensive empirical validation) and because of the ease and speed with which these methods can be applied to engineering problems. Traditional methods can be classified into two general categories: integral methods and correlation methods. Numerous survey papers are available (e.g., ref. 18 and pp. 181-229 of ref. 28) which attempt to evalu-

ate the accuracy and limits of applicability of various traditional methods for compressible two-dimensional turbulent flows.

The objectives of this section are to describe and discuss the merits of each category of traditional methods. In addition, several illustrative examples of each category will be discussed and compared with experimental data. Comments concerning the accuracy and applicability of these prediction methods will be made. A discussion of compressibility transformations is first presented since transformations are frequently used in both correlation methods and integral methods; next, a discussion of correlation methods including compressible law-of-the-wall/law-of-the-wake formulations is given; finally, integral methods are discussed. Integral methods may use a transformation technique and/or a correlation method in the complete solution procedure.

Transformations

One of the earliest approaches to predicting compressible turbulent flows was to seek a transformation which, when applied to the governing equations for compressible flow, yields identically the incompressible equations. This technique has been used with success for laminar boundary-layer flows which satisfy certain requirements on the relationship between kinematic viscosity and temperature. (Reynolds stress terms do not appear in the laminar boundary-layer equations.) The obvious advantage of this approach for turbulent flows is that, if successful, the more extensive knowledge of the mechanism of turbulent momentum transfer for incompressible flows can be used to predict compressible flows. The transformation concept assumes that the companion incompressible flow resulting from the transformation is physically observable; in addition, it is usually necessary to assume an invariance hypothesis concerning some transformation scale. Beckwith (ref. 18) points out several examples where the physical concepts of a compressibility transformation are violated because of a lack of correspondence of the transformed incompressible flow. These include the following: (1) Normal pressure gradients which may be important in high-speed flows do not exist in incompressible flow and, therefore, are not transformed; (2) dissipation effects in heating calculations are not properly transformed; (3) large normal temperature gradients in the transformed incompressible flow result from the transformation and, according to the equation of state, cannot exist in the constant-density flow; (4) fluctuating density terms in the compressible formulation have no counterpart in the corresponding constant-density flow.

The earliest transformation for turbulent flow was presented by Dorodnitsyn (ref. 67) who considered only the Von Kármán momentum integral equation. Mager (ref. 68) was the first to attempt to transform the partial-differential equations for turbulent boundary-layer flow. Examples of other attempts to define a transformation in the same time frame were Culick and Hill (ref. 69), Burggraf (ref. 70), and various reference temperature or enthalpy methods for zero-pressure-gradient flows (e.g., refs. 71, 72, and 73).

Some years later, Coles (ref. 15), criticizing the assumption made in references 68 and 70 of invariant turbulent shear and stream function under the transformations, proposed a more physically acceptable transformation in which the adiabatic, compressible, and the constant-density flows are assumed to be

related by three scaling parameters $\sigma(x)$, $\eta(x)$, and $\zeta(x)$. The first parameter relates the stream functions of the two flows, the second is a multiplicative factor of the Dorodnitsyn-Howarth scaling of the normal coordinate, and the third relates the streamwise coordinates of the two flows. An additional assumption pertaining to the invariance of a Reynolds number characterizing the law-of-the-wall region of the boundary layer is necessary to complete the transformation. This assumption, which Coles called the substructure hypothesis, provides a substitute for a reference state utilized with many theoretical approaches. Coles' transformation was then modified or extended as follows: (1) Crocco (ref. 74) modified Coles' transformation to include effects of heat transfer and pressure gradient; (2) Baronti and Libby (ref. 75) replaced Coles' substructure hypothesis with a sublayer hypothesis based on experimental observation; (3) Jeromin (ref. 76) extended Coles' transformation to include effects of mass transfer; (4) Lewis, Kubota, and Webb (ref. 77) defined new coordinates consistent with Coles' transformation and eliminated the need for a substructure or sublayer hypothesis (they found, however, that dissipation effects for compressible flows invalidate the transformation for high wall temperatures); (5) Economos and Boccio (ref. 78) empirically modified Coles' law of the wall/law of the wake and introduced two compatibility equations which provide the closure conditions. Coles' approach and the subsequent companion work represent the primary advances in transformation theory in recent years.

Comparisons with experimental data have shown that transformations yield good results only for moderate Mach numbers ($M \leq 6$) and for moderate wall heating ($T_w/T_t \geq 0.5$) with zero or mild pressure gradients (refs. 75, 77, 79, and 80). (In ref. 79, it was observed that while compressibility had little effect on mixing length for flat-plate-type turbulent boundary layers, Mager's transformation predicts a large effect.) By empirically modifying Coles' transformation, Economos and Boccio (ref. 78) were able to extend the range of agreement with experimental data beyond any other method. While this empirical modification was not physically appealing (transformation of impermeable wall case yields mass transfer in transformed plane), agreement with experiment was substantially improved. This is illustrated in figure 12 where the methods of Baronti and Libby (ref. 75) and Economos and Boccio are compared with experiment; here, local skin friction values were obtained from experimental velocity profiles according to each transformation approach (by fitting law-of-the-wall profiles to experimental profiles) and normalized by a reference value. (See ref. 80 for details.) This reference value is equivalent to the measured skin friction as illustrated in figure 12. As the ratio of wall temperature to total temperature is decreased, a systematic error appears in the skin friction obtained using Coles' transformation with the sublayer hypothesis as recommended by Baronti and Libby. The empirical modification of Economos and Boccio apparently eliminates this disagreement.

The ability of Coles' original transformation to predict flat plate skin friction and heating for Mach 4 to 13 and $0.14 \leq T_w/T_t \leq 0.7$ is illustrated in figure 13. The experimental data are transformed according to Coles' method and compared with a good incompressible prediction (ref. 81). The prediction of skin friction is generally poor; this poor agreement results from an effect of T_w/T_t not accounted for in the transformation. (See ref. 82.) The improved heating prediction in figure 13 reflects the use of a Reynolds analogy factor ($2N_{St}/C_f$) to adjust the level of the data.

Both references 77 and 78 applied their versions of Coles' transformation with an incompressible integral method, and examples of the results are shown in figure 14. Here, the skin friction and momentum thickness for the waisted body of revolution from reference 83 are compared with predicted values from each method. These comparisons properly belong in a later section on integral methods but are shown here to illustrate the accuracy of these transformation methods. The agreement of the method of reference 78 (fig. 14(a)) with experiment is good and rivals some of the more advanced numerical methods, while the predictions of reference 77 (fig. 14(b)) are obviously poor and unacceptable for engineering purposes. (However, curvature and laminarization effects may be present in some of the data of ref. 83 and thus could influence these comparisons.)

These comparisons of the results from transformation methods with experimental data and other comparisons in the cited references lead to the general conclusion that while some success for adiabatic flows is evident, transformation methods are not presently desirable for general applications, a conclusion also reached in references 18 and 28 (pp. 181-229).

Correlation Methods

Correlation methods are perhaps the most popular of the traditional methods because they are generally simple to apply and some are quite accurate. Even though these methods are strictly applicable only for two-dimensional or axisymmetric flows with zero pressure and wall temperature gradients, they are widely used for parametric design studies and preliminary estimates. The empirical input to some of these methods enhances the accuracy and allows easy modification of the method to include new empiricism. Some of these methods provide predictions for wall shear stress only, while others also allow specification of the boundary-layer profiles. Additional assumptions for the Reynolds analogy factor $2N_{St}/C_f$ and the recovery factor are required in order to calculate wall heat transfer for those methods which only predict wall shear.

Spalding and Chi (ref. 81) have presented an excellent summary of available correlation methods for compressible turbulent flow up to 1964. Since 1964 the only correlation method to arise is that of White and Christoph (ref. 84). According to Spalding and Chi, correlation methods may be classified as follows:

- (1) Methods using Prandtl or Von Kármán differential equations (i.e., Prandtl or Von Kármán mixing length concepts)
- (2) Theories based upon other differential equations
- (3) Theories based upon a fixed velocity profile
- (4) Theories based upon incompressible formulae with reference properties

In categories 1 and 2 the shear stress is assumed to be constant through the boundary layer and equal to its wall value; in category 3 the velocity profile is assumed independent of compressibility; in category 4 the incompressible relations are assumed to apply for compressible flows if the gas properties are evaluated at a reference temperature or enthalpy where the reference temperature

is a function of Mach number, ratio of wall to edge temperature, and recovery factor. Some examples of the more popular methods in each category are as follows:

Category 1 - Van Driest I (ref. 13) and Kutateladze and Leont'ev (ref. 85), which use a Prandtl mixing length, and Wilson (ref. 86), Van Driest II (ref. 87), Harkness (ref. 88), Deissler and Loeffler (ref. 39), and Moore (ref. 89), which use a Von Karman mixing length.

Category 2 - Li and Nagamatsu (ref. 90) and Kosterin and Kashmarov (ref. 91).

Category 3 - Cope (ref. 92) and Monaghan (ref. 93).

Category 4 - Summer and Short (ref. 73) and Eckert (ref. 72).

In addition to these methods, Spalding and Chi (ref. 81) present a method which uses a Van Driest type analysis to determine a function F_C and empirical data to determine a function F_R . In their method the assumption is made that $F_C C_f$ varies uniquely with $F_R R$ according to an incompressible law (R is a Reynolds number) and that F_C and F_R are functions only of Mach number, ratio of wall temperature to edge temperature, and recovery factor.

Numerous survey papers (refs. 16, 80 to 82, 84, and 94 to 98) have attempted to determine which of the correlation techniques best predicts available experimental data for compressible turbulent boundary-layer flow. The method which is found to be the "best" in each of these survey papers is usually either Van Driest II (ref. 87), Spalding and Chi (ref. 81), or a reference temperature approach (e.g., Eckert, ref. 72). The choice of a "best" method is influenced in each of the survey papers by particular selections of virtual origin, Reynolds analogy factor for heating calculations, and recovery factor. (See ref. 82.)

Comparisons of experimental skin friction and heat transfer data with predicted values obtained from the methods of Van Driest (ref. 87), Spalding and Chi (ref. 81), and Eckert (ref. 72) for Mach numbers 4 to 10 and ratios of wall temperature to total temperature from 0.14 to 0.7 are shown in figures 15 to 17. The data were obtained in windtunnels on flat-plate models with $dp/dx = 0$ and $dT_w/dx = 0$; skin friction was measured with balances and wall heating was measured by transient techniques. The comparisons are presented in the form $F_C C_f$ against $F_R R_\theta$ or $F_R R_{x,vo}$ where $F_C C_f$ is equivalent to the incompressible value of skin friction and $F_R R_\theta$ or $F_R R_{x,vo}$ is equivalent to the corresponding incompressible value of Reynolds number. (See ref. 82 for further explanation.) In this manner, all the transformed experimental data can be compared directly with values from a good incompressible skin friction law (law from ref. 81 used herein) to judge the efficacy of each method.

The comparison of the data with predicted values from the Van Driest II method (ref. 87) is shown in figure 15. For this comparison, a momentum thickness Reynolds number is used, and a Reynolds analogy factor of 1.0 is assumed, as recommended for best results with the Van Driest II method by Hopkins and Inouye in reference 98. The comparison is favorable for heat transfer, but the

transformed skin friction data fall generally below the prediction. As reported in reference 82, the prediction error also appears to be a function of T_w/T_t . A similar comparison for the method of Spalding and Chi (ref. 81) is shown in figure 16. Here, the virtual origin location was assumed to be near the end of boundary-layer transition, and Von Kármán's Reynolds analogy factor (used as suggested in the appendix of ref. 95) was applied as recommended for the Spalding and Chi method in reference 82. The prediction of both the heating and skin friction data in figure 16 is quite good. The results from Eckert's method (ref. 71) are shown in figure 17 using the same virtual origin and Reynolds analogy factor as previously used with the Spalding and Chi method. The comparison between data and prediction is again very good in figure 17, but there appears to be a discernible variation of prediction errors with T_w/T_t . (See ref. 82.) Considering the wide range of flow conditions of the data, each of the three approaches provides a credible prediction method for zero-pressure-gradient turbulent-boundary-layer flows.

Comparisons of predictions from Eckert's method (ref. 72) with data from flight are shown in figures 18 and 19. Data obtained on conventional aircraft such as the A-5A, the Mirage IV, and the XB-70-1 (refs. 99 to 101) are shown in figure 18. The agreement with Eckert's method is good in each case. Heating data from sharp and blunt cones in flight are shown in figure 19 (from ref. 96) where Colburn's Reynolds analogy (ref. 102) was used for the calculation and the virtual origin was assumed to occur at the stagnation point or cone tip. A cone/flat plate transformation after Van Driest (ref. 103) was applied. The agreement between prediction and data is surprisingly good over the wide range of data included ($3 \leq M \leq 13$, $0.2 \leq T_w/T_e \leq 2.3$). It appears therefore that these correlation methods provide accurate predictions of turbulent skin friction and heat transfer for a wide range of flow conditions (for $dp/dx \approx 0$, $dT_w/dx \approx 0$) in flight as well as in wind tunnels.

Compressible law of the wall.- The law-of-the-wall velocity profile has been useful in arriving at quantitative analytical results for incompressible flows. This incompressible law is empirical in nature but can be derived directly from mixing length concepts; that is,

$$\tau = \bar{\rho} l^2 \left(\frac{\partial \bar{u}}{\partial y} \right)^2$$

and

$$l = Ky \quad (\text{Prandtl})$$

so

$$\tau = \bar{\rho} K^2 y^2 \left(\frac{\partial \bar{u}}{\partial y} \right)^2 \quad (20)$$

Integration yields ($\rho = \text{Constant}$ and $\tau = \tau_w = \text{Constant}$)

$$\frac{\bar{u}}{u_\tau} = u^+ = \frac{1}{K} \ln y^+ + C \quad (21)$$

$$y^+ = \frac{yu_\tau}{\nu_w}$$

$$u_\tau = \left(\frac{\tau_w}{\rho_w}\right)^{1/2}$$

which is the incompressible law of the wall and is valid only very near the wall but not in the viscous sublayer. Coles (ref. 104) extended equation (21) to include the wake portion of the boundary layer, and the resulting equation is

$$u^+ = \frac{1}{K} \ln y^+ + c + \frac{\pi}{K} w \quad (22)$$

where $(\pi/K)w$ is a wake function which accounts for the wake-like behavior of the outer portion of the turbulent boundary layer. Alternately, by evaluating equation (22) at the edge of the boundary layer and subtracting the resulting equation from equation (22), the velocity defect equation is obtained

$$\frac{u_e - u}{u_\tau} = -\frac{1}{K} \ln \frac{y}{\delta} + \frac{\pi}{K} (2 - w) \quad (23)$$

An expression for the incompressible profile from the wall to the outer edge of the buffer layer (beginning of fully turbulent region) was presented by Spalding (ref. 105) and Kleinstein (ref. 106). Modifications to the law of the wall for surface roughness (e.g., ref. 107) and wall injection (e.g., ref. 108) are available. Equation (23), the velocity defect distribution, is independent of surface roughness. The law-of-the-wall/law-of-the-wake expressions have been used extensively and with great success in studies of turbulent boundary layers either to obtain such parameters as C_f and δ from experimental velocity profiles or as an auxiliary equation in integral or numerical prediction methods.

The successful application of the law-of-the-wall/law-of-the-wake velocity profile for incompressible flows has naturally led to numerous attempts to apply similar concepts to compressible flows. A brief description of some of the more prominent of these studies follows.

Van Driest (ref. 13) in 1951 derived a compressible law of the wall for zero-pressure-gradient flows by solving the turbulent-boundary-layer equations with Prandtl's mixing length formulation and a laminar and turbulent Prandtl number of unity. By comparing the resulting law of the wall from Van Driest's analysis with the incompressible law of the wall, it is clear that the effects of compressibility can be accounted for by defining a generalized velocity u^* in place of u . (See Maise and McDonald (ref. 79).) This generalized velocity is defined as

$$u^* = u_\infty \frac{1}{A} \sin^{-1} \left[\frac{2A^2(\bar{u}/u_\infty) - B}{(B^2 + A^2)^{1/2}} \right] = \int \left(\frac{\rho}{\rho_w}\right)^{1/2} du$$

where ρ is from Crocco's relation and

$$A^2 = \frac{[(\gamma - 1)/2]M_\infty^2}{T_w/T_\infty}$$

$$B = \frac{1 + [(\gamma - 1)/2]M_\infty^2}{T_w/T_\infty} - 1$$

More recently Maise and McDonald (ref. 79) applied these concepts by assuming that Coles' law of the wall was valid for compressible flow if the velocities are defined as the generalized velocity. The resulting equation for the velocity defect was

$$\frac{u_\infty^* - u^*}{u_\tau} = -\frac{1}{K} \ln \frac{y}{\delta} + C(2 - w)$$

where w is Coles' tabulated wake function (ref. 104). Using Clauser's results (ref. 1) for incompressible flow to define the constants, the final expression is

$$\frac{u_\infty^* - u^*}{u_\tau} = -2.5 \ln \frac{y}{\delta} + 1.25(2 - w) \quad (24)$$

Maise and McDonald found that experimental velocity profiles for adiabatic, compressible turbulent boundary layers from Mach 1.5 to 5 through a wide range of Reynolds numbers were well correlated by equation (24). However, the velocity profiles for nonadiabatic flows in the same range of Mach number were poorly correlated.

Fernholz (ref. 109) used a similar analysis with generalized velocities but did not use Clauser's constants. Instead, experimental data were used to correlate the constant as a function of the ratio of wall temperature to adiabatic wall temperature and Reynolds number. The formulation was

$$\frac{u^*}{u_\tau} = \frac{1}{K} \ln \frac{yu_\tau}{v_w} + F_1 \quad (25)$$

where

$$F_1 = f\left(\frac{T_{aw} - T_w}{T_{aw}}, \frac{\rho_e u_e \theta}{\mu_w}\right)$$

Fernholz also included the velocity defect law but redefined the δ -coordinate as was done for incompressible flows. The resulting equation was

$$\frac{u_\infty^* - u^*}{u_\tau} = -\hat{M} \ln \frac{y}{\Delta^*} - \hat{N} \quad (26)$$

where

$$\Delta^* = \delta \int_0^1 \frac{u_e^* - u^*}{u_\tau} d \frac{y}{\delta}$$

$\hat{M} = 4.7$ and $\hat{N} = 6.8$ for adiabatic walls. Equation (25) provided a good correlation of experimental velocity profiles for Mach 5 to 8 with moderate heat transfer. Equation (26) also correlated the defect region of these profiles for $R_\theta = \rho_e u_e \theta / \mu_w$ greater than 1000 to 1500.

Mathews, Childs, and Paynter (ref. 110) using generalized velocity concepts fitted the velocity defect equation (eq. (24)) to experimental velocity profiles (by the method of least squares) and thereby obtained the skin friction and boundary-layer thickness which allowed the best profile fit. The test cases involved both normal and conical shock interactions with turbulent adiabatic boundary layers at supersonic speeds as well as a flat-plate supersonic flow. The velocity profile fits were good, and the resulting skin friction and boundary-layer thickness values compared favorably with experiment and other predictions.

Sun and Childs (ref. 111) modified the analysis of reference 110 by using a more realistic shear stress distribution through the boundary layer. Instead of assuming $\tau = \tau_w = \text{Constant}$, the expression

$$\frac{\tau}{\tau_w} = 1 - \left(\frac{y}{\delta}\right)^b \quad (27)$$

was used. Equation (27) with $b = 1$ is a reasonable fit to experimental data for both subsonic and supersonic flows (ref. 25). This modification satisfies the physical condition that the velocity gradient be zero at $y = \delta$ and provides more accurate values of boundary-layer thickness. The profile fit and the resulting skin friction were little changed from the analysis of reference 109.

Kane (refs. 112 and 113) used the compressible counterpart of equation (1) which is

$$u^{++} = \frac{1}{K} \ln y^+ + C \quad (28)$$

where

$$u^{++} = \int_0^{u^+} \left(\frac{\rho/\rho_w}{\tau/\tau_w}\right)^{1/2} du^+ \quad (29)$$

Equation (29) was evaluated by using the Crocco temperature profile and Squire's definition of τ/τ_w (ref. 114) which includes the effects of wall injection. Inclusion of an empirical extension of Kleinstein's buffer layer profile (ref. 106) to compressible flow as well as Coles' wake parameter completed the formulation of the compressible law of the wall/law of the wake. Kane finds that three profile functions remain undefined in his compressible law of the wall/law of the wake which must be obtained from a fit of experimental velocity profile data. A multiple regression analysis is then used to define the best functional variation of these three functions with appropriate fluid variables.

Squire (ref. 114) used an approach similar to Kane's method to extend the compressible law of the wall to flows with wall injection. By fitting experimental velocity profile data, the integration constant in the law of the wall was determined as a function of v_w/u_τ and Mach number. The slope of the log region K was found to be independent of mass injection. Chen (ref. 115) extended the generalized velocity concepts used by Maise and McDonald (ref. 79) to flows with rough wall, heat transfer, and pressure gradient. White and

Christoph (ref. 116) included effects of longitudinal pressure gradient on the shear stress distribution and then, using a method similar to Squire (ref. 114) with $v_w = 0$, obtained a closed form solution for the law-of-the-wall velocity profile.

Danberg (ref. 115) used Coles' law-of-the-wall/law-of-the-wake profile and a reduced velocity

$$u' = \int \left(\frac{\rho}{\rho_w} \right)^{1/2} du$$

to account for compressibility effects. Four profile parameters were determined from least square fits of Danberg's compressible law of the wall to experimental velocity profile data from Mach 2 to 6 for adiabatic wall conditions. Danberg attempted a similar definition of a law of the wall for the temperature profile, but a paucity of experimental data prevented definitive results.

This discussion of the status and development of a compressible law of the wall indicates that reliable expressions for a compressible law of the wall exist for adiabatic wall conditions and Mach numbers less than 6. However, for flows with significant heat transfer, the definition of a compressible law of the wall is still unclear. The unresolved question of the effect of heat transfer on the applicability of a compressible law of the wall is clearly illustrated when the results of Maise and McDonald (ref. 79), which show poor correlation of compressible velocity profiles with heat transfer, are compared with the results of Gran, Lewis, and Kubota (ref. 118) which show good correlation of compressible velocity profiles with pressure gradient and heat transfer, both studies using nearly the same compressible law-of-the-wall formulation; the difference between the two formulations was that Δ^* (see eq. (26)) was used instead of δ in the velocity defect law in reference 117. It thus appears that further progress in defining a general law-of-the-wall velocity profile for compressible turbulent boundary layers will be paced by progress in obtaining detailed and accurate experimental data through a wide range of flow variables.

Integral Methods

All integral methods solve the (Von Kármán) integral momentum equation along with various auxiliary relations. The two-dimensional Von Kármán momentum integral equation is obtained by integrating the x-momentum equation. When normal stress terms are neglected, the following equation is obtained:

$$\frac{d\theta}{dx} + \frac{\theta}{u_e} \frac{du_e}{dx} \left(H + 2 + \frac{u_e}{\rho_e} \frac{d\rho_e}{du_e} \right) + \frac{1}{\rho_e u_e^2} \frac{d}{dx} \left(\rho_e \delta^3 - \int_0^\delta p \, dy \right) = \frac{C_f}{2} \quad (30)$$

where

$$\theta = \int_0^\delta \frac{\rho u}{\rho_e u_e} \left(1 - \frac{u}{u_e} \right) dy$$

$$H = \frac{\delta^*}{\theta}$$

$$\delta^* = \int_0^{\delta} \left(1 - \frac{\rho u}{\rho_e u_e} \right) dy$$

If p is independent of y and the free-stream flow is adiabatic, then

$$\frac{u_e}{\rho_e} \frac{d\rho_e}{du_e} = -M_e^2$$

and equation (30) becomes

$$\frac{d\theta}{dx} + \frac{\theta}{u_e} \frac{du_e}{dx} (H + 2 - M_e^2) = \frac{C_f}{2}$$

There are two basic types of integral methods - those which solve the equations in the physical plane and those which use a compressibility transformation and then solve the equations in the incompressible plane. Most of the earlier methods used a compressibility transformation, while more recent methods favor solving the equations in the physical plane. Examples of auxiliary relations used in the numerous methods available in the literature are as follows:

- (1) Moments of the integral momentum equation, which are obtained by multiplying the momentum equation by y or u and integrating across the boundary layer (these moment equations contain unknowns involving turbulent shear stress or dissipation integrals which must be defined in terms of known quantities)
- (2) Entrainment equation and/or lag equation
- (3) Specification of velocity, temperature, and/or shear stress profiles
- (4) Specification of form factor, wall shear, and/or wall heating (Reynolds analogy)

By using selected auxiliary relations, the problem is reduced to solving a set of quasilinear, coupled ordinary differential equations by an available solution technique.

Integral methods have advantages which have assured their continued use through the years. Primary advantages are the following: (1) Solution procedures are fast and easily programmed; (2) starting procedure is simple; (3) less detailed information on turbulence is necessary; (4) integration process eases restriction on accuracy of profile shapes. The disadvantages of such methods are that considerable empiricism is necessary to close the equation set (i.e., relying upon empirical input restricts accuracy and range of application) and that nonequilibrium effects are difficult to include. The latter restriction becomes particularly important for high Mach number flows. Of course, if a compressibility transformation is used, the integral method is subject to all the uncertainties inherent in the transformation.

Most earlier integral methods utilized a compressibility transformation in the solution procedure. Examples of these are the methods Reshotko and Tucker (ref. 119), Englert (ref. 120), Mager (ref. 68), Culick and Hill (ref. 69), and Spence (ref. 121). More contemporary methods using transformations are those of Sasman and Cresci (ref. 122), Camarata and McDonald (ref. 123), Flaherty (ref. 124), Zwarts (ref. 125), and Küster (ref. 30, pp. 19-1 - 19-11); extensions of Head's entrainment method (ref. 126) to compressible flows by transformations were given by Standen (ref. 127), So (ref. 128), and Green (ref. 129).

In recent years, integral methods which do not use a compressibility transformation but rather use auxiliary relations which are valid in the compressible plane have found considerable favor. A representative list of such methods includes those of Miller (ref. 130), Michel, Quémard, and Cousteix (ref. 131), Johnson and Boney (ref. 132), Pinckney (ref. 133), Reeves (ref. 30, pp. 6-1 - 6-A2-2), and White and Christoph (ref. 84). In addition, Green (refs. 129 and 134) and Green, Weeks, and Brooman (ref. 135) extended Head's entrainment method (ref. 126) to compressible flows also using physical variables. Obviously, discussion of all these methods is not feasible in the present paper; therefore, a representative example of each type of method is discussed. The particular methods chosen were a method using a transformation (Flaherty, ref. 124), a method using entrainment concepts in physical variables (Green, Weeks, and Brooman, ref. 135), a method specially configured for adverse gradients (generated by concave surfaces) also in physical variables (Pinckney, ref. 133), and a method in physical variables but using a compressibility transformation for a portion of the solution (Reeves, ref. 30, pp. 6-1 - 6-A2-2). The structural highlights of each of these four calculation procedures will be discussed along with comparisons with typical experimental data.

Method of Flaherty.- This method (ref. 124) is basically a modification of the procedure of Reshotko and Tucker (ref. 119) and solves the momentum integral and moment-of-momentum equations in the transformed plane defined by using Stewartson's transformation (ref. 136). The skin friction coefficient is obtained from the Ludwig and Tillman incompressible equation (ref. 137) using reference temperature concepts (ref. 72). An empirical expression is used by Flaherty for the shear stress integral through the boundary layer and is the main improvement over the earlier Reshotko and Tucker method which used a constant shear stress. A provision for calculating wall heat transfer based upon the energy deficit in the boundary layer is also included.

Comparisons of predictions from Flaherty's method with two sets of experimental data are shown in figure 20. These example data were chosen to illustrate the ability of the method to predict boundary-layer growth along flat or curved surfaces with favorable pressure gradient. Good prediction of the boundary-layer thickness data from reference 138 at Mach 1.5 (fig. 20(a)) is achieved over the entire length of the test plate. Reasonable agreement with the data from reference 83 at Mach 2 (fig. 20(b)) on the waisted body of revolution is also obtained, but the agreement of prediction with both momentum thickness and skin friction data deteriorates in the region of adverse pressure gradient ($x/L > 0.7$). Comparisons of this method with other available data in references 30 (pp. 181-229) and 124 indicate generally good predictions of boundary-layer integral properties up to Mach 6 with moderately cooled walls and moderate pressure gradient.

Method of Green, Weeks, and Brooman.- This integral method (ref. 135) is essentially an extension of Head's method (ref. 126) to compressible flow and attempts to account for the influence of upstream flow history on the turbulent stresses. The procedure consists of solving in the physical plane the integral momentum equation, the entrainment equation, and a rate equation for the entrainment coefficient. This rate equation or lag equation is developed from an equation for shear stress derived from the turbulent kinetic energy equation. In addition, an empirical factor is introduced to account for the variation of integral parameters with Mach number in equilibrium flows. The method as formulated is restricted to adiabatic flows.

Two comparisons of predictions from this method with experimental data are shown in figure 21. The first is a comparison with the data of reference 83 (fig. 21(a)). The prediction is in good agreement with the experimental surface shear and momentum thickness, even at the rear (adverse pressure gradient) of the waisted body. Good agreement is also obtained with the data of Lewis, Gran, and Kubota (ref. 139), as shown in figure 21(b). Here the pressure gradient is zero up to $x \approx 35.6$ cm, adverse from $x \approx 35.6$ cm to 45.7 cm, and then favorable thereafter. The good agreement seen in figure 21 is also evident in other comparisons shown in reference 135 for adiabatic conditions up to Mach 4.

Method of Pinckney.- This method (ref. 133) was especially tailored to predict turbulent boundary-layer development on compression (concave) surfaces common to hypersonic air breathing engines. The set of equations which is solved consists of the momentum integral equation, the moment-of-momentum equation, and the integral energy equation. Auxiliary relations consist of (1) assuming a Crocco-like temperature profile which satisfies the total energy deficit across the boundary layer as determined from the net heating along the surface (history effect), (2) assuming an empirical shear stress distribution across the boundary layer, and (3) assuming the Spalding and Chi (ref. 81) skin friction prediction (suitably shifted) is valid in pressure gradient flows (as well as the resulting heat transfer coefficient obtained from Spalding and Chi skin friction with Von Kármán's Reynolds analogy factor (ref. 140)). Provisions are made to allow calculations to proceed through transition and into fully turbulent boundary-layer flow.

Comparisons of Pinckney's method with experimental data from reference 141 are shown in figure 22. These integral boundary-layer-thickness data were obtained on an axisymmetric compression surface for both Mach 5 adiabatic flow and Mach 8 cold-wall conditions. Predictions from the integral method are generally in good agreement with the integral thicknesses for both experimental conditions shown. Comparisons with other data in reference 133 are also favorable and confirm reasonable accuracy for this prediction method at least up to Mach 8 with moderate wall cooling.

Method of Reeves.- This method (ref. 30, pp. 6-1 - 6-A2-2) solves the compressible turbulent boundary-layer equations including mass transfer by assuming a two-layer boundary-layer model. Mixing length concepts are assumed to apply in the inner layer, and this results in a compressible law-of-the-wall expression; this expression is inserted into the boundary-layer conservation equations which are integrated away from the wall to a matching location. The outer (or wake) layer solution uses an integral momentum method, the results from which

are matched to the inner layer solution at a prescribed match point. The outer layer integral solution employs a compressibility transformation. An empirical expression for the shear stress integral for the outer layer is specified. Apparently the dynamics of the boundary-layer solutions from this method depend on coupling and interaction between the inner and outer solutions.

Two comparisons of predictions from Reeves' method with experimental data are shown in figure 23. The predictions of the integral thicknesses for the data of reference 138 (fig. 23(a)) at Mach 1.5 are excellent. While the prediction of momentum thickness for the data of reference 83 (fig. 23(b)) at Mach 2.4 is good, the skin friction data are not well predicted. Reeves found good agreement between his predictions and experimental data up to Mach 10 for a wide range of wall temperature ratios with and without wall mass transfer. Some computational stability problems occurred for negative pressure gradients. The method was computationally quite rapid.

In summary, this brief review of various available integral solution procedures for two-dimensional compressible turbulent boundary-layer flow indicates that reasonably accurate predictions are possible using integral techniques for a wide range of flow conditions. Caution must be exercised in applying integral methods to flows with severe pressure gradients as well as other nonequilibrium effects and to flows where the empirical correlations used in the method do not apply. While integral methods provide fast and inexpensive calculations necessary for design and analysis of fluid systems, the limitations of any method must be clearly understood to prevent erroneous conclusions. As discussed earlier, transformation theory has not, thus far, developed into a tool for general application, and therefore, integral methods using a "complete" compressibility transformation should probably be avoided at present.

NUMERICAL SOLUTION PROCEDURES

This section considers the various alternative numerical procedures currently being used to solve the nonlinear partial-differential equations describing compressible turbulent boundary layers (which are parabolic in the marching or longitudinal direction). There are several numerical difficulties peculiar to the calculation of turbulent (as opposed to laminar) compressible boundary layers. These problem areas include (1) presence of a thin sublayer, which requires either a separate wall treatment or variable grid (or coordinate transformation), (2) rapid growth of the boundary layer with longitudinal distance, which requires a transformation or streamline mapping procedure, and (3) algebraic terms in the turbulence modeling expression which can alter the stability of the numerical calculation procedure.

Solution Techniques

The numerical solution procedures used to solve the compressible turbulent boundary-layer problem can be conveniently categorized in the following manner:

Conventional Finite-Difference Methods

Implicit (refs. 45 (pp. 375-383), 53, and 142 to 157)
Explicit (ref. 158)

Finite-Difference Variants

Shooting method (refs. 28 (pp. 551-554), 40, 159, and 160)
Box method (ref. 161)
Micro-integral (ref. 9)

Methods Employing Analytical Functions

Wortman approach (ref. 162)
BLIMP (ref. 163)
Method of weighted residuals or method of integral relations (refs. 164 and 165)
Finite element (ref. 166)

Method of Characteristics (ref. 36)

The conventional finite-difference methods have been the most popular. They usually employ Crank-Nicolson differencing and the Thomas algorithm for inversion of the coefficient matrix. The advantages of these procedures include ease of coding, numerical stability, and overall simplicity. Their disadvantages are mainly due to their essentially "brute force" approach, in that 100 nodes in the vertical direction are usually needed to adequately represent a turbulent profile (even with nonuniform mesh spacing). Therefore, the procedures generally require relatively large storage and long machine time, especially when chemical reaction effects are included.

The shooting procedure uses finite differences in the longitudinal or x-direction but solves an ordinary differential equation (two-point boundary-value problem) in the transverse or y-direction. Several users of this approach have encountered serious stability problems, especially with wall heating or cooling and pressure gradient cases. The solutions seem to be sensitive to guesses of the inner boundary conditions. Only a few codes presently use the shooting method, and it is probably not one of the best procedures available.

The box method is quite efficient for boundary layers and is of more recent vintage than the conventional finite-difference and shooting procedures. By a change of dependent variables the equations are reduced to a first-order nonlinear system, which is solved by Newton iteration and two-point differencing. This procedure has several advantages, which include high order spatial accuracy, even with a rapidly varying nonuniform grid, and the small number of nodes required for solution (obtained by Richardson extrapolation). As a result of these advantages, this procedure produces solutions in 7 times less machine time and with much less storage than conventional finite-difference methods.

In the micro-integral method, developed at Imperial College of Science and Technology, the boundary-layer growth is accounted for by use of a stream function as a transverse variable, thus reducing the number of nodes required. Most versions of this procedure also use a Couette flow analysis near the wall, which significantly reduces the required calculation time, as the use of small nodal spacing near the wall to resolve the sublayer is no longer necessary. Also, in

this method the convective terms are integrated between grid nodes before differentiation. This solution procedure is one of the more efficient ones available, but the Couette flow analysis near the wall must change with different boundary conditions, and, since the usual formula for grid control (stream-function boundary condition) is explicit, there may be problems for large longitudinal increments.

The Wortman approach is fairly recent and bears some faint resemblance to the shooting method in that finite differences are taken in the longitudinal direction only. An integrating factor is used to reduce the order of the equations and the procedure is referred to as an iterative operator method. The method appears to be quite fast and has a high order of spatial accuracy.

BLIMP (boundary-layer integral matrix procedure) has undergone extensive development, especially for application to flow chemistry problems. The procedure is fairly involved, and the method was specifically developed to minimize the number of grid nodes (especially important for the large equation set which results when chemical effects are included). The method is characterized by finite differences in the longitudinal direction, and strip integrals in the transverse direction with cubic spline fits and Newton-Raphson iteration.

The method of weighted residuals (or method of integral relations) is somewhat similar to strip integral procedures. The method uses weighting and approximating functions which must be assumed. The advantage to the procedure is again the small number of nodes involved, but the coding is fairly complex and considerable insight is often needed to select reasonable functional forms. For turbulent flows the computation time can be of the same order as for the conventional finite difference and the method (and the several variants thereof; including finite element which is a global as well as a local method of weighted residuals) has not been very popular.

In the method of characteristics a solution is obtained in the outer region of the boundary layer only and matched to a law of the wall. For this procedure the viscous terms in the boundary-layer equations must be neglected.

Systems of Independent Variables

The simplest set of independent variables to use would be the actual nondimensional physical quantities x, y (ref. 167). An advantage of this variable system, when compared with the more usual transformations, is the decreased labor involved when changes are made in the physical specification of the problem (i.e., one does not have to keep untransforming and retransforming for quantities or boundary conditions which are specified functions of physical variables). Therefore, these variables are particularly useful for inclusion of alternate turbulence models and to determine the influence of a specified variation of pressure in the transverse direction. However, this system of variables does not account for boundary-layer growth with longitudinal distance without periodic nodal point redistribution and is therefore seldom used in production codes which are expected to apply over changes in Reynolds number of several orders of magnitude.

One method of solving this boundary-layer growth problem is to use a normalizing factor on y which is a function of x , such as δ , δ^* , etc. This will keep the boundary layer within the computational grid, but longitudinal derivatives of the normalizing factors are required; if δ^* is used, this quantity can become negative for cold walls.

More generally, solutions are obtained using some variant of the Levy-Lees transformation (e.g., ref. 11)

$$\xi \propto \int \rho_e u_e dx \quad (31)$$

$$\eta \propto \frac{1}{\xi^{\bar{n}}} \int \rho dy \quad (32)$$

originally developed for laminar boundary layers. These variables reduce the boundary-layer growth and the influence of variable density in the computational domain. As a rule of thumb, $\bar{n} \approx 0.5$ for laminar flows and $\bar{n} \approx 0.8$ for turbulent flows. However, in general $\bar{n} = f(x)$ and the boundary layer may still grow out of (or into) the mesh (i.e., $\eta_e \neq \text{Constant}$ for turbulent flows without solving for $\bar{n}(x)$).

Another alternate set of independent variables involves the use of a stream function ψ as the normal or transverse coordinates (ref. 9). This approach automatically tracks the boundary-layer growth, but the boundary conditions must be specified or determined. One could also use the Crocco or velocity variables (ref. 168) where the normal coordinate is a function of u/u_e . This allows an accurate solution with a nearly constant $\Delta u/u_e$ step size, which corresponds to a highly nonuniform Δy ; that is, the number of necessary nodes is very effectively minimized. However, this variable set is not suitable for cases where $u/u_e > 1$ (as transformation involves $\sqrt{1 - (u/u_e)}$), and therefore, wall jet flows would be difficult to compute with the code.

Two examples are given here of the possible problems and inaccuracies which can be encountered in numerical solutions. Figure 24 (taken from ref. 169) indicates the error in C_f associated with a change in nodal point spacing. The usual assumption made in numerical analysis is that the solution becomes more accurate as the integration interval is reduced. However, as the figure shows, for single-precision IBM machines with approximately 7 decimal place accuracy, decreasing the step size can actually increase the discrepancy between a theoretical and numerical solution (as a result of roundoff error). When double-precision arithmetic is used (approximately 15 decimal place accuracy), the expected trend is obtained. The other example is given in figure 25 (from ref. 170). Here $\hat{K} = \Delta \eta_{n+1} / \Delta \eta_n$ and is the conventional means of including variable nodal spacing in a finite-difference procedure (e.g., ref. 53). These results from reference 170 show that, for $\hat{K} \neq 1.0$, there is some error involved in using variable grid spacing (at least as used in ref. 170) and that this error can become appreciable for $\hat{K} \approx 1.05$ (usual values of \hat{K} used in solution procedures are 1.02 to 1.04). These examples are only given to indicate that certain simple accuracy checks should be made on any numerical code before the numbers can be fully believed.

MEAN FIELD CLOSURE

This is probably the most widely used recent closure approach for computing compressible turbulent boundary layers. In this procedure the Reynolds stress ($\overline{\rho u'v'}$) is related directly to the mean velocity and density fields. This assumption is nearly exact for equilibrium and near equilibrium boundary layers where turbulence production is approximately equal to turbulence dissipation (e.g., pp. 275-299 of ref. 45). That is,

$$\overline{u'v'} \frac{\partial \bar{u}}{\partial y} \propto \frac{e^{3/2}}{l} \quad (33)$$

Using the Prandtl model (ref. 45, pp. 275-299)

$$\overline{u'v'} \propto \sqrt{e} l \frac{\partial \bar{u}}{\partial y} \quad (34)$$

Solving equation (34) for e and inserting this into equation (33), one obtains

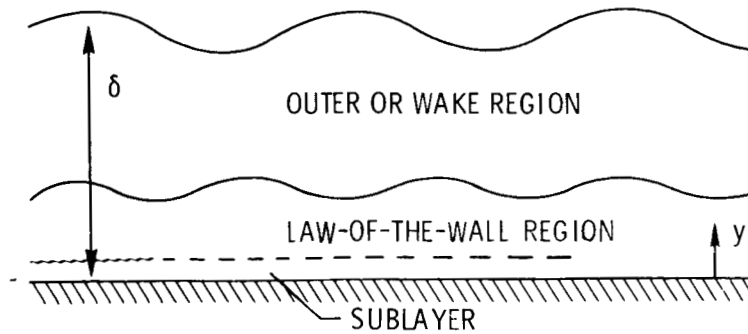
$$\overline{u'v'} \frac{\partial \bar{u}}{\partial y} \propto \frac{(\overline{u'v'})^3}{l^4 (\partial \bar{u} / \partial y)^3} \quad (35)$$

or

$$\overline{u'v'} \propto l^2 \left(\frac{\partial \bar{u}}{\partial y} \right)^2 \quad (36)$$

which is the usual mixing-length model; that is, $\overline{u'v'}$ is a function of mean velocity profile. The popularity of the mean field closure procedures is due to several reasons: (1) Many compressible turbulent-boundary-layer flows are either equilibrium or near equilibrium; (2) a wide range of boundary conditions can be easily and accurately incorporated ($p(x)$, $v_w(x)$, variable edge entropy, transition, roughness, etc.); (3) the higher order mean turbulence field models usually use a mean field model in the near-wall region (e.g., refs. 171 and 172); (4) less computer time and storage are required, compared with mean turbulence field methods; (5) except for highly nonequilibrium flows, mean field methods yield almost the same answers as mean turbulence field methods. (For example, see refs. 8, 24, and 173.)

Details of the mean field closure can be conveniently discussed using sketch (a) where the boundary layer is shown subdivided into the usual three regions. The sublayer is the region nearest the wall. The no-slip and usual impervious wall boundary conditions ("wall discipline") require a wall damping expression as a modifier to whatever turbulence model is used in the other two regions. In the law-of-the-wall or fully turbulent region of the boundary layer, the turbulent motions are scaled as a function of y and experience indicates that the mixing length model is almost universally valid. The outer or wake region can be strongly influenced by "history" or relaxation effects and here the turbulent motions are scaled as a function of δ .



Sketch (a)

Starting in the law-of-the-wall region, the most commonly used mean field closure model is the mixing length

$$-\overline{u'v'} = \iota^2 \left| \frac{\partial \bar{u}}{\partial y} \right| \frac{\partial \bar{u}}{\partial y} \quad (37)$$

For $\iota \propto y$ (law-of-the-wall region)

$$-\overline{u'v'} = K^2 y^2 \left| \frac{\partial \bar{u}}{\partial y} \right| \frac{\partial \bar{u}}{\partial y} \quad (38)$$

where K is the Prandtl or Von Kármán constant, which is approximately equal to 0.4.

In the outer, or wake region, there are two expressions commonly used, a mixing length expression

$$-\overline{u'v'} = \delta^2 \left(\frac{1}{\delta} \right)_{\max}^2 \left| \frac{\partial \bar{u}}{\partial y} \right| \frac{\partial \bar{u}}{\partial y} \quad (39)$$

and an eddy viscosity expression (ref. 1)

$$-\overline{u'v'} = \underbrace{\alpha u_e}_{\sigma} \delta_i^* \frac{\partial \bar{u}}{\partial y} \quad (40)$$

where, from computational experience (ref. 28), δ_i^* must be used instead of δ^* for the compressible case.

For the sublayer, or wall damping region, several expressions are available (e.g., refs. 34, 40, 174, and 175), but results in reference 169 indicate that, at least for some cases, most of these expressions yield very similar results. The most commonly used wall damping expression was developed by Van Driest (ref. 174) and is an exponential damping upon the mixing length $\iota(1 - e^{-y/A})$ where

$$\frac{Au_{\tau}}{\nu} = A^+ \quad (A^+ = 26 \text{ for } dp/dx \text{ and } v_w \approx 0) \quad (41)$$

Therefore, in the wall region the mixing length model becomes

$$-\overline{u'v'} = (Ky)^2(1 - e^{-y/A})^2 \left| \frac{\partial \bar{u}}{\partial y} \right| \frac{\partial \bar{u}}{\partial y} \quad (42)$$

In addition to modeling the Reynolds stress term in equation (2), solutions of the compressible turbulent boundary-layer problem also require a model for the Reynolds heating term (eq. (4)). This is generally handled through use of a turbulent conductivity expression

$$-\overline{v'h'} = \kappa_t \frac{\partial \bar{h}}{\partial y} \quad (43)$$

which then allows the definition of a turbulent Prandtl number

$$\kappa_t = \frac{\epsilon}{N_{Pr,t}} \quad (44)$$

Once $N_{Pr,t}$ is known, the model for $-\overline{u'v'}$ can be used in equation (44) to determine κ_t .

Therefore, in the usual mean field closure models, there are four closure "constants" which must be determined or specified before a solution can be obtained: A^+ for the wall damping region, K for the law-of-the-wall region, $(1/\delta)_{\max}$ or α for the wake or outer region, and $N_{Pr,t}$. These constants will now be examined in some detail, with particular emphasis upon their possible variation due to (1) compressibility, (2) low Reynolds number, (3) wall blowing, (4) pressure gradient, and (5) roughness.

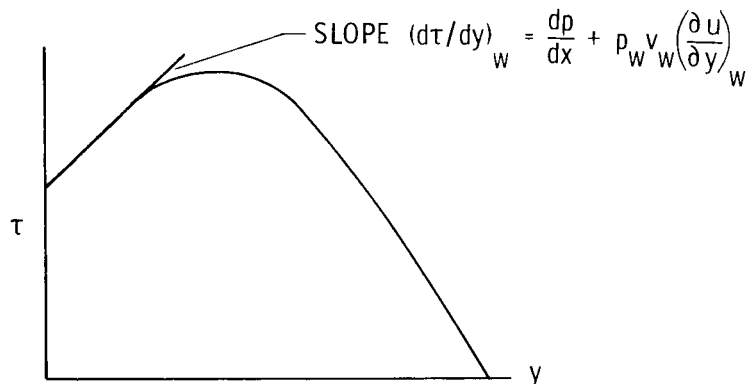
Wall Damping Constant

This is the most variable of the four "constants." Available data, although not definitive, show no discernible effect of Mach number upon A^+ (e.g., refs. 176 and 177). However, when A is computed from A^+ for compressible flow ($A = A^+v/\sqrt{\tau/\rho}$), v , τ , and ρ can be evaluated at several places (at the wall, locally as a function of y , and at the edge of the sublayer). Computational experience indicates evaluation at the wall is slightly better (refs. 53, 176, 177, and 178).

There is no discernible influence of low Reynolds number upon A^+ , or at least none has yet been identified (e.g., ref. 179). The influence of wall blowing upon A^+ , however, is quite large, and there exist several ways of accounting for this effect. One of the first procedures was a simple correlation plot of A^+ and the wall injection similarity parameter $2F/C_f$ (ref. 53). The data for this plot (fig. 26) were obtained from an examination of low-speed blowing data. By analogy to the $F = 0$ case, the A^+ -value was taken as the y^+ -location where the data were faired into a typical law-of-the-wall variation (i.e., the outer edge of the sublayer-buffer region). This variation (fig. 26) worked quite well (ref. 53), and most of the other models tend to give similar results (ref. 180). The changes in A^+ with wall mass transfer are quite large and some modification to A^+ must be included in order to obtain a reasonable C_f

prediction. Probably the most general method of adjusting A^+ for blowing is given by Launder (ref. 171), who suggests $A^+ = 26/(\tau/\tau_w)^{1.7}$ (i.e., since $\tau/\tau_w = f(y)$, $A^+ = f(y)$).

The variation of A^+ with pressure gradient is also quite large. Cebeci and Smith (ref. 12) give a correction procedure, as does Kays (ref. 181). (See also ref. 19.) Again, probably the simplest approach is to use the Launder expression $A^+ = 26/(\tau/\tau_w)^{1.7}$ which accounts quite well for the effects of both mass injection and pressure gradient. The basic problem with the variation of A^+ with blowing and pressure gradient is indicated in sketch (b). As shown in



Sketch (b)

the sketch, the wall damping occurs in a region where $\tau \neq \text{Constant}$, and the various approaches involve either letting $A^+ = f(\partial\tau/\partial y)$ (ref. 179) or using the local $\tau(y)$ to correct the A^+ or τ_w value; that is (from ref. 171, for example),

$$A^+ = \frac{26}{(\tau/\tau_w)^{1.7}} \quad (45)$$

Another parameter which has a large effect upon A^+ is roughness. McDonald and Fish (ref. 182) give a correction term for roughness as follows:

Wall damping with roughness = (Wall damping without roughness)

$$+ \left[1 + \frac{k^+}{30(y^+ + 1)} \right] \exp\left(\frac{-2.3y^+}{k^+}\right) \quad (46)$$

where

$$k^+ = \frac{ku_\tau}{v}$$

$$y^+ = y \frac{u_\tau}{v}$$

u_τ is based on $\tau(y)$ and k is the roughness height. It should be noted that this damping term (with roughness) could be greater than 1.

The influence of moderate acceleration (approaching laminarization, involving significant alteration of the sublayer) upon A^+ was investigated by Launder and Jones (ref. 183). They proposed the following expression:

$$A^+ = 11 + 7900L \quad (L > 0.0019) \quad (47)$$

where the pressure gradient parameter L is

$$L = C_f^{-2/3} \frac{v}{u_e^2} \frac{du_e}{dx}$$

This expression has not yet received detailed consideration for compressible flows.

Prandtl Wall Constant

From available data, there is no appreciable effect upon K of either compressibility (general computational experience, ref. 184), low Reynolds number (refs. 179, 185, and 186), wall blowing (refs. 184 and 185), or surface roughness (refs. 45 (pp. 396-398) and 187). There is, however, a moderate influence of pressure gradient upon K , as shown in figure 27 (taken from ref. 188). From the work of Lewis, Gran, and Kubota (ref. 139), the Clauser pressure gradient parameter β_K (and therefore fig. 27) is applicable to compressible flow if δ^* is taken as δ_i^* . Except for apparent pressure gradient effects (results similar to those in fig. 27 were also observed in ref. 30 (pp. 10-1 - 10-13) for supersonic flow), the wall slope K is the most constant of the mean field closure "constants."

Outer or Wake Constant

The present section discusses the behavior of $(1/\delta)_{\max}$ (eq. (39)) instead of α ; the behavior of α (eq. (40)) is quite similar, and in most instances the two expressions (eqs. (39) and (40)) give similar results. Figure 28 provides a typical comparison between the use of equations (39) and (40) for calculation of surface shear. For this low hypersonic case with moderate wall cooling, the mixing length is in slightly better agreement with the data. From the classic work of Maise and McDonald (ref. 79), there is no appreciable Mach number effect upon $(1/\delta)_{\max}$. There is, however, a large low Reynolds number effect. Recent research (ref. 189) has strongly indicated that this low-Reynolds-number effect is caused by the residue of the boundary-layer transition process.

One method of correlating the low-Reynolds-number effect is with a scaling parameter δ^+ , where

$$\delta^+ = \frac{\delta u_{\tau, \max}}{(v)_{\tau \max}} \quad (48)$$

In references 176, 186, and 189 this parameter successfully correlated the low Reynolds number effect over a wide Mach number range. For the low-speed case a parameter Re_θ is sometimes used (ref. 175) when $dp/dx = 0$. Working with this expression for δ^+ , one can show that $\delta^+ \propto \epsilon/\mu$ or a turbulence Reynolds number as follows:

$$\delta^+ = \frac{\delta \sqrt{\tau} \sqrt{\rho}}{\mu} \quad (49)$$

From the Townsend or Bradshaw assumption of the relationship between e and τ ,

$$\rho \overline{u'v'} \propto e \bar{\rho} \propto \tau \quad (50)$$

Therefore,

$$\delta^+ \propto \delta \frac{\bar{\rho} \sqrt{e}}{\mu} \quad (51)$$

From the Prandtl model for ϵ

$$\epsilon \propto \nu \rho \sqrt{e} \quad (52)$$

and identifying ν with δ one obtains

$$\delta^+ \propto \frac{\epsilon}{\mu} \quad (53)$$

The extent of the low-Reynolds-number amplification is indicated in figure 29(a) (from ref. 189) where $(1/\delta)_{\max}$ was derived from experimental velocity profiles for flat plates, cones, and cylinders. Increases of a factor of 2 or more in $(1/\delta)_{\max}$ above the usual levels (0.07 to 0.09) for values of δ^+ near 100 are observed. Since $\overline{u'v'} \approx (1/\delta)_{\max}^2$, this represents an increase of a factor of 4 or more in turbulent shear. The evidence that this increase is a function of distance downstream of transition is given by comparison of figure 29(a) with figure 29(b) (also from ref. 189) where $(1/\delta)_{\max}$ actually decreases with decreasing δ^+ for the nozzle wall case (where transition generally occurs far upstream in the settling chamber). The correlation for inclusion of low Reynolds number effects should therefore be a function of both δ^+ (or ϵ/μ) and $\Delta x/\delta$, the number of boundary-layer thicknesses downstream of the end of transition. (According to ref. 190, a value of $\Delta x/\delta$ of approximately 30 to 50 is needed to "wash out" the low Reynolds number effect.)

As Mach number increases, edge Reynolds numbers (such as $Re_{e,x}$, $Re_{e,\theta}$, etc.) become proportionally much larger than Reynolds numbers based on wall conditions (such as δ^+ , etc.). This is due to the large difference, at least for wind-tunnel conditions, between the wall and boundary-layer-edge temperatures. Therefore, as shown quantitatively in figure 30, a given value of δ^+ (which seems to correlate the transition-induced low Reynolds number effects) can correspond to a very large value of $Re_{e,x}$. This implies that the low Reynolds number amplification can effect a rather large portion of the boundary-layer flow on a hypersonic vehicle.

The outer or wake constant $(1/\delta)_{\max}$ is also influenced by wall blowing and pressure gradient. From the data shown in figure 31 (from ref. 53) the level of $(1/\delta)_{\max}$ decreases as the profile becomes less full and $d\delta/dx$ increases. Reference 186 contains an excellent explanation for this effect, which involves the problem of flow history effects. A detailed discussion of this problem is postponed until later when nonequilibrium flows are considered. As a final point, for the outer region model there seem to be only moderate increases of $(1/\delta)_{\max}$ with roughness (ref. 191).

Turbulent Prandtl Number

When dealing with $N_{Pr,t}$, there is a basic question of which term to model, $\overline{v'H'}$ or $\overline{v'h'}$. Since $H' = h' + \bar{u} u'$, then $\overline{v'H'} \approx \overline{v'h'} + \bar{u} \overline{u'v'}$ and therefore $N_{Pr,T} \equiv \epsilon/\kappa_T$ (where $\overline{v'H'} = \kappa_T(\partial\bar{H}/\partial y)$) cannot equal $N_{Pr,t} \equiv \epsilon/\kappa_t$ (where $\overline{v'h'} = \kappa_t(\partial\bar{h}/\partial y)$), except for $M \approx 0$. This question is discussed in some detail in references 53 and 192. The results of reference 177 clearly show that $N_{Pr,t}$ is much more invariant with Mach number than $N_{Pr,T}$. Typical $N_{Pr,t}$ distributions inferred from profile data are shown in figure 32 for low-speed and supersonic flow. Figure 32 shows data from references 181 and 193 to 196. An expanded scale is used, and the scatter, except near the wall, is typically ± 10 percent about a hypothetical mean line through the data. The scatter near the wall is probably caused by inaccurate mean profile data in that region. The data from reference 177 showing the problems with $N_{Pr,T}$ and $N_{Pr,t}$ are shown in figure 33. The $N_{Pr,t}$ data at $M = 7.2$ agree fairly well with the low-speed data in figure 32, indicating that there may not be a strong Mach number effect on $N_{Pr,t}$.

The evidence for a possible influence of low Reynolds number upon $N_{Pr,t}$ is primarily circumstantial, but indicates little or no influence (at least for air). Figure 34 summarizes some of the more accurate Reynolds analogy data (from refs. 197 to 201) for the low Reynolds number case. Since $N_{Pr,t}$ is a measure of the relationship between turbulent shear and turbulent heating, any large changes in $N_{Pr,t}$ might be expected to affect the Reynolds analogy factor. The available data do not seem to exhibit a strong trend with δ^+ , at least over the limited range for which data are available.

A second piece of circumstantial evidence as to the effect of low Reynolds number on $N_{Pr,t}$ is indicated in figure 35 (taken from ref. 12). The curves shown in this figure are the result of purely theoretical calculations based upon an assumed model of turbulence, but they do indicate only a very small effect of ϵ/μ upon $N_{Pr,t}$ for the $N_{Pr} \approx 0.7$ case. However, if the low Reynolds number effect comes from the persistence of transitional flow structures, this evidence is not really generic. In the absence of further data no firm conclusion can be drawn concerning the influence of low Reynolds number on $N_{Pr,t}$ except that no large effect has yet surfaced.

The variations of $N_{Pr,t}$ with y^+ (fig. 32) could also be interpreted as indicating a variation of $N_{Pr,t}$ with ϵ/μ , but this influence of low Reynolds number near the wall results in reduced shear (e.g., ref. 202) as opposed to the influence of low Reynolds number in transitional flow structures, which results in increased shear. Therefore, as stated previously, ϵ/μ (or δ^+ or y^+) is

not sufficient to adequately identify or correlate the various low Reynolds number influences. These low Reynolds number problems obviously require further definitive research, especially in regard to $N_{Pr,t}$.

The data from references 196, 203, and 204 indicate only a small influence of wall blowing on $N_{Pr,t}$. In reference 204, data with near equilibrium pressure gradients indicate that $N_{Pr,t}$ values do become somewhat lower in the law-of-the-wall region for the positive dp/dx case.

Intermittency Normal to the Wall

Another ingredient often used in mean field closure procedures is a normal intermittency factor Γ_y , which is generally defined as the percentage of time that the flow is turbulent. This factor accounts for the superlayer or intermittent nature of the outer region in turbulent boundary layers. For high Reynolds number calculations ($(\epsilon/\mu)_{max} > 100$ to 200) the inclusion of Γ_y is generally a second-order effect (refs. 45 (pp. 366-374), 53, and 205); however, Γ_y can become important for $(\epsilon/\mu)_{max} < 100$ (ref. 53).

Typical distributions of Γ_y are shown in figure 36 (from ref. 25) for the low-speed and hypersonic cases. These data indicate that a fully turbulent flow occurs much farther out in the boundary layer for the high Mach number case, and that, even for the simple $dp/dx \approx 0$ case, Γ_y is a function of M . In addition to this Mach number effect, the data of Fiedler and Head (ref. 206) show that Γ_y can be a strong function of pressure gradient. The influence of roughness on Γ_y is evidently fairly small (ref. 207).

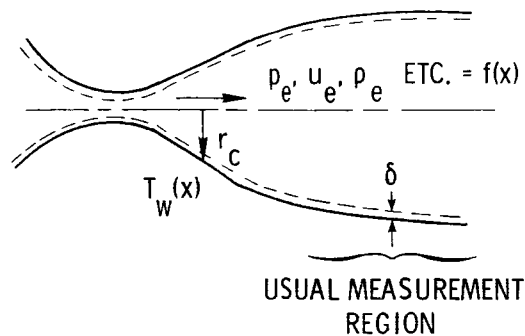
APPLICATIONS OF MEAN FIELD CLOSURE METHODS

Particularly during the last 8 years the literature has been rife with comparison between theory and data for mean field prediction methods. These comparisons indicate that mean field closure approaches yield predictions which are quite accurate over a wide range of conditions. (See especially refs. 12, 28, and 30.) In this section, comparisons of prediction and data for the more usual cases (such as $dp/dx = 0$, wall blowing, or equilibrium flows) will not be considered, but instead, the more unusual situations, such as a diagnosis of nozzle wall boundary layers and transitional flows, among others, will be treated.

The Case of the Nozzle Wall Turbulent Boundary Layer

Thick, fully developed turbulent boundary layers have been difficult to obtain on models at high Mach number as a result of (1) the increase in transition Reynolds number with Mach number (e.g., ref. 208), (2) the notorious difficulty in tripping high Mach number boundary layers, and (3) the general decrease in test section size of hypersonic facilities compared with the low-speed facilities. Therefore, a great deal of the hypersonic turbulent boundary-layer profile data were taken in nozzle wall boundary layers, which are readily available and usually of the order of 5 to 50 cm thick.

However, as can be readily seen with the help of sketch (c), there are several problems with these nozzle wall boundary-layer data. First of all, the measuring stations usually cover a small range of $\Delta x/\delta$ (data taken in test section region only with δ quite large). These data are therefore not very satisfactory as test cases for the mean field methods, as these procedures are of the parabolic type and the solution proceeds in the streamwise direction. The data are usually taken at a specified x -location for a range of unit Reynolds number, rather than over a respectable range of $\Delta x/\delta$ at a given unit Reynolds number.



Sketch (c)

The second problem involves so-called "history" effects. Although the flow may locally inhabit a region where $dT_w/dx = 0$ and $dp/dx = 0$, just a few boundary-layer thicknesses upstream the gradients in these quantities are often quite large and there is a question of how fast the wall boundary layer loses the "memory" of these gradients. Of course, it is possible to make measurements at several stations along the nozzle, starting with a measured profile near the high gradient (large dp/dx) region (such as in ref. 47). This produces a quite interesting but theoretically undemanding test case (boundary-layer recovery from a favorable pressure gradient).

An additional problem in the nozzle wall data is that of low Reynolds number similitude. This problem concerns the early transition (usually in the settling chamber) and subsequent early "loss of memory" of the transitional flow structures. This problem was covered previously in connection with figure 29 and indicates that the nozzle wall data for low values of δ^+ may be applicable only to a limited class of applied flows, such as where roughness induces early transition on the nose of a vehicle before the boundary layer undergoes the expansion to afterbody flow conditions.

Several investigators have studied these various nozzle wall problems (such as refs. 176 and 209 to 212). Figure 37 indicates typical total temperature and velocity relationships obtained on flat plates, cones, and cylinders (small dp/dx and $T_w(x)$ history), and figure 38 illustrates the nozzle wall case. These figures (taken from ref. 208) are now quite old (made up approximately 8 years ago); however, the differences between the flat plate and nozzle wall data (that is, the differences between a linear variation of T_t and u as opposed to a quadratic variation) have also been consistently observed in the more recent data. The development of the quadratic variation is clearly seen in figure 39 (taken from ref. 212).

In summary, the current status of the nozzle wall data indicates that for $M > 5$, an adiabatic wall, and large values of δ^+ (greater than 2000), the nozzle wall profile data in the test section region are fairly typical (in approximate agreement with the flat plate case). (See ref. 190.) For large values of δ^+ , $M > 5$, and a nonadiabatic wall, the velocity profiles are still fairly typical (ref. 190), but the T_t profiles are evidently out of equilibrium (ref. 209). For low values of δ^+ (without relaminarization downstream of the throat), the profiles are evidently correct only for practical cases where transition is far upstream.

Influence of Wall Blowing Upon Skin Friction

The conventional method of representing the influence of porous wall injection upon skin friction is with a similarity plot of $C_f/C_{f,0}$ against $2F/C_{f,0}$. An exhaustive review article by Jeromin (ref. 33) presents the available data in these coordinates. (See fig. 1 of ref. 33.) Jeromin's plot indicates a strong Mach number effect upon skin friction reduction due to blowing. Several predictors (refs. 213 to 215) have examined the question of a Mach number effect in these coordinates, two of these since the publication of Jeromin's review. Reeves (ref. 30 (pp. 6-1 - 6-A2-2)) calculated a weak Mach number effect, but his results indicated separate influences of Reynolds number and the ratio of wall temperature to total temperature, which could account for some of the apparent Mach number effects. Squire and Verma's (ref. 213) calculations (fig. 28 of ref. 213), in which a conventional mean field turbulence modeling procedure was employed, indicated very little influence of either Reynolds number, Mach number, or T_w/T_t , at least for $Re_{e,\theta} > 8000$ (the lower limit for their calculations). This result is similar to conclusions reached in the early work of Rubesin (ref. 215). Landis (ref. 214) attributed most of Jeromin's Mach number effect to the influence of T_w/T_t .

The data which indicate the strongest Mach number effect are those of Danberg (ref. 216). When the low Reynolds number effects are included in the analysis of Danberg's data (value of $C_{f,0}$ redefined), the final result for the available Mach number range (data and theory) is shown in figure 40 (from ref. 217). There is apparently very little Mach number effect, and the data are correctly predicted by the mean field closure methods. There is insufficient experimental data to determine any possible effect of the ratio of wall temperature to total temperature.

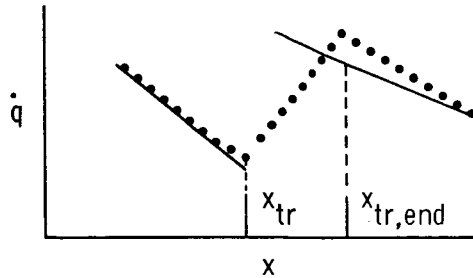
Transitional Flow Calculations

The now classical approach to calculation of the transitional flow region between laminar and turbulent flow is to multiply the usual $\overline{u'v'}$ model by a streamwise intermittency factor Γ_x to account for the increasing presence of turbulent bursts (e.g., refs. 142, 153, and 164). Using the definitions of x_{tr} and $x_{tr,end}$ indicated in sketch (d), the expression usually used for the intermittency factor is (from ref. 218)

$$\Gamma_x = 1 - e^{-0.412 \left(\frac{x - x_{tr}}{\Delta x} \right)^2}$$

where

$$\Delta x = \frac{x_{tr,end} - x_{tr}}{2.96} \quad (54)$$



Sketch (d)

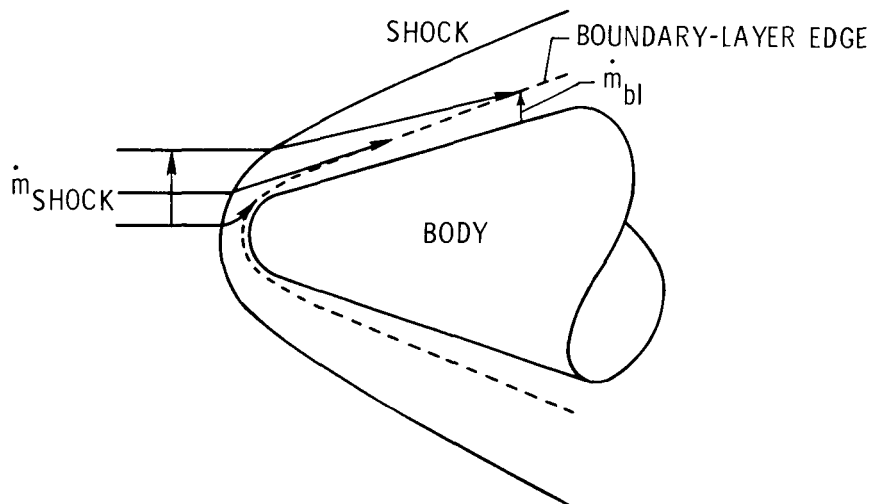
To apply this expression to a problem or a set of data, the x_{tr} and $x_{tr,end}$ values must be known. Typical values of the ratio $x_{tr,end}/x_{tr}$ (or the ratio $R_{tr,end}/R_{tr}$, which is the same thing for $dp/dx = 0$) are shown in figure 41 (from ref. 219). A nominal value of 2 for the ratio of $x_{tr,end}$ and x_{tr} is seen to be a reasonable approximation over a large Mach number range. (See also ref. 201.) Therefore, the problem is reduced to a specification of x_{tr} , a discussion of which is beyond the scope of the present report. (See, for example, ref. 220.) A comparison between equation (54) (which gives low-speed values of Γ_x) and hypersonic measurements of Γ_x is shown in figure 42 (from ref. 59). The high-speed data are in relatively good agreement with the curve from equation (54), indicating that the latter may be used with some confidence.

For accurate transitional flow calculation in compressible flow, the precursor effects (discussed previously) should be included. An example of the increased agreement obtained when these precursor and low Reynolds number effects are included is given in figure 43 (from ref. 58).

Additional "Nontypical" Applications of Mean Field Closure Methods

Variable edge entropy.- This problem is caused by the mass "swallowed" or entrained by the boundary layer along the afterbody of slightly blunted vehicles. (See sketch (e).) As the boundary layer swallows the high entropy streamlines, the edge properties possess a variable entropy condition. The actual edge conditions are determined by equating mass flow in the boundary layer at a given body station \dot{m}_{bl} to the mass flow in an entering stream tube \dot{m}_{shock} . This problem was treated in reference 221, using a mean field closure approach. Figure 44 (from ref. 221) indicates the better agreement resulting from consideration of variable entropy.

Transverse curvature influence.- Cebeci and Smith (ref. 12) have treated this case quite well, using a mean field approach. The problem arises when $\delta/r_c \approx 0(1)$, where r_c is the local body transverse radius of curvature.



Sketch (e)

According to reference 12, the outer region formulation is unchanged. The inner and wall damping regions are altered to

$$v = K \left(\frac{r}{r_c} \right)^{1/2} r_c \ln \left(\frac{r}{r_c} \right) \left[1 - e^{-\frac{r_c}{A} \ln \left(\frac{r}{r_c} \right)} \right] \quad (55)$$

Using this expression Cebeci and Smith obtained good agreement with data on a 0.061-cm-diameter needle at $M_\infty = 5.8$.

Longitudinal curvature influence.— The definitive review work in this area is a fairly recent report by Bradshaw (ref. 222). The usual effect is for convex curvature to reduce the Reynolds stress and entrainment and for concave curvature to increase the shear over the no-curvature level for the same pressure gradient. There are evidently four distinct effects of longitudinal curvature upon compressible turbulent boundary-layer physics and calculations. The first of these effects is the influence of additional longitudinal curvature terms in the mean flow equations. These extra terms were included in the calculation methods of references 167 and 223 and calculations in reference 224 using the code of reference 167; the results of these calculations indicate better agreement for a flow with mild concave curvature when these terms are included.

The second effect is unique to compressible flows, in that longitudinal curvature can induce a large pressure gradient in the boundary layer. This influences the flow even beyond the boundary layer and creates a nonuniform free stream (i.e., induces $u_e(y)$ for $y > \delta$). This occurs primarily as a result of the Prandtl-Meyer type of flow turning which is a typical feature of compressible flows. Therefore, the expression $\partial p / \partial y = 0$ is no longer true, and the correct $p(x, y)$ behavior must be included in boundary-layer prediction procedures; that is, one must have the correct value of p_{local} to compute a density, and $\partial p / \partial x$ is now a function of y . The codes of references 167 and 223 both include this capability.

The third effect of longitudinal curvature is the influence on the turbulent structure itself. Bradshaw (see ref. 222) has given a correction factor of the form

$$\frac{1}{\delta} = \left(\frac{1}{\delta}\right)_t \left(1 - B \frac{\bar{u}/r_c}{\partial \bar{u}/\partial y}\right) \quad (56)$$

where

$$B \approx 0(10)$$

This term is generally applied in an average sense to the outer region flow using the wall curvature for r_c and provides a first-order correction for moderate curvature (herein defined as convex radius of curvature large enough so that laminarization does not occur and concave radius of curvature large enough so that Goertler vortices are not important and separation does not occur).

The fourth effect of longitudinal curvature is illustrated by experimental data, which indicate that for $\delta/r_c > 0.005$ (which is not very large), concave curvature can generate steady, longitudinal Goertler vortices embedded in the outer portion of the turbulent boundary layer (ref. 225). The presence of Goertler vortices converts a readily solvable two-dimensional boundary-layer problem into a more complex three-dimensional turbulence problem of the parabolic-elliptic type (recirculation in the crossplane). Much more research is needed before quantitative predictions about the latter type of flow can be made.

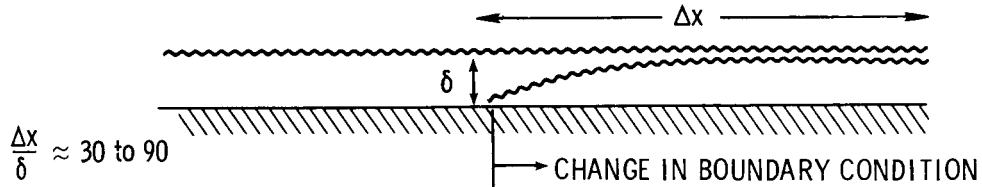
Calculations for adverse pressure gradient in compressible flow.- There is currently some controversy concerning the capacity of turbulent boundary-layer calculation methods to compute adverse pressure gradient flows for the compressible case. Bradshaw, in reference 226, partly on the basis of disagreements between his procedure and data, suggests that a mean dilatation correction is needed before satisfactory results can be obtained. Part of the problem in this area is due to the fact that the early (pre-1969) data for adverse pressure gradient compressible turbulent flows were taken on bodies where positive values of dp/dx were induced by longitudinal curvature, thereby introducing all the possible problems just discussed. However, Bradshaw (in ref. 226) considers the newer data, where the waves causing the adverse pressure gradient are impressed upon a flat surface.

One example of an adverse pressure gradient calculation (on a flat surface) is given in figure 45, and the external Mach number distribution for this flow is given in figure 46. The data are from reference 139 and the mean field calculation method is taken from reference 12. In this case the comparison is quite good. A check calculation made by the present authors using the method of reference 53 yielded similar agreement with the data. On the basis of these results, the question of whether Bradshaw's dilatation correction factor (ref. 226) is really required to compute adverse pressure gradient compressible flow is still open.

NONEQUILIBRIUM AND MEAN TURBULENT FIELD CLOSURE

Physical Problem

Primarily as a result of the large difference in scales between the inner (near wall) and outer portion of turbulent boundary layers, the inner portion (with scales of the order of y) reacts much faster to a change in boundary conditions than the outer region (with scales of the order of δ). This is shown schematically in sketch (f). The value of $\Delta x/\delta$ necessary for the outer region



Sketch (f)

flow to "relax" and equilibrate with the new boundary conditions is of the order of 30 to 90.

Therefore, as discussed earlier, for rapid changes in boundary conditions a rate equation is needed for the computation of $u'v'$ in the outer region (and perhaps for A^+ as well; see ref. 181). The turbulent field cannot instantaneously follow or track rapid changes in the mean flow. A nonequilibrium situation can be set up by the sudden removal or application of a pressure gradient, wall injection or suction, wall temperature gradient, or wall roughness. Larger changes, such as those caused by shock-wave impingement and large obstacles or steps, may cause the flow to violate the boundary-layer assumptions. In addition to the computation of nonequilibrium flows, $u'v'$ rate equations and mean turbulence field models are also necessary for including free-stream disturbance boundary conditions and for calculating the various turbulent second-order correlations.

There is a zeroth-order nonequilibrium modeling which involves a rate equation for the mixing length or outer region constant. This equation is usually of the form

$$\delta_i^* \frac{d\epsilon}{dx} = C(\epsilon_{\text{equilibrium}} - \epsilon) \quad (57)$$

Simple expressions or rate equations of this general form were used in references 30 (pp. 6-1 - 6-A2-2 and 29-1 - 29-10), 45 (pp. 375-383), 227, and 228 and do tend to give at least the correct qualitative behavior, the problem being that the decay constant can change with the particular flow involved; that is, the equation has the correct form but the absolute rate of return to equilibrium is uncertain. Therefore, the balance of this section is devoted to methods based upon rate equations derived from the Navier-Stokes equations (second-order correlations or Reynolds stress transport equations).

Second-order equation closure methods (or mean turbulence field methods) have been applied rather extensively to low-speed turbulent boundary layers.

(See refs. 21, 172, and 229 for reviews of this work.) However, their application to compressible flows has been rather limited, perhaps as a result of the following: (1) relative success of the mean field methods, (2) dearth of accurate data for nonequilibrium compressible turbulent boundary-layer flows (i.e., very few interesting test cases), (3) questions concerning possible importance of p' and ρ' terms in these equations, and (4) lack of sufficient data on the fluctuation field for the compressible case (for modeling purposes).

Equations and Modeling for Compressible Nonequilibrium Flows

The Reynolds stress transport equations (or $R_{i,j}$ equations) are generally obtained by (1) multiplying the Navier-Stokes equations for u_i by u_j , (2) multiplying the Navier-Stokes equations for u_j by u_i , (3) adding these two equations, (4) substituting for instantaneous values the usual mean plus fluctuation portions and Reynolds averaging, (5) subtracting out the kinetic energy equation for the mean flow, and (6) imposing the usual boundary-layer order of magnitude analysis. The result of all this is an equation for $\overline{u_i u_j}$. From this equation one can obtain (1) an equation for $\overline{u_j^2}$ ($i = j = 1, 2, 3$), (2) an equation for $\overline{u'v'}$ ($i = 1, j = 2$), and (3) an equation for $e = \overline{u'^2 + v'^2 + w'^2}$ (sum of equations for $\overline{u_j^2}$). The general form of these second-order equations is usually the following:

$$\text{Convection} = \text{Production} + \text{Diffusion} - \text{Dissipation}$$

Details of the derivation of these equations are available, for example, in references 36, 42, 148, 159, and 230 for the compressible turbulent kinetic energy equation and in references 43 and 156 for more complete sets of the second-order compressible equations. Reference 12 represents probably one of the best references for general discussion and derivation of the second-order equations for both low and high speeds.

From computational experience, the critical portion of the development of a good nonequilibrium turbulent boundary-layer calculation procedure is an accurate equation for the length scale of turbulence (refs. 36 and 45, pp. 275-299). The results of the calculations for nonequilibrium flows are usually not extremely sensitive to the details of the modeling used in the second-order correlation equation, but the length scale determination must be nearly correct for a good prediction.

There are three approaches usually used to derive a length scale equation: (1) form an equation for the turbulence dissipation D and relate this to L through the usual model for D ($D \approx e^{3/2}/L$) (ref. 8); (2) use an equation for the two-point correlations, which introduces a length scale quite naturally; and (3) use the turbulent vorticity equation and relate to L , for example, through the expression $L = e^{1/2}/\omega$ (refs. 231 and 232). An alternate approach to the length scale problem is to use an algebraic relationship (such as a function of y/δ , for example), which is assumed known (ref. 148). This latter method does not yield satisfactory results for truly nonequilibrium flows (if the length scale being solved for is the one used in modeling the Reynolds stress).

Single-Equation Models

Bradshaw approach.- This method (ref. 36) gives a second-order outer region solution based upon the conversion of the turbulent kinetic energy equation into an equation for $\overline{u'v'}$ by assuming that $a_1 = \tau/2\rho e = \text{Constant}$. The only length scale which appears is in the dissipation term; this is a very important aspect of the method, as Huffman (ref. 233) has shown that this length scale L (for dissipation) is much more invariant than the usual mixing length (which is used to model turbulence production), as can be seen by comparing figures 47 and 48 (from ref. 233). Bradshaw's a_1 is also relatively invariant, even for nonequilibrium flows, as indicated in figures 49 (from ref. 233) and 50 (from ref. 234). Bradshaw, by using a_1 , evidently sidesteps the problem of modeling the production term with a length scale and then having to derive and solve an equation for that scale. The length scale which Bradshaw uses (in the dissipation term) is evidently fairly invariant, and therefore, his one-equation method ($\overline{u'v'}$ equation plus algebraic length scale) should yield predictions which are as accurate as the more common two-equation models (e and ϵ equations).

Method of Shamroth and McDonald and method of Chan.- These procedures (refs. 159 and 155) use the integral form of the turbulent kinetic energy equation and Bradshaw modeling (a_1 and L). The procedures are, at least approximately, integral forms of the Bradshaw closure approach and seem to be fairly successful in predicting nonequilibrium flows. The method is inherently fast and relatively accurate and is a good choice for a simple nonequilibrium boundary-layer calculation procedure.

Two-Equation (and More) Models for Compressible Flows

Method of Wilcox and Alber.- This procedure (ref. 231) solves the turbulent kinetic energy equation and the fluctuating vorticity equation. Mass-weighted averages are used along with the Prandtl model for $\overline{u'v'} \approx e^{1/2} \epsilon (\partial u / \partial y)$.

Method of Spalding and Gibson.- This method (ref. 232) is quite similar to that of reference 231 in basic concept (e , ω equations used) but quite different in detail and application. Neither of these procedures has yet seen much application in highly nonequilibrium compressible flows.

Method of Donaldson and Sullivan.- This method (ref. 156) solves the complete set of second-order boundary-layer equations (u'^2 , v'^2 , w'^2 , $\overline{u'v'}$, $\overline{T'T'}$, $\overline{u'T'}$, and $\overline{v'T'}$) and therefore does not have to use a turbulent Prandtl number. However, most of the p' type terms were neglected. The latest version of this method (in publication) includes a length scale equation. The type of detailed information obtainable from this type of closure is shown in figures 51 and 52.

At the present time there are insufficient detailed data available to develop "calibrated" nonequilibrium (mean turbulence field) closure methods for compressible turbulent boundary layers.

CALCULATION OF THREE-DIMENSIONAL COMPRESSIBLE

TURBULENT BOUNDARY LAYERS

Status

A general method for solving three-dimensional compressible turbulent boundary-layer flows is not currently available; however, a limited number of problems have been solved using special techniques for each case. Blottner (ref. 235) presents a review of specialized and approximate solutions of the laminar three-dimensional boundary-layer equations. General three-dimensional boundary-layer computer codes require the following: (1) an efficient and accurate numerical procedure, including the required logic to automatically change the difference molecule as a function of local flow conditions, (2) a generalized curvilinear coordinate system convenient for the design engineer, (3) accurate turbulence models for the Reynolds stresses, and (4) a three-dimensional inviscid flow field solution which is compatible with the boundary-layer coordinate system.

A number of general numerical procedures and computer codes have been developed for two-dimensional and axisymmetric turbulent boundary-layer flows (e.g., see refs. 53, 142, 164, 202, and 236 to 242). This success was extended to a particular class of three-dimensional flows designated as quasi-two-dimensional (retains computational advantage of two independent variables while allowing large cross-flow components) by Hunt, Bushnell, and Beckwith (ref. 243). Numerical solutions for general three-dimensional flows did not materialize until after 1972 because of computer systems limitations (storage and processing speed) and the lack of accurate three-dimensional inviscid flow field solutions required for boundary-layer-edge input conditions.

Since 1972 an intensive research program on three-dimensional boundary-layer flows has been under way at a number of research centers. This effort is stimulated by increasing awareness of potential savings in cost and man-hours through numerical simulation of complex flows; often these flows cannot be simulated in ground test facilities (such as, for example, real-gas boundary-layer flow over the space shuttle). Substantial progress has been made as a result of the increasing availability of large-storage, high-speed computer systems and the maturing of accurate numerical procedures and computer codes for solving the three-dimensional inviscid equations for complex configurations. (See refs. 244 and 245.) Some of the more important areas of three-dimensional boundary-layer research are as follows: coordinate systems and transformations, numerical solution techniques, turbulence modeling, geometry, initial conditions, inviscid boundary conditions, inflow lines, regions of influence and dependence, and numerical optimization for perfect-gas flows as opposed to real-gas flows. These specific areas will be discussed in detail in subsequent sections of the present review.

The primary purpose of this section is to discuss in detail problems associated with development of three-dimensional compressible turbulent boundary-layer codes for application to complex aeronautical and aerospace vehicles and to indicate progress to date in achieving this goal. Comparisons of numerical results

with experimental data for several operational three-dimensional boundary-layer computer codes will also be presented.

Problems associated with obtaining accurate three-dimensional flow field results will not be discussed. In reality, the prediction of the inviscid flow field with the accuracy required presents a challenge as difficult as solving the three-dimensional compressible turbulent boundary-layer equations; however, the inviscid flow field input will be assumed available in the present review. (See, for example, ref. 246.)

Boundary-Layer Equations

An orthogonal curvilinear coordinate system is generally used to define the surface over which the boundary layer is flowing. The coordinate normal to the surface is x_3 with x_3 being zero on the surface. The lines $x_1 = \text{Constant}$ and $x_2 = \text{Constant}$ define the system of orthogonal coordinates on the surface. (See fig. 53.) The square of the element of arc (ds) in the boundary layer is

$$ds^2 = (h_1 dx_1)^2 + (h_2 dx_2)^2 + (h_3 dx_3)^2 \quad (58)$$

where h_1 , h_2 , and h_3 are metric coefficients (or scale factors):

$$h_1 = h_1(x_1, x_2) \quad h_2 = h_2(x_1, x_2) \quad (59)$$

The metric coefficient h_3 is generally assumed to be unity ($h_3 = 1$) since the boundary layer is assumed to be thin. The governing equations (first order) can then be written as follows, where h_3 is included for generality:

Continuity

$$\frac{\partial}{\partial x_1}(h_2 h_3 \rho u_1) + \frac{\partial}{\partial x_2}(h_1 h_3 \rho u_2) + \frac{\partial}{\partial x_3}(h_1 h_2 \overline{\rho u_3}) = 0 \quad (60)$$

x_1 -momentum

$$\begin{aligned} \frac{\rho u_1}{h_1} \frac{\partial u_1}{\partial x_1} + \frac{\rho u_2}{h_2} \frac{\partial u_1}{\partial x_2} + \frac{\overline{\rho u_3}}{h_3} \frac{\partial u_1}{\partial x_3} - \rho u_1 u_2 K_1 + \rho u_2^2 K_2 = & - \frac{1}{h_1} \frac{\partial p}{\partial x_1} \\ & + \frac{1}{h_3} \frac{\partial}{\partial x_3} \left(\frac{\mu}{h_3} \frac{\partial u_1}{\partial x_3} - \overline{\rho u_1' u_3'} \right) \end{aligned} \quad (61)$$

x_2 -momentum

$$\begin{aligned} \frac{\rho u_1}{h_1} \frac{\partial u_2}{\partial x_1} + \frac{\rho u_2}{h_2} \frac{\partial u_2}{\partial x_2} + \frac{\overline{\rho u_3}}{h_3} \frac{\partial u_2}{\partial x_3} - \rho u_1 u_2 K_2 + \rho u_1^2 K_1 = & - \frac{1}{h_2} \frac{\partial p}{\partial x_2} \\ & + \frac{1}{h_3} \frac{\partial}{\partial x_3} \left(\frac{\mu}{h_3} \frac{\partial u_2}{\partial x_3} - \overline{\rho u_2' u_3'} \right) \end{aligned} \quad (62)$$

Energy

$$\frac{\rho u_1}{h_1} \frac{\partial H}{\partial x_1} + \frac{\rho u_2}{h_2} \frac{\partial H}{\partial x_2} + \frac{\overline{\rho u_3}}{h_3} \frac{\partial H}{\partial x_3} = \frac{1}{h_3} \frac{\partial}{\partial x_3} \left[\frac{\mu}{N_{Pr} h_3} \frac{\partial H}{\partial x_3} + \mu \left(1 - \frac{1}{N_{Pr}} \right) \frac{1}{h_3} \frac{\partial}{\partial x_3} \left(\frac{u_1^2 + u_2^2}{2} \right) - \overline{\rho u_3' H'} \right] \quad (63)$$

where

$$\overline{\rho u_3} = \rho u_3 + \overline{\rho' u_3'}$$

The geodesic curvatures of the surface coordinate lines are

$$K_1 = - \frac{1}{h_1 h_2} \frac{\partial h_1}{\partial x_2} \quad (64)$$

$$K_2 = - \frac{1}{h_1 h_2} \frac{\partial h_2}{\partial x_1} \quad (65)$$

The governing equations are completed with the perfect-gas equation of state (see refs. 245 and 247 for real-gas flows)

$$p = \rho RT \quad (66)$$

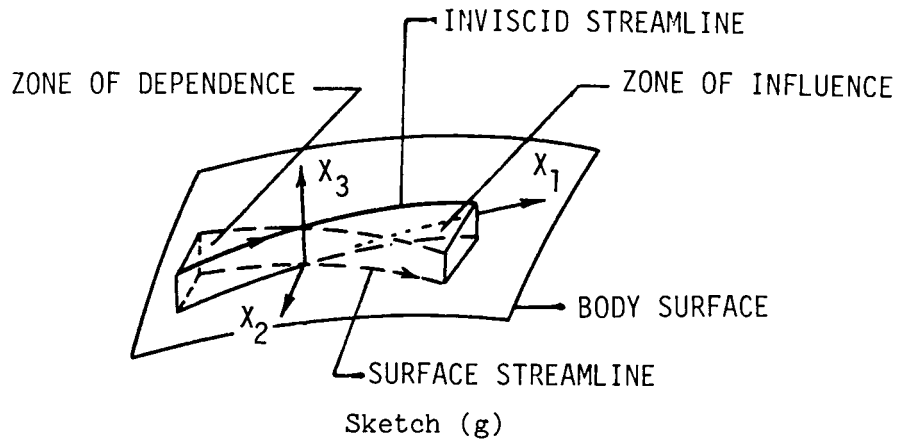
a viscosity law

$$\mu = f(T) \quad (67)$$

and suitable models or transport equations for the Reynolds stress terms appearing in the equations.

Obvious differences between the equations for three-dimensional (eqs. (60) to (67)) and two-dimensional (eqs. (1) to (4)) boundary-layer flows are the appearance of the cross-flow terms in the continuity and streamwise momentum equations and the addition of a second momentum equation for the cross-flow direction. However, the most important difference between two- and three-dimensional equations is that the three-dimensional equations are hyperbolic rather than parabolic in coordinate planes parallel to the wall boundary. The hyperbolic character of the three-dimensional equations has been recognized by a number of authors (see refs. 248 to 257) and arises naturally from the variation of the cross flow along the coordinate line normal to the wall boundary ($x_1 = \text{Constant}$, $x_2 = \text{Constant}$). Streamlines originating at different points along this normal line diverge in the downstream direction. These streamlines originate at different upstream locations; consequently, wedge-shaped regions of influence and dependence are associated with three-dimensional viscous flow and extend upstream and downstream from the computational point along the normal to the wall boundary. This characteristic of the three-dimensional boundary-layer equations is generally referred to in the literature as the influence

principle. (See ref. 248.) A schematic showing the regions of dependence and influence is presented in sketch (g). A more complete discussion is presented by Raetz (ref. 248), Kitchens, Gerber, and Sedney (refs. 254 and 257) and Wang (ref. 256).



The required boundary conditions for the governing equations (eqs. (61) to (63)) are as follows:

$$\left. \begin{aligned}
 x_3 = 0 \quad (\text{wall}) \\
 u_1 = 0 \\
 u_2 = 0 \\
 u_3 = u_w(x_1, x_2) \\
 T = T_w(x_1, x_2) \quad \text{or} \quad \left(\frac{\partial T}{\partial x_3} \right)_w = \dot{q}_w(x_1, x_2) \\
 \\
 x_3 \rightarrow \infty \quad (\text{edge}) \\
 u_1 = u_{1,e}(x_1, x_2) \\
 u_2 = u_{2,e}(x_1, x_2) \\
 T = T_e(x_1, x_2)
 \end{aligned} \right\} \quad (68)$$

The governing equations for the inviscid flow at the outer edge ($x_3 \rightarrow \infty$) are evaluated from equations (61) to (63) as follows, where the static temperature is utilized instead of the total enthalpy:

x_1 -momentum

$$\frac{u_{1,e}}{h_1} \frac{\partial u_{1,e}}{\partial x_1} + \frac{u_{2,e}}{h_2} \frac{\partial u_{1,e}}{\partial x_2} - u_{1,e} u_{2,e} K_2 + u_{2,e}^2 K_1 = - \frac{1}{\rho_e h_1} \frac{\partial p}{\partial x_1} \quad (69)$$

x_2 -momentum

$$\frac{u_{1,e}}{h_1} \frac{\partial u_{2,e}}{\partial x_2} + \frac{u_{2,e}}{h_2} \frac{\partial u_{2,e}}{\partial x_2} - u_{1,e} u_{2,e} K_1 + u_{1,e}^2 K_2 = - \frac{1}{\rho_e h_2} \frac{\partial p}{\partial x_2} \quad (70)$$

Energy

$$\rho_e c_p \left(\frac{u_{1,e}}{h_1} \frac{\partial T_e}{\partial x_1} + \frac{u_{3,e}}{h_2} \frac{\partial T_e}{\partial x_2} \right) = \frac{u_{1,e}}{h_1} \frac{\partial p}{\partial x_1} + \frac{u_{2,e}}{h_2} \frac{\partial p}{\partial x_2} \quad (71)$$

Variable entropy and vorticity can be treated by the system of equations; however, its proper treatment is very complex for three-dimensional flows. The reader is referred to Mayne (ref. 255) and Popinski and Davis (ref. 258) for blunt cone flows and to Kendall et al. (ref. 245) for general configurations. The proper treatment of variable entropy is of primary importance for some applications such as the space shuttle.

Two general approaches may be followed in evaluating the required edge conditions: (1) the pressure gradient terms required in equations (61) and (62) (dp/dx_i , $i = 1, 2$) can be obtained by direct solution of the Euler equation, or (2) the pressure $p(x_1, x_2)$ can be specified together with the appropriate boundary and initial conditions and $u_{i,e}$ and T_e obtained directly from the solution of equations (69) to (71). The optimum approach is to develop simultaneously an accurate three-dimensional inviscid computer code with a coordinate system compatible with that developed for the three-dimensional boundary-layer program; in any event, accurate and consistent edge conditions are required if accurate boundary-layer solutions are to be obtained.

The sufficient conditions required to start the boundary-layer solution have been presented by Ting (ref. 259). In principle the system of equations can be solved numerically by marching parabolically away (downstream) from specified initial data planes; however, the influence principle must be carefully treated.

Coordinate Systems and Transformations

Coordinate systems.— A number of papers have been published on the solution of three-dimensional boundary-layer flows; however, these papers have generally used specialized coordinate systems for each test problem. The coordinate system was generally chosen to simplify the governing equations for the particular flow of interest. The primary concern in the selection of a coordinate system is that it should allow the procedure to start from the initial conditions and proceed in a logical fashion over the entire surface without having to match together two or more distinct coordinate systems.

The majority of the references available have used streamline coordinates. (See ref. 260, for example.) The streamline coordinate system is an orthogonal surface coordinate system formed by the projection of the inviscid streamlines and their orthogonal trajectories on the surface. The system has a number of distinct advantages; however, its calculation is a major numerical effort in itself and must unfortunately be repeated for each change in flow conditions

(angle-of-attack changes, for example). Another disadvantage is encountered in the design of wings and control surfaces where displacement surface effects must be accurately treated (for example, supercritical wing design). The coordinate system has to be recalculated for each iterative cycle between the three-dimensional inviscid and boundary-layer programs. This represents a major undertaking and would be prohibitively expensive in terms of computer processing time. Streamline coordinates also tend to diverge greatly in highly three-dimensional flow, which results in large truncation errors unless additional streamlines are introduced in order to retain a reasonable mesh point spacing in the direction normal to the streamline coordinate. Consequently, it should be realized that while streamline coordinates are optimum for many simple flows (for example, three-dimensional stagnation point flows), they do not appear at the present to be optimum for general three-dimensional flows. It is then advantageous to seriously consider the development of a body-oriented surface coordinate system that would completely eliminate the requirement of coordinate system recalculation for each change in flow condition.

A body-oriented surface coordinate system could be made compatible with the inviscid three-dimensional computer program used to specify the required edge conditions. The only disadvantage of an orthogonal surface coordinate system is that the initial data lines cannot in general be made to coincide with the body coordinate lines even for simple geometry, such as a blunt nose cone at angle of attack. Blottner and Ellis (ref. 261) have presented an orthogonal surface coordinate system whose origin is at the stagnation point for analytic bodies at angle of attack. McGowan and Davis (ref. 262) have utilized an orthogonal surface coordinate system for sharp right circular and elliptical cones at angle of attack. However, these applications are for analytic bodies of revolution and not for general aerodynamic vehicles. The body-oriented coordinate system appears optimum from the viewpoints of geometry input and direct coupling with existing three-dimensional inviscid computer codes. The system completely avoids the time-consuming and difficult problem of streamline trajectory calculation for each change in flow conditions; consequently, inviscid-viscous coupling procedures can be greatly simplified for problems where displacement surface effects are important. The difficulties associated with developing efficient procedures for numerically generating the coordinates and required metric coefficients for an orthogonal body-oriented surface coordinate system are more than compensated by program flexibility from the viewpoint of the engineer who must use the computer program as a design tool.

The body-oriented surface coordinate system can be chosen to be either orthogonal or nonorthogonal. Regardless of whether the system is orthogonal or nonorthogonal, the x_3 -coordinate must be chosen normal to the wall boundary. Consequently, for the orthogonal system the selection of one coordinate x_1 or x_2 automatically fixes the remaining coordinate because of the orthogonality requirements. For example, if x_1 is chosen to lie along the rays of a sharp right circular cone, then the x_2 -coordinate for $x_1 = \text{Constant}$ cuts the cone in circular elements; however, for sharp elliptical cones a warped cross-section element is formed. (See fig. 2 of ref. 262.) The nonorthogonal coordinate system appears desirable from a number of viewpoints: (1) It can be made to coincide with the location of the initial data planes; (2) it can be generated as easily as the orthogonal system; and (3) the difference grid can be developed to completely cover the computational region of interest - for example, swept,

tapered wings. (See fig. 2 of ref. 244.) Further, the nonorthogonal system results in only a minimal increase in the number of correction terms arising from the metric tensor (see ref. 245) provided the cross-flow diffusion terms are not considered (in other words, if only the classical three-dimensional boundary-layer equations are used).

From the viewpoint of the design engineer it appears that a general computer code for solving the three-dimensional boundary-layer equations should be developed in nonorthogonal, body-oriented surface coordinates. This system would also allow complete flexibility and could utilize streamline coordinates if so desired for special flow cases. This viewpoint is currently being incorporated in the computer program under development by Cebeci et al. (ref. 244) for wing surfaces.

Transformations.- The selection of suitable transformations for three-dimensional laminar or turbulent boundary-layer flow presents a problem since no one transformation can be considered general. The selection of primitive variables introduces problems since the boundary layer is thin and grows at different rates in the x_1 - and x_2 -coordinates; furthermore, the equations are singular at the tip of sharp bodies. When physical coordinates are used, the solution is extremely sensitive to the surface mesh point distribution; consequently, procedures developed in physical coordinates generally require either excessively small grid spacing distributions for the x_1 - and x_2 -coordinates or special treatment of the spatial derivative terms in the finite-difference equations if accurate results are to be obtained. This results directly in excessive computer storage and/or processing time. Specific problems associated with physical coordinates are as follows: (1) excessive growth of the boundary layer in the computational domain requiring additional mesh points in the x_3 -coordinate as the solution proceeds downstream, (2) large gradients in the wall region for turbulent flows requiring either closely spaced mesh points in the normal direction or the inclusion of the law-of-the-wall relationship (not really satisfactory for three-dimensional flow), and (3) singularities such as at the tip or leading edge of sharp-edge bodies. The problem associated with the boundary-layer growth can be treated with suitable stretching and normalization as presented by Kendall et al. (ref. 245).

Transformation to similarity variables has been shown to be useful for computing similar flows (see ref. 263, for example); however, their usefulness is questioned by some authors (see, for example, ref. 245) for three-dimensional flows which are highly nonsimilar in character. The majority of the three-dimensional boundary-layer solution procedures now in existence use similarity type variables. (See ref. 245.)

As in two-dimensional boundary layers the physics of turbulent flow presents a numerical problem since wall gradients are large in comparison to laminar flow; the viscous sublayer generally requires a minimum of two to three mesh points. Generally a geometric-progression grid point spacing normal to the wall is employed; that is $\Delta x_{3,i+1} = \hat{K} \Delta x_{3,i}$, where $\hat{K} = 0(1.02)$. It has also been suggested that a logarithmic spacing be utilized as indicated by the law of the wall. The main object, regardless of the transformation or stretching selected for the normal coordinate, is to minimize the total number of mesh points normal to the wall boundary in order to minimize the required computer

storage and processing time. It should also be noted that the x_3 -transformation generally complicates the Reynolds stress models and their inclusion in the computer code; this is one advantage of using primitive variables with suitable thickness normalization. (See ref. 245.)

To date no general transformation has been developed for three-dimensional turbulent boundary-layer flows. Several transformations have been studied and are presented by Blottner (ref. 242). Some of these transformations will be discussed in a subsequent section where three particular computer programs will be presented, with numerical results compared with experimental data.

Turbulence Modeling

Research on turbulent transport equation models and turbulence structure (e.g., refs. 30 (pp. D-1 - D-14 and B-1 - B-24) and 264) is very important since the goal of this research is to develop one set of equations with one set of constants or functional values which will adequately model all turbulent flows; however, to date no transport equation procedure has been shown to be superior to simple eddy-viscosity models for two-dimensional, equilibrium, boundary-layer flows. (This is not the case for free shear, jet, and wake flows.) It is agreed by most investigators of turbulence modeling that eddy-viscosity models leave a great deal to be desired since the physics of the flow is in general neglected; however, from the design engineers viewpoint, the eddy-viscosity concept works well for a wide class of two-dimensional turbulent boundary-layer flows.

A number of rather difficult questions must be answered concerning the extension of the two-dimensional eddy-viscosity models to three-dimensional flow; for example, the cross-flow momentum equation requires the specification of an eddy-viscosity coefficient for the cross-flow direction. The simplest approximation is to assume that $\epsilon_{x2} = \epsilon_{x1}$ (isotropic eddy viscosity). This simple assumption implies that the turbulent stresses and mean flow rate of strain are always parallel. However, measurements of the complete turbulent stress tensor by Van den Berg et al. (ref. 265) indicate that the turbulent shear stress level in three-dimensional boundary-layer flow is lower than would be expected from extrapolation of two-dimensional theory; also, the local shear stress direction does not in general coincide with the direction of the velocity gradient. Experimental data indicate that the eddy viscosity should be lower in the cross-flow direction; that is, $\epsilon_{x2}/\epsilon_{x1} < 1$. One might assume that $\epsilon_{x2} = \alpha\epsilon_{x1}$ where $\alpha < 1$; however, this approximation is unsatisfactory (see ref. 266) unless some empirical functional relationship between ϵ_{x1} and ϵ_{x2} can be determined which allows accurate numerical prediction of a wide class of three-dimensional boundary-layer flows. This approach may become feasible as accurate three-dimensional experimental data are obtained. Two-dimensional eddy-viscosity models were developed to their current level primarily as a result of the availability of a wealth of experimental data; the same data base must be provided for three-dimensional flows for successful models to be developed.

In the present paper, closure through the solution of transport equations will not be discussed in further detail. The reader interested in this approach is referred to references 172 and 267 to 269 for examples.

Closure of equations (61) to (63) requires that an effective viscosity μ_{eff} and thermal conductivity κ_{eff} be expressed in terms of the mean flow variables. The Reynolds stress terms are defined as follows:

$$\left. \begin{aligned} -\rho \overline{u_1' u_3'} &= \epsilon_{x1} \frac{\partial u_1}{\partial x_3} \\ -\rho \overline{u_2' u_3'} &= \epsilon_{x2} \frac{\partial u_2}{\partial x_3} \\ -\rho \overline{u_3' H'} &= \epsilon_{\theta} \frac{\partial H}{\partial x_3} \end{aligned} \right\} \quad (72)$$

The further assumption is made that $\epsilon_{x1} = \epsilon_{x2} = \epsilon$ and a turbulent Prandtl number is defined which relates the effective conductivity and effective viscosity. The following relations can then be formulated:

$$\mu_{\text{eff}} = \mu \left(1 + \frac{\epsilon}{\mu} \Gamma \right) \quad (73)$$

and

$$\kappa_{\text{eff}} = \frac{c_p \mu}{N_{Pr}} \left(1 + \frac{\epsilon}{\mu} \frac{N_{Pr}}{N_{Pr,t}} \Gamma \right) \quad (74)$$

The streamwise intermittency function Γ_x (ref. 218) models the transitional region of flow and is a function of x_1 and x_2 ($0 \leq \Gamma_x \leq 1$; $\Gamma_x = 0$ for laminar flow; $\Gamma_x = 1$ for turbulent flow). The effect of pressure gradient on intermittency is presented in reference 270. For the present discussion it is assumed that the initiation and completion of the transitional flow region are specified; however, correlation relations could be directly incorporated into a computer code.

The simplest eddy-viscosity approach (see fig. 54) is to assume that the eddy viscosity is a scalar function independent of coordinate direction (refs. 168 and 243). The following models are considered since they are used in most current three-dimensional, compressible, turbulent, boundary-layer programs:

Single-layer model

$$\epsilon = \rho l_1^2 \left\{ \frac{1}{h_3^2} \left[\left(\frac{\partial u_1}{\partial x_3} \right)^2 + \left(\frac{\partial u_2}{\partial x_3} \right)^2 \right] \right\}^{1/2} \Gamma_y \quad (75)$$

where

$$\frac{l_1}{x_{3,e}} = k_2 \tanh \left(\frac{k_1}{k_2} \frac{x_3}{x_{3,e}} \right) D \quad (76)$$

$$D = 1 - \exp\left(-\frac{x_3}{A}\right) \quad (77)$$

$$A = A^+ \left(\frac{\mu}{\rho}\right)_w \left(\frac{\tau_t}{\rho}\right)_w^{-1/2} \quad (78)$$

$$\Gamma_y = \frac{1 - \operatorname{erf}\left(k_5 \frac{x_3}{x_{3,e}} - k_6\right)}{2} \quad (79)$$

$$\tau_t = \left(\tau_{x1}^2 + \tau_{x2}^2\right)^{1/2} \quad (80)$$

Two-layer model

Inner law

$$\epsilon_{\text{inner}} = \rho l_2^2 \left\{ \frac{1}{h_3^2} \left[\left(\frac{\partial u_1}{\partial x_3} \right)^2 + \left(\frac{\partial u_2}{\partial x_3} \right)^2 \right] \right\}^{1/2} \Gamma_y \quad (0 \leq x_3 \leq x_{3,c}) \quad (81)$$

Outer law

$$\epsilon_{\text{outer}} = k_4 \rho V_e \delta^* \Gamma_y \quad (x_{3,c} < x_3 \leq x_{3,e}) \quad (82)$$

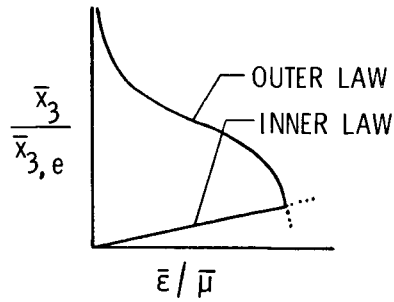
where

$$l_2 = \kappa x_3 D \quad (83)$$

$$V_e = \left(u_{1,e}^2 + u_{2,e}^2\right)^{1/2} \quad (84)$$

$$\delta^* = \int_0^{x_{3,e}} \left[1 - \frac{(u_1^2 + u_2^2)^{1/2}}{V_e} \right] dx_3 \quad (85)$$

The point where the inner and outer laws are matched $x_{3,c}$ is obtained from the continuity of eddy viscosity; that is, $\epsilon_{\text{inner}} = \epsilon_{\text{outer}}$. (See sketch (h).) No attempt is generally made to assure continuous derivatives for the two laws; however, the single law is continuous and appears to be as satisfactory as the more complex two-layer relationship (ref. 271). Three-layer models have been proposed by Pletcher (ref. 158), but there does not appear to be any advantage to the multilayer models above the single-layer mixing length model (eq. (75)) or the two-layer model (eqs. (81) and (82)). The normal intermittency factor



Sketch (h)

(eq. (79)) proposed by Klebanoff (ref. 272) is generally approximated by the following relationship:

$$\Gamma_y = \left[1 + 5.5 \left(\frac{x_3}{x_{3,e}} \right)^6 \right]^{-1} \quad (86)$$

For high Reynolds number flows the constants k_i appearing in equations (75) to (83) are generally assigned the following values: $k_1 = 0.4$ to 0.435 , $k_2 = 0.09$, $A^+ = 26$, $k_4 = 0.0168$, $k_5 = 5$, $k_6 = 0.78$, and $N_{Pr,t} = 0.95$. These values represent the classical values generally used for equilibrium, high Reynolds number, turbulent flows (see ref. 12); however, it should be noted that although the assigned values are sufficient over a broad range of flow and wall boundary conditions, modifications to these values are required for certain classes of flow as discussed in previous sections of the present review. Typical turbulent Prandtl number variations are given in references 273 to 275 and in figure 32.

The accuracy of the various eddy-viscosity models can only be assessed by careful numerical experimentation in which numerical results are compared with experimental data. These models have been compared over a wide range of test conditions for two-dimensional high Reynolds number, turbulent boundary-layer flows; however, their extension to general three-dimensional flows still requires extensive study. The models (eqs. (75), (81), and (82)) have been shown to accurately predict the data of Rainbird (ref. 276) for a sharp right circular cone (adiabatic wall) at angle of attack. (See refs. 271 and 277.) However, more demanding three-dimensional flows should be calculated and the numerical results compared with data. The previously mentioned problem with ϵ_{x2} must receive careful attention. It is not sufficient to simply assume ϵ_{x2} is some percentage of ϵ_{x1} ; this has been indicated in reference 265 for infinite swept-wing flow.

Numerical Solution Procedures

A number of research papers have been published over the past few years dealing with numerical procedures for solving the three-dimensional boundary-layer equations for laminar and turbulent compressible flow. Currently, there is no general method for solving the three-dimensional boundary-layer equations (ref. 235); however, significant progress has been made in the development of

such procedures by Kendall et al. (ref. 245), Cebeci et al. (ref. 244), and Wortman (ref. 162). A limited number of problems have been solved by applying special techniques to each specific problem (stagnation point flow, leading-edge attachment flow, swept infinite wings, and sharp and blunt cones). For these particular problems it has been possible to use simple geometrical relationships (coordinate system) and similarity type transformations to reduce the complexity of the governing equations. As previously mentioned, two of the more difficult numerical problems are (1) the generation of the surface coordinate systems and the required metric coefficients h_1 , h_2 , and h_3 and (2) the proper treatment of the inviscid edge conditions.

The properties of the three-dimensional boundary-layer equations were first studied in detail by Raetz (ref. 248). It was noted that the governing equations are hyperbolic in planes parallel to the wall boundary as opposed to parabolic for two-dimensional flow. Raetz introduced the concept of the influence principle into the three-dimensional boundary-layer literature which results directly from the hyperbolic character of the equations. The zones of influence and dependence for the three-dimensional boundary-layer equations have also been examined in detail by Wang (ref. 256). The hyperbolic character of the equations has been utilized by Bradshaw (ref. 278) through the application of the well-known method of characteristics, the wall region of the flow being patched to the characteristics solution for the outer region.

In order to obtain the correct solution to the three-dimensional equations, the solution procedure must correctly account for the zone of dependence. The stability of the procedure and the region where the solution can be obtained with specified initial conditions are determined by the zone of dependence. This zone thus prescribes the minimum amount of initial data that must be specified in order to advance the solution. Kitchens, Gerber, and Sedney (refs. 254 and 257) have made detailed studies of this requirement during which they systematically violated the zone of dependence requirement. Their results clearly demonstrate that errors accumulate and grow in the numerical solution if the zone of dependence is not satisfied. The most interesting result, presented in reference 254, is that satisfying the zone of dependence criteria is not sufficient to assure stability in all cases. The conclusion is drawn that the zone of dependence concept is not necessarily the same as the concept of stability. This particular result of reference 254 should be further studied since most investigators have treated these concepts as either the same or closely related.

For two-dimensional boundary-layer flows the zone of dependence is automatically satisfied, the equations are parabolic, and the procedure can march downstream, provided the necessary initial, boundary, and edge conditions are specified. For three-dimensional boundary-layer flows it is necessary to internally adjust the mesh aspect ratio (see ref. 254), such that

$$\frac{\Delta x_2}{\Delta x_1} \geq \max \left(\frac{|u_e|}{u_1} \right) \quad (87)$$

over all interior points

Then the largest allowable Δx_1 from one data plane to the next is

$$\Delta x_1 < \tilde{\alpha} \frac{\Delta x_2}{\max(|u_2|/u_1)_{\text{over entire data plane}}} \quad (88)$$

where $\tilde{\alpha} \leq 1$. The requirement that equations (87) and (88) be satisfied in the solution plane introduces numerical complexity for the three-dimensional boundary-layer equations.

The numerical procedures currently being applied to solve the three-dimensional boundary-layer equations have resulted, in general, from a direct extension of procedures developed during the 1960's for two-dimensional and axisymmetric boundary-layer flows. The present review is not intended to give a complete survey of the extension of these methods to three-dimensional boundary-layer flows. Reviews of three-dimensional laminar boundary layers have been presented by Cooke and Hall (ref. 279), Stewartson (ref. 280), Crabtree, Kùchemann, and Sowerby (ref. 281), Mager (ref. 282), and Hansen (ref. 283). A recent review of two- and three-dimensional flows has been presented by Blottner (ref. 235). Solutions of the three-dimensional boundary-layer equations have been considered by Fannelöp and Humphreys (ref. 253). The reader interested in the initiation of numerical research in three-dimensional boundary-layer flows should carefully review these references, as well as The European Research Programme on Viscous Flows (ref. 266) and the results of Euromech 60 (ref. 284). The purpose of the present section is to present three solution procedures which are representative of current programs for three-dimensional turbulent boundary-layer flows; two of these procedures are currently being developed as production codes for arbitrary configurations.

Crocco variables.- The primary advantage of a Crocco-type transformation is that the solution domain in the normal coordinate is bounded between the definite limits of $0 \leq \zeta \leq 1$. The procedure is also attractive in that the grid points can be uniformly placed in the velocity plane and still satisfy the demanding mesh point distribution for the wall region of turbulent flows. The only disadvantage of the method appears to be the restraint that velocity overshoot in the u_1 velocity component is not allowed; that is, $u_1/u_{1,e}$ must increase monotonically from the specified wall value (slip at surface can be allowed) to unity at the edge boundary. The transformation has been used for laminar flows (see refs. 255, 258, 262, and 285) and for turbulent flows over cones at angle of attack by Harris and Morris (ref. 168). A discussion of Crocco-type variables is presented by Davis (ref. 286).

A three-dimensional compressible turbulent code has been developed at Langley Research Center for Crocco-type variables (ref. 168). The program is currently restricted to analytic geometry; however, work is currently under way to extend the code to a general curvilinear coordinate system for arbitrary geometry.

In the subject program, equations (60) to (63) are first nondimensionalized, and a similarity-type transformation is introduced for the x_3 -coordinate and velocity as follows:

$$\bar{h}_3 = \tilde{\xi} \frac{\rho_e}{\rho} \frac{L}{\sqrt{R_{\infty,L}}} h_3 \quad (89)$$

$$\bar{u}_3 = \frac{1}{\xi \sqrt{R_{\infty, L}}} \frac{\rho_e}{\rho} u_{\infty} u_3 \quad (90)$$

where u_{∞} is the reference velocity and $\xi = \sqrt{x_1}$ for a sharp cone. The metric coefficients h_2 and h_3 are arbitrary functions of the coordinates. The equations are next cast into Crocco form as follows:

$$\zeta = \left(1 - \frac{u_1}{u_{1,e}}\right)^{1/2n} \quad (91)$$

The exponent n can be selected to minimize the number of nodal points in the ζ -direction (normal to the wall boundary). The continuity and x_1 -momentum equations are combined to form the shear equations, where the shear parameter Φ is defined by

$$\Phi = -\frac{1}{h_3} \frac{\mu}{T} \left(1 + \frac{\varepsilon}{\mu} \Gamma_x\right) \quad (92)$$

Consequently, $u_1/u_{1,e}$ is replaced by Φ as a new dependent variable, and $\tilde{H} = u_3/u_{1,e}$ is uncoupled from the system of equations. The system therefore reduces to three coupled nonlinear partial differential equations in Θ , G , and Φ , together with an explicit algebraic relationship for \tilde{H} . The system assumes the following form:

$$\frac{\partial^2 \omega}{\partial \zeta^2} + \alpha_1 \frac{\partial \omega}{\partial \zeta} + \alpha_2 \omega + \alpha_3 + \alpha_4 \frac{\partial \omega}{\partial \xi} + \alpha_5 \frac{\partial \omega}{\partial \eta} = 0 \quad (93)$$

where ω represents Θ , G , and Φ , and α_1 , α_2 , α_3 , α_4 , and α_5 are nonlinear coefficients.

The boundary conditions on equation (93) are as follows:

When $\zeta = 0$

$$G = 1 \quad \Theta = 1 \quad \Phi = 0 \quad (94)$$

When $\zeta = 1$

$$\left. \begin{aligned} \Theta = \Theta_w \quad \text{or} \quad \left(\frac{\partial \Theta}{\partial \zeta}\right)_w &= f(\xi, \eta) \\ G = 0 \\ \left(\frac{\partial \Phi}{\partial \zeta}\right)_w &= -\left(a_1 \tilde{H} + a_2 \frac{\bar{l} \Theta}{\Phi} + \Phi\right)_w \end{aligned} \right\} \quad (95)$$

where a_1 and a_2 are functions of geometry and the inviscid edge conditions and $\bar{l} = \mu/T$.

Equation (93) is solved in an iterative mode with a marching implicit finite-difference technique suggested by Dwyer (ref. 287) and modified by Krause

(ref. 288). The method is second-order accurate and unconditionally stable (conditional stability for reverse cross flow; see ref. 288). For turbulent flows a minimum of two mesh points in the ζ -plane must be located in the viscous sub-layer; consequently, careful consideration must be given to the placement of the mesh points in the ζ -coordinate in order to minimize computer storage and processing time requirements. Two approaches to the minimization problem have been considered: the specification of a variable mesh point distribution for $n = 1$ of the form $\Delta\zeta_{k+1}/\Delta\zeta_k = \text{Constant}$ for $k = 2, 3, \dots, N - 1$ (geometric progression), and the selection of $n = 3/4$ which appears optimum for turbulent flows. Variable mesh-point distributions are also used in the ξ - and η -planes to minimize the computer processing time and storage requirements. A schematic of the difference molecule is presented in figure 55(a). Equation (93) is written at the point $(i-1/2, j, k)$ and solved for the values of the dependent variables Θ , G , Φ , and H at the point (i, j, k) . The difference relationships used in the procedure for the Krause (ref. 288) "zig-zag" scheme are presented in reference 271.

When a converged solution cannot be obtained at the most leeward plane, $\phi = 180^\circ$ (for example, separation on leeward surface), a cubic Crank-Nicolson differencing scheme (see fig. 55(b)) is used at the maximum η -station (ref. 261). If this procedure were not incorporated into the program logic, one η -station would be lost for each additional $\Delta\xi$ step because of the Krause differencing scheme.

The marching procedure cannot be initiated without the existence of two orthogonal initial data planes. For a sharp right circular cone these planes of initial data are generated directly from the governing equations by using a second-order Crank-Nicolson scheme for the two planes ($\xi = 0$, $0 \leq \eta \leq \eta_{\max}$ and $0 \leq \xi \leq \xi_{\max}$, $\eta = 0$) where similarity exists. A discussion of problems associated with obtaining initial data planes for general configurations is presented in reference 260.

Substitution of the difference quotients (see ref. 271) into equation (93) results in a system of coupled algebraic equations whose coefficient matrix is of tridiagonal form which can be efficiently solved for the dependent variables (Thomas' algorithm). The primary problem associated with equation (93) is that the coefficients (α_1 , α_2 , etc.) are highly nonlinear. The shear equation controls the convergence rate of the numerical procedure (the number of iterations required as the system is sequentially iterated). Equation (93) can be written for Φ as

$$\frac{\partial^2 \Phi}{\partial \zeta^2} + \left(\frac{h_1}{\zeta} + \frac{\beta_1}{\Phi^2} \right) \frac{\partial \Phi}{\partial \zeta} - \frac{h_1}{\zeta^2} \Phi + \frac{\beta_2}{\Phi} + \frac{\beta_3}{\Phi^2} \frac{\partial \Phi}{\partial \xi} + \frac{\beta_4}{\Phi^2} \frac{\partial \Phi}{\partial \eta} = 0 \quad (96)$$

where the coefficients β_1 , β_2 , β_3 , and β_4 are functions of geometry, inviscid edge conditions, and previous iterate values of the dependent variables $u_1/u_{1,e}$ and Θ and their derivatives. The problem is further complicated by the inclusion of the turbulence models (eqs. (75) to (85)) since in the transformed plane Φ appears explicitly in the transformed relationships. Consequently, the coefficients (β_1 , β_2 , etc.) also depend on Φ for turbulent flows (for laminar flows this dependence is removed). The system of equations will not converge if the shear equation is written as shown in equation (96) because

of the Φ^{-1} term. Convergence can be achieved by using a Taylor's series expansion of Φ^{-1} about the previous iterate value Φ_G ; that is,

$$\frac{1}{\Phi} = \frac{1}{\Phi_G} \left(2 - \frac{\Phi}{\Phi_G} \right) + O(\Phi^2) \quad (97)$$

Substitution of equation (97) into equation (96) yields

$$\frac{\partial^2 \Phi}{\partial \zeta^2} + \left(\frac{h_1}{\zeta} + \frac{\beta_1}{\Phi^2} \right) \frac{\partial \Phi}{\partial \zeta} + \left(-\frac{h_1}{\zeta^2} - \frac{\beta_2}{\Phi_G^2} \right) \Phi + \frac{2\beta_2}{\Phi_G} + \frac{\beta_3}{\Phi^2} \frac{\partial \Phi}{\partial \zeta} + \frac{\beta_4}{\Phi^2} \frac{\partial \Phi}{\partial \eta} = 0 \quad (98)$$

Equation (98) converges in an average of five to seven iterations for high Reynolds number turbulent flow. The wall boundary condition on Φ (see eq. (95)) also presents a problem since Φ_w is unknown; however, the wall derivative relationship can be directly incorporated in the iterative solution procedure. In principle, it should be possible to reduce the average number of iterations substantially to a maximum of three. Research continues in the areas of (1) restructuring equation (98), (2) treatment of the Φ_w wall boundary conditions, and (3) the problems associated with Φ in the transformed turbulence models. Note however that the procedure requires essentially the same processing time per mesh point (0.002 sec) as the Cebeci-Keller box method (refs. 289 to 291) and that this time may be substantially reduced through convergence accelerator procedures and/or the inclusion of Newton-Raphson iteration.

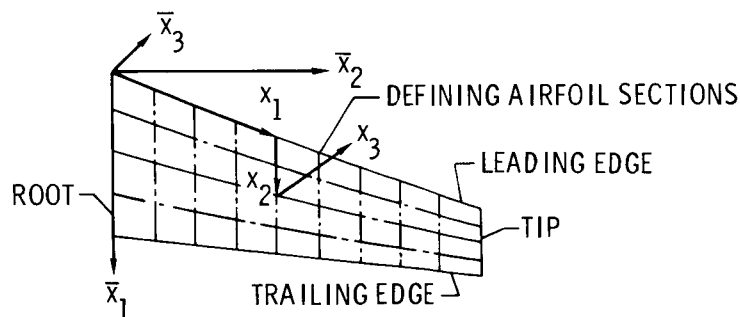
The numerical procedure and turbulence models have been applied to a number of flows (current geometry limited to sharp right circular and elliptic cones). Numerical results compared with experimental wall and profile data for a cone (ref. 276) with a 12.5° semiapex angle at an angle of attack of 15.75° are shown in figure 56. The free-stream Mach number, total pressure, and total temperature for the experiments were 1.8, 172.4 kN/m^2 , and 294 K, respectively. Transition was assumed to be initiated and completed in the region $0.03 \leq \bar{x}_1/\bar{L} \leq 0.08$ ($\bar{L} = 105.6 \text{ cm}$). The adiabatic wall boundary condition was imposed on the energy equation (see eq. (95)); that is, $(\partial \Theta / \partial \zeta)_w = 0$. No experimental data were input into the viscous flow solution. The inviscid pressure distribution $p_e = f(\xi, \eta)$ was obtained from a numerical solution of the three-dimensional inviscid flow equations.

The numerical results for $u_1/u_{1,e}$, G , and Θ are compared with experimental data in figure 56 for circumferential locations of ϕ , 0° and 135° . In order to evaluate the effect of nodal-point spacing in the ζ -plane, a parametric study was made for $N = 301, 201, 101, 61,$ and 21 with $\Delta \zeta_{k+1} / \Delta \zeta_k = 1.02$. The results for $N = 301$ and 201 were essentially identical, and those for $N = 101$ were within 0.5 percent of the $N = 301$ results. The agreement between the experimental and numerical results is very good for 301 points and, in general, good for as few as 21 points. The two turbulence models (eqs. (75) to (85)) produced essentially identical results. The two-layer model results presented in figure 56 are for $N = 301$; however, the two-layer results for $N = 21$ were essentially identical to the $N = 21$ results of the single-layer model.

The results for $\Delta \zeta_{k+1} / \Delta \zeta_k = 1.02$ presented in figure 56 were obtained for $n = 1$. (See eq. (91).) Numerical results for $\Delta \zeta_{k+1} / \Delta \zeta_k = 1$ (equal mesh distribution), $N = 21$, and $n = 3/4$ were in slightly better agreement with the

$N = 301$ results for the variable mesh point distribution; however, the difference between the two cases for $N = 21$ was minor. The major points that should be noted in these comparisons are that the numerical procedure is efficient and accurate and that the turbulence models are satisfactory for high Reynolds number equilibrium turbulent boundary-layer flows. The Crocco-type transformation and the numerical procedure allow the generation of accurate solutions for a minimum of 21 points normal to the wall boundary. The computer code requires 60000g storage (the $i-1, j, k$ data plane is stored on disk) and approximately 0.002 second per grid point processing time on a CDC-6600 computer system. Current studies indicate that it may be possible to substantially reduce the processing time through convergence accelerators for the shear equation (eq. (98)) and/or the inclusion of a Newton-Raphson iteration procedure. The current program is comparable in both storage and processing time with the Cebeci-Keller box method (ref. 260).

Arbitrary wings.— An accurate and efficient computer code for the three-dimensional boundary-layer flow over wings is required for the design and evaluation of supercritical wings and laminar flow control surfaces ($u_{3,w} = g(x_1, x_2)$). Studies of wing geometry specifications have indicated that a nonorthogonal surface coordinate system is optimum from the viewpoint of the design engineer. Cebeci et al. (ref. 260) have developed an efficient and accurate procedure for solving the three-dimensional boundary-layer equations for laminar, transitional, and turbulent perfect-gas flow over general wings. The advantage of this geometry routine are as follows: (1) Calculation of the coordinate system (ξ, η, h_1, \dots) for each angle-of-attack or flow condition change is eliminated; (2) discontinuities associated with patched coordinate systems are eliminated; (3) the method is optimum from the viewpoint of the design engineer. (See sketch (i).) Only one disadvantage is encountered in that the nonorthogonal metric tensor results in additional terms appearing in the system of equations. However, this increase in terms is minimal if cross-flow diffusion terms are neglected. Preliminary results obtained in reference 260 for a typical supercritical wing indicate computation times of approximately 30 sec on an IBM 370/165 computer system for a $30 \times 20 \times 20$ grid.



Sketch (i)

The governing equations are written for a nonorthogonal surface coordinate system for ease of placement of the mesh distribution over the wing surface. The wing is defined in an orthogonal $\bar{x}_1, \bar{x}_2, \bar{x}_3$ coordinate system where \bar{x}_1 is in the direction of the airplane's longitudinal axis, \bar{x}_2 is in the spanwise direction, and \bar{x}_3 is orthogonal to the plane of \bar{x}_1 and \bar{x}_2 . The wing is described

by a series of airfoil sections in planes of $\bar{x}_2 = \text{Constant}$. The equations relating the airfoil section specification and the \bar{x}_1 -coordinate system are presented in reference 260 in terms of percentage chord. The equations required for the calculation of the nonorthogonal surface mesh and the procedure with which they are solved are also presented in reference 260.

The x_1 -momentum equation is as follows (see eq. (61) for orthogonal system):

$$\frac{\rho u_1}{h_1} \frac{\partial u_1}{\partial x_1} + \frac{\rho u_2}{h_2} \frac{\partial u_1}{\partial x_2} + \overline{\rho u_3} \frac{\partial u_1}{\partial x_3} - \rho K_1 u_1^2 \text{ctn } \theta + \rho K_2 u_2^2 \text{csc } \theta + \rho K_{12} u_1 u_2$$

$$= - \frac{\text{csc}^2 \theta}{h_1} \frac{\partial p}{\partial x_1} + \frac{\text{ctn } \theta \text{csc } \theta}{h_2} \frac{\partial p}{\partial x_2} + \frac{\partial}{\partial x_3} \left(\mu \frac{\partial u_1}{\partial x_3} - \overline{\rho u_1 u_3} \right) \quad (99)$$

where θ represents the angle between the coordinate lines $x_1 = \text{Constant}$ and $x_2 = \text{Constant}$. For an orthogonal coordinate system, $\theta = \pi/2$ and equation (99) reduces identically to equation (61) for $h_3 = 1$. The geodesic curvatures are given by the relationships

$$K_1 = \frac{1}{h_1 h_2 \sin \theta} \left[\frac{\partial}{\partial x_1} (h_2 \cos \theta) - \frac{\partial h_1}{\partial x_2} \right] \quad (100)$$

$$K_2 = \frac{1}{h_1 h_2 \sin \theta} \left[\frac{\partial}{\partial x_2} (h_1 \cos \theta) - \frac{\partial h_2}{\partial x_1} \right] \quad (101)$$

The parameter K_{12} is defined as follows:

$$K_{12} = \frac{1}{\sin \theta} \left[- \left(K_1 + \frac{1}{h_1} \frac{\partial \theta}{\partial x_1} \right) + \cos \theta \left(K_2 + \frac{1}{h_2} \frac{\partial \theta}{\partial x_2} \right) \right] \quad (102)$$

It should be noted that the addition of correction terms for nonorthogonal coordinates to the system of equations is minor for the classical three-dimensional boundary-layer equations; however, if one wants to include the cross-flow diffusion terms in the x_2 -momentum equation, then a significant number of additional correction terms would be required. (See ref. 12.)

The system of governing equations is transformed through the introduction of a two-component vector potential and a similarity-type transformation. (See ref. 260.) The Cebeci-Keller box method (refs. 162, 289, and 290) is used to solve the resulting system of equations. One of the basic concepts of the box procedure is to rewrite the system of equations as a first-order system of partial-differential equations. Consequently, derivatives of some quantities with respect to the x_3 -coordinate must be introduced as new unknown variables. Derivatives with respect to all other variables occur only to the first order because of the boundary-layer approximations. Centered difference quotients and averages at the midpoints of net rectangular and net segments are used in order to produce second-order-accurate finite-difference equations. The method is unconditionally stable for positive cross flow but appears to be unconditionally unstable for negative cross flow. The equations are highly nonlinear and implicit in structure. Newton's method is used to solve the system; a block-tridiagonal factorization scheme is used which is efficient and stable. The

numerical formulation of the system of equations is presented in detail in reference 28. Numerical results are compared with the data of East and Hoxby (ref. 291) in figure 57 for several x_1/L stations. Numerical results for a supercritical wing calculation are presented in figure 58.

Reacting gas flows.- The Aerotherm Division of the Acurex Corporation is currently developing a laminar, transitional, and turbulent three-dimensional boundary-layer computer code for application to arbitrary configurations such as the space shuttle. (See ref. 245.) The numerical procedure is an extension of the method presented in reference 238. This particular code includes equilibrium and/or frozen flow chemistry. A body-oriented orthogonal surface coordinate system is used to describe the vehicle surface. The computer code is compatible with the accurate three-dimensional supersonic inviscid flow field program developed by Marconi, Yaeger, and Hamilton (ref. 246). Three-dimensional entropy-layer effects are included in the solutions. This is of particular importance for vehicles such as the space shuttle.

The governing equations are numerically solved in primitive variables with suitable stretching and normalization in the x_3 -coordinate. Similarity transformations are not used since the program will in general be applied to highly nonsimilar flows. The governing equations, in nondimensional form, are presented in reference 245. The solution domain is covered by a mesh point network shown in figure 59. The initial data planes are assumed known at $x = x_i$; the solution is to be obtained at $x_{i+1} = x_i + \Delta x_i$. The functional form of the derivatives is specified and substituted into the governing equations together with the required boundary conditions. This procedure results in a system of algebraic relations between the unknown dependent variables at the nodal point in the plane located at x_{i+1} . Normal to the wall boundary, the dependent variables are represented by a splined Taylor series between each mesh point as follows (where the prime denotes differentiation with respect to x_3):

$$\left. \begin{aligned} u_{j+1} &= u_j + u_j' \Delta x_3 + u_j'' \frac{\Delta x_3^2}{2} \\ u_{j+1}' &= u_j' + u_j'' \Delta x_3 \end{aligned} \right\} \quad (103)$$

Where j represents the grid index ($j = 1, 2, \dots, JMAX$). The equations are integrated with respect to x_3 between each mesh point. This insures that the conservation laws are satisfied exactly between the mesh points and greatly simplifies the calculation of the diffusion terms since all second derivatives are eliminated.

In the cross-flow direction (x_2 -coordinate) second-order-accurate centered difference quotients are used to replace the cross-flow derivatives; that is, for equal nodal spacing

$$\left(\frac{\partial u}{\partial x_2} \right)_{i,j,k} = \frac{u_{i,j,k+1} - u_{i,j,k-1}}{\Delta x_{2,k+1}} \quad (104)$$

where k is the index for the x_2 mesh point distribution. Axial derivatives are approximated by the backward difference quotients of the form

$$\left(\frac{\partial u}{\partial x_1}\right)_{i,j,k} = \frac{u_{i+1,j,k} - u_{i,j,k}}{\Delta x_{1,i}} \quad (105)$$

where i is the index associated with the mesh point distribution in the x_1 -coordinate.

A fully implicit solution is obtained in the procedure. Equations (103) and (104) are evaluated in the $x_{1,i+1}$ -plane; introduction of the boundary conditions results in a nonlinear system of algebraic equations for the primary variables (u , ρ , etc.) and secondary variables (u' , ρ' , etc.) at each nodal point in the $x_{1,i+1}$ -plane. The resulting system of algebraic equations is solved by the Newton-Raphson procedure. The solution reduces to the problem of inverting a large matrix and thereby solving the linear system of algebraic equations for the unknowns. The large matrix is treated as a system of submatrices. The matrix is block tridiagonal in structure since cross-flow derivatives are represented by centered difference quotients. The submatrices along the main diagonal are dense, whereas the off-diagonal submatrices are sparse. A schematic of a typical diagonal submatrix for one x_1 -plane is presented in figure 4 of reference 245.

Data required for the initial planes are obtained directly in the solution procedures at stagnation points and leading-edge attachment lines. Similarity variables are used for the generation of these solutions. The entropy layer effects and the procedure through which they are included in the numerical procedure are discussed in detail by Kendall et al. (ref. 245). The eddy-viscosity model currently used is the single-layer model (see eq. (75)), where the Lewis and Prandtl numbers are assumed constant. More general models will be incorporated into the code once it is completely operational and detailed studies have been made of comparisons of numerical results with experimental data.

A comparison of numerical results with experimental data (ref. 292) for flow over a sharp cone at angle of attack is presented in figure 60. Solutions for the flow over a space shuttle are currently being obtained.

Status of Three-Dimensional Boundary-Layer Computational Techniques

Significant progress has been made in the development of numerical techniques for solving the compressible three-dimensional turbulent boundary-layer equations (see appendix, table A2); however, more efficient and reliable methods must be developed for application to general aerospace vehicles. This becomes clearly apparent when one considers the prohibitive computer processing times which can occur for either complex reacting gas flows or turbulent flows over large-scale aerospace vehicles (ref. 260). Early numerical research in the area of compressible, three-dimensional boundary-layer flows was primarily directed towards developing second-order-accurate, stable numerical schemes for solving the laminar equations for flows where simplifying assumptions were possible. Current research is directed towards (1) improving these numerical procedures for application to complex flows, (2) developing more general coordinate systems, and (3) detailed studies of turbulence modeling procedures for three-dimensional turbulent-boundary-layer flows. Reynolds stress models require accurate experimental data where the stress components are measured. The wealth of

two-dimensional experimental data which made possible the successful development of two-dimensional eddy-viscosity models may provide little reliable guidance for complex three-dimensional boundary-layer flows.

The problems associated with solving the three-dimensional inviscid equations for complex vehicles are rapidly being solved; however, efficient and reliable procedures for automatically coupling the inviscid and boundary-layer codes must be developed in order to avoid time-consuming and difficult data manipulation. Compatible coordinate systems must be developed for the inviscid and viscous codes in order to reduce or completely eliminate the inherent errors associated with data interpolation and smoothing between coordinate systems. Current studies and experience indicate that a nonorthogonal curvilinear coordinate system is optimum for general three-dimensional boundary-layer flows.

Flexibility must also be programed into the boundary-layer codes which will assure that the optimum difference scheme is utilized at various locations in the solution domain in order to automatically satisfy the zone of dependence requirements as well as to maximize the region over which the solution may be obtained. Care must be exercised in order to determine whether the classical three-dimensional boundary-layer equations are valid in a specific area where the solution is required; that is, boundary region flow, inflow regions, and regions of separated flow require special treatment. For these cases either the parabolized Navier-Stokes or the full Navier-Stokes equations must be solved.

A number of difficult problems remain to be solved before compressible, three-dimensional, turbulent, boundary-layer codes are developed to the current confidence level of existing two-dimensional codes. An optimistic review of current research programs, together with the increasing capabilities of digital computer systems and the maturing of three-dimensional inviscid flow field codes, indicates that general purpose, three-dimensional boundary-layer codes for compressible turbulent flows will become available in the near future.

RÉSUMÉ

Compressibility Influence on Turbulent Boundary-Layer Shear Stress

From comparisons of high-speed data with low-speed closure procedures using variable mean density, there does not appear to be any appreciable influence of compressibility upon turbulent shear stress modeling in compressible turbulent boundary layers, even for extreme cases such as Mach 14 to 20 with a change in density across the layer of up to a factor of 100. Other evidence of an apparent lack of any compressibility-caused new physics which may alter the shear stress for the compressible boundary-layer case includes the following:

- (1) Fluctuation Mach number is generally less than 1;
- (2) the shear stress distribution through the boundary layer is not a function of Mach number for zero pressure gradient flows;
- (3) the Morkovin hypothesis is valid up to Mach 5 (based on fluctuation data);
- (4) profile N power is not a function of Mach number, at least up to Mach 10;
- (5) the nondimensional burst period is approximately the same as that for low speed.

Computational Capability of Existing Procedures

Compressible equilibrium and near equilibrium boundary-layer flows, at least up to Mach 20, can be computed fairly accurately using mean field methods, provided that the influence of such items as low Reynolds number effects, pressure gradient, and wall blowing are properly accounted for through adjustments in the modeling constants. By and large, these adjustments can be obtained from low-speed data. Several calculation methods are available for the nonequilibrium case, but these have not yet received sufficient exercise on compressible highly nonequilibrium flows (primarily as a result of lack of data) to determine their relative or absolute accuracy.

Important Unresolved Issues

The following is a brief listing of what are the more important unresolved issues (or research frontiers) in the calculation of compressible turbulent boundary layers, as discussed in the present paper:

1. Considerable further development and calibration of nonequilibrium methods is required for compressible flows. Further experimental data in highly nonequilibrium flows must be obtained before this effort can be really meaningful.

2. Definitive experiments are needed to determine directly the influence of compressibility upon shear stress production in compressible turbulent boundary layers (conditional sampling measurements at high Mach numbers and measurements of fluctuating pressure terms in Reynolds stress equations).

3. Further definition is needed of the boundaries between boundary-layer and nonboundary-layer behavior; that is, where can boundary-layer methods be reasonably expected to work? Bradshaw addresses this with his "extra rates of strain," but definitive guidelines are needed (such as how much concave longitudinal curvature is necessary before longitudinal vortices develop and the flow is no longer a boundary layer). Obviously one can employ Navier-Stokes codes and complete Reynolds stress modeling to attack such situations, but currently the boundary-layer codes are so much faster to run on computers (as compared with the Navier-Stokes solvers) that they should be used whenever possible; this necessitates having well-known limits within which accurate answers can be obtained (without new physics making either the basic equation set or the turbulent modeling inapplicable).

4. Obviously, three-dimensional compressible turbulent-boundary-layer calculations are in an early stage, and considerable experimentation is necessary before the efficacy of mean field methods for the three-dimensional case is determined.

Langley Research Center
National Aeronautics and Space Administration
Hampton, VA 23665
April 7, 1977

APPENDIX

SUMMARY OF CALCULATION PROCEDURES FOR NONSIMILAR TWO- AND THREE-DIMENSIONAL COMPRESSIBLE TURBULENT BOUNDARY LAYERS (FINITE DIFFERENCE, FINITE ELEMENT, AND WEIGHTED RESIDUAL METHODS)

The purpose of this summary (or catalog) of numerical prediction methods is to indicate the wide variety of such procedures which are available. (Table A1 has 31 entries.) In most cases information for the various entries were obtained from the individual authors, who kindly filled out and returned data sheets on their methods. Several authors have made a special effort to optimize the numerical solution procedure (e.g., refs. 9, 12, 162, and 163) to reduce the required machine time and storage per case. Most of the procedures have detailed user's manuals, and in many cases the codes are available either without charge or for the cost of mailing. Many of the special effects treated by the various methods (such as nonequilibrium or equilibrium chemistry, transition, roughness, etc.) are indicated in tables A1 and A2, as is the fundamental closure approach.

If these tables serve no other function, they should at least cause researchers to think quite carefully before producing the 32nd entry; that is, several of the procedures are quite similar, and future research should obviously concentrate on using the best numerical methods to investigate such items as nonequilibrium flows, rather than on producing another compressible turbulent-boundary-layer deck.

APPENDIX

TABLE A1.- CALCULATION PROCEDURES FOR NONSIMILAR TWO-DIMENSIONAL COMPRESSIBLE

TURBULENT BOUNDARY LAYERS

Method	Major reference	User's manual	Numerical solution method	Closure assumption	Unique features	Computing machine; language; storage	Code source
Adams	154, 293	Not available	Iterative implicit finite difference	Mixing length; $N_{Pr,t} = \text{Constant}$; wall damping uses local properties	Originally developed for transitional flows	IBM 370/165; FORTRAN IV; 47000g core storage	J. C. Adams, Jr. Von Kármán Gas Dynamics Facility, AEDC Arnold Air Force Station TN 37389
Albers and Gregg	160, 40	Ref. 160	Shooting method	Herring and Mellor inner and outer ϵ formulation (ref. 40)	Longitudinal wall curvature effects	IBM 7094/7044; FORTRAN IV; 67000g core storage	COSMIC 112 Barrow Hall University of Georgia Athens, GA 30602 (request LEM-12178; can also be punched from ref. 160)
Anderson and Lewis	294	Ref. 146	Implicit finite difference	Mixing length; Cebeci wall damping modifications (ref. 12); Clauser σ in outer region	Both perfect gas and equilibrium chemistry	IBM and CDC; FORTRAN IV	C. H. Lewis Aerospace Engineering Dept., VPI & SU Blacksburg, VA 24061 (can also be punched from ref. 146)
A. J. Baker	166	Ref. 295, 296	Finite element	Either eddy viscosity or second-order turbulent field closure	Small number of nodal points (due to finite element approach); wall shear specific-able; ideal gas and equilibrium hydrogen-air chemistry	IBM 360/65 or CDC 6600; FORTRAN IV; 160000g core storage	R. E. Smith, Jr. M.S.125, NASA Langley Research Center Hampton, VA 23665
R. J. Baker and Launder	186, 203	Ref. 9	Finite difference (Imperial College micro-integral method)	Mixing length with universal wall damping function; low Reynolds number amplification on outer mixing length	Unique near wall damping function	IBM or CDC; FORTRAN; 47000g core storage	Mechanical Engineering Dept. Imperial College of Science and Technology Exhibition Rd., London SW7, England (price, \approx \$100)

APPENDIX

TABLE A1.- Continued

Method	Major reference	User's manual	Numerical solution method	Closure assumption	Unique features	Computing machine; language; storage	Code source
Bradshaw and Ferriss	36, 297	Ref. 298	Method of characteristics	Mean turbulence field; uses relationship between $u'v'$ and e (a_1 parameter)	Includes models for extra rates of strain (ref. 172); companion code will handle infinite swept wings with non-equilibrium turbulent field	CDC 6400; FORTRAN IV; less than 500008 core storage	P. Bradshaw, Aeronautics Dept. Imperial College of Science and Technology Exhibition Rd. London SW7, England
Bushnell and Beckwith	53, 167, 243, 299	Ref. 241, 299	Iterative implicit finite difference	Mixing length; latest versions include low Reynolds number amplification for outer region mixing length	Alternate version for slot injection; also, code available in nondimensional physical variables with $p(x,y)$ and longitudinal curvature terms; original version includes infinite swept wings	CDC 6600; FORTRAN IV; 750008 core storage	Barbara H. Pitts M.S. 163, NASA Langley Research Center Hampton, VA 23665
Cebeci and Keller	12, 290	Not available	Keller box method	Mixing length near wall; Clauser σ in outer region (two-layer model); wall damping includes influence of m_w and dp/dx	Uses very efficient numerical scheme; run times are quite short	IBM 370; FORTRAN IV; 770008 core storage	Generally available for company use only; limited outside distribution

APPENDIX

TABLE A1.- Continued

Method	Major reference	User's manual	Numerical solution method	Closure assumption	Unique features	Computing machine; language; storage	Code source
Chan	155, 300	Not available	Implicit finite difference	Essentially a version of Bradshaw closure using integral form of turbulent kinetic energy equation; this equation tracks outer region mixing length constant	Relatively simple (but accurate) method for nonequilibrium turbulent flows	IBM 360/67; FORTRAN IV	Y. Y. Chan High-Speed Aerodynamic Section National Aeronautical Establishment Ottawa, Canada
Crawford and Kays	301	Ref. 301	Patankar-Spalding (ref. 9)	Turbulent kinetic energy equation or mixing length/eddy viscosity; mixing length always used in sublayer	Wall damping is a function of wall injection and pressure gradient; both internal and external flows		Can be punched from ref. 301
Deboy and Abbott	165	Included in ref. 165	Method of weighted residuals	Nominal Cebeci-Smith two-layer eddy viscosity (ref. 12)	Code used for studying numerical problems (with MWR) for turbulent boundary-layer flows		Code can be punched from ref. 165; procedure is not meant as a general-use prediction method
Donaldson and Sullivan	156	Ref. 302	Implicit finite difference	Complete mean turbulence field approach	Includes equations for all pertinent second-order correlations	CDC 7600 or IBM 1130; FORTRAN	M. W. Rubesin M.S. 229-3 NASA Ames Research Center Moffett Field, CA 94035 (code is still considered a research tool for studying second-order correlations, rather than a general predictive method)

APPENDIX

TABLE A1.- Continued

Method	Major reference	User's manual	Numerical solution method	Closure assumption	Unique features	Computing machine; language; storage	Code source
Dwyer	152, 198	Ref. 152	Implicit finite difference	Nominal Cebe-Smith two-layer eddy viscosity (ref. 12)	Includes transverse curvature, chemistry equilibrium	FORTRAN IV	Can be punched from ref. 152
Fivel and Masek	151, 303	Ref. 303	Implicit finite difference	Nominal Cebe-Smith two-layer eddy viscosity (ref. 12)	Nonequilibrium, equilibrium, and frozen chemistry, finite wall catalysis	CDC 6600; FORTRAN IV; 620008 core storage	R. A. Jones M.S. 168 NASA Langley Research Center Hampton, VA 23665
Carr and Fox	143	Not available	Implicit finite difference	Nominal Cebe-Smith two-layer eddy viscosity (ref. 12)	Uses physical coordinates		Not available
Gibson and Spalding	232	Ref. 232	Imperial College micro-integral approach	Mean turbulence field; equations for turbulent kinetic energy and fluctuating vorticity	"Couette" wall functions; second-order, two-equation turbulence closure		Could be punched from ref. 232 (uses basic Patankar-Spalding code, (ref. 9)
Harris	142	Ref. 240	Implicit finite difference	Nominal Cebe-Smith two-layer eddy viscosity (ref. 12)	Simultaneous solutions of equations; transition region calculation using streamwise intermittency function	CDC 6600; FORTRAN IV; 750008 core storage	Julius E. Harris M.S. 163 NASA Langley Research Center Hampton, VA 23665

TABLE A1.- Continued

Method	Major reference	User's manual	Numerical solution method	Closure assumption	Unique features	Computing machine; language; storage	Code source
Kendall and Anderson (BLIMP)	34, 163, 304	Ref. 305	Integral matrix	Two-layer eddy viscosity with unique wall damping treatment	Ideal gas or equilibrium chemistry; transverse curvature and entropy layer treatments; ablation cases with chemistry; numerical method permits small number of nodes	CDC 7600, CDC 6600 or UNIVAC 1108; FORTRAN (Note: This is the JANNAF standard reacting boundary-layer calculation procedure)	Klaus Gross M.S. EP23 NASA Marshall Space Flight Center Huntsville, AL 35812
Kuhn	164	Ref. 306	Method of weighted residuals	Two-layer eddy viscosity	Transitional flow calculation	CDC 6600; FORTRAN IV; 500008 core storage	S. Z. Pinckney M.S. 168 NASA Langley Research Center Hampton, VA 23665
Levine (MABLE)	149	Ref. 150	Implicit finite difference	Nominal Cebeci-Smith two-layer eddy viscosity (ref. 12)	Transformation for variable mode spacing in y; equilibrium hydrogen-air chemistry and ideal gas	IBM 360 or UNIVAC 1108 (developed for liquid rocket nozzle flows)	T. Reedy APL/JHU 8621 Georgia Ave. Silver Spring, MD 20910
Mayne	223, 221 for ear-lier version (without normal pressure gradient and curvature)	Not available	Implicit finite difference with Von Mises variables (modification and extension of Patankar-Spalding method, ref. 9)	Mixing length	Includes $p(y)$ due to longitudinal curvature and other longitudinal curvatures; transition region calculation	IBM 370/155; FORTRAN IV; 550008 core storage	A. W. Mayne, Jr. Von Kármán Gas Dynamics Facility, AEDC Arnold Air Force Station TN 37389

APPENDIX

TABLE A1.- Continued

Method	Major reference	User's manual	Numerical solution method	Closure assumption	Unique features	Computing machine; language; storage	Code source
McDonald	159, 307	Ref. 308	Implicit finite difference	Integral turbulent kinetic energy (with Bradshaw-type assumptions) or mixing length	Transitional flow; rough walls; free-stream turbulence; equilibrium and nonequilibrium chemical reactions	UNIVAC 1108 or 1110 or CDC 6600; FORTRAN; 2500010 or 4000010, depending upon option or overlay	B. H. Anderson M.S. 86 NASA Lewis Research Center 21000 Brookpark Rd. Cleveland, OH 44135
Omori	148	Ref. 148	Implicit finite difference (uses basic code of ref. 150)	Turbulent kinetic energy equation with algebraic length scale and Prandtl model relating $u', v',$ and w'	Both ideal gas and equilibrium chemistry; one-equation turbulent kinetic energy closure	UNIVAC 1108; FORTRAN IV; 5900010 core storage	Klaus Gross M.S. EP23 NASA Marshall Space Flight Center Huntsville, AL 35812
Patankar and Spalding	9	9	Imperial College micro-integral method	Mixing length or turbulent kinetic energy closure (one- and two-equation models)	Generality of closure methods; also handles pipe and diffuser flows	Decks available for most computers using FORTRAN language	D. B. Spalding Mechanical Engineering Dept. Imperial College of Science and Technology Exhibition Rd. London SW7, England
Pletcher	158	Unpublished guide and notes available from author	Explicit finite difference	Mixing length	Explicit numerics	IBM 360/65 or IBM 370/158; FORTRAN IV	R. H. Pletcher Iowa State Univ. Ames, IA 50010
Reyhner	45 (pp. 375-383)	Ref. 309	Implicit finite difference	Two-layer eddy viscosity with simplified ϵ equation for nonequilibrium flows	Uses physical coordinates; simplified differential equation to compute ϵ in nonequilibrium flows	CDC 6600; FORTRAN IV; 2700010 core storage	Available by purchase from The Boeing Co., Seattle, WA 98124

APPENDIX

TABLE A1.- Concluded

Method	Major reference	User's manual	Numerical solution method	Closure assumption	Unique features	Computing machine; language; storage	Code source
Rie	144, 310		Implicit finite difference	Two-layer eddy viscosity	Transverse curvature effect; equilibrium chemistry	Honeywall 6060; FORTRAN	A. Martellucci GE-RES, P. O. Box 8555 Philadelphia, PA 19101 (user's manual available by purchase)
Shang and Hankey	147, 170 274	Not available	Implicit finite difference	Two-layer eddy viscosity	Transition region using intermittency function.	CDC; FORTRAN	J. S. Shang Wright-Patterson Air Force Base OH 45433
Verma	213	Ref. 311	Implicit finite difference	Two-layer eddy viscosity	Well exercised	IBM 360/165	Can be punched from ref. 311
Waiter and LeBlanc	153, 312	Ref. 153	Implicit finite difference	Two-layer eddy viscosity	Uses physical variables; variable entropy	IBM 360/370; FORTRAN IV	Not available
Wilcox and Chambers	231, 313	Not available (basic code same as ref. 240)	Implicit finite difference	Two-equation mean turbulence field (Saffman model)	Surface roughness; transition	UNIVAC 1108 or CDC; FORTRAN	DCW Industries 13535 Ventura Blvd. Sherman Oaks, CA 91423
Wortman	162, 314	Not available	Operator method	Mixing length or one- or two-equation mean turbulent field	Efficient numerical method	IBM or CDC	

APPENDIX

TABLE A2.- CALCULATION PROCEDURES FOR NONSIMILAR THREE-DIMENSIONAL
COMPRESSIBLE TURBULENT BOUNDARY LAYERS

Method	Major reference	Numerical solution procedure	Turbulence closure procedure	Unique features	Code source
Kendall et al.	245	Integral matrix	Scalar-invariant eddy-viscosity mixing-length model	Equilibrium and frozen flow; orthogonal body-oriented coordinate system; Primitive variables; fast, low storage	R. M. Kendall Acurex Corp. Aerotherm Division 485 Clyde Ave. Mountain View, CA 94043 or J. E. Harris, LaRC
Cebeci et al.	244, 260	Keller box method, implicit finite difference	Scalar-invariant eddy-viscosity two-layer model	Perfect gas; nonorthogonal body-oriented coordinate system; fast, low storage	T. Cebeci Douglas Aircraft Co. 3855 Lakewood Blvd. Long Beach, CA 90808 or J. E. Harris, LaRC
Harris	271	Implicit finite difference	Scalar-invariant eddy-viscosity two-layer model; mixing-length model	Perfect gas; orthogonal body-oriented coordinate system; Crocco transformation; fast, low storage	J. E. Harris M.S. 163 NASA Langley Research Center Hampton, VA 23665
Frieders and Lewis	248	Implicit finite difference	Scalar-invariant eddy-viscosity two-layer model	Binary gas mixture with wall mass transfer; orthogonal, body-oriented coordinate system; stream function with Levy-Lees transformation	M. L. Laster R&D Directorate AEDC, Arnold Air Force Station, TN 37389
Adams	315, 316	Implicit finite difference	Scalar-invariant eddy-viscosity two-layer model	Perfect gas; streamline coordinate system	J. C. Adams, Jr. Von Karman Gas Dynamics Facility, AEDC Arnold Air Force Station, TN 37389

APPENDIX

TABLE A2.- Concluded

Method	Major reference	Numerical solution procedure	Turbulence closure procedure	Unique features	Code source
Baker et al.	317, 318	Finite element	Scalar-invariant eddy-viscosity two-layer model	Equilibrium and frozen flow; orthogonal coordinate system	A. J. Baker Computational Mechanics Consultants 3601A Chapman Highway Knoxville, TN 37920
Wortman	162	Operator procedure	Scalar-invariant eddy-viscosity two-layer model	Equilibrium and frozen flow; orthogonal coordinate system	
Spalding	319, 320	Micro-integral (ref. 9)	Mixing-length and higher order modeling	Equilibrium and frozen flow; orthogonal coordinate system	D. B. Spalding Imperial College of Science and Technology Exhibition Rd. London SW7, England
Nash and Patel	267	Explicit finite difference	Scalar-invariant eddy-viscosity mixing-length order modeling	Perfect gas; orthogonal coordinate system	J. F. Nash Sybucon Inc. 9 Perimeter Rd. NW Atlanta, GA 30339
Fanneiöp and Humphreys	253	Implicit finite difference	Scalar-invariant eddy-viscosity two-layer model	Perfect gas; streamline coordinates	T. K. Fanneiöp The Aeronautical Research Institute of Sweden Stockholm, Sweden
Krause et al.	321	Implicit finite difference "Mehrstellen" method	Scalar-invariant eddy-viscosity two-layer model	Perfect gas; Nonorthogonal body-oriented coordinate system	E. Krause Aerodynamisches Institut der RWTH 51 Aachen Wullnerstra Be zw 5-7 West Germany

REFERENCES

1. Clauser, Francis H.: The Turbulent Boundary Layer. Volume IV of Advances in Applied Mechanics, H. L. Dryden and Th. von Kármán, eds., Academic Press, Inc., 1956, pp. 1-51.
2. Lin, C. C., ed.: Turbulent Flows and Heat Transfer. Volume V, High Speed Aerodynamics and Jet Propulsion, Princeton Univ. Press, 1959.
3. Dorrance, William H.: Viscous Hypersonic Flow. McGraw-Hill Book Co., Inc., c.1962.
4. Kutateladze, S. S.; and Leont'ev, A. I. (D. B. Spalding, transl.): Turbulent Boundary Layers in Compressible Gases. Academic Press, Inc., 1964.
5. Schlichting, Hermann (J. Kestin, transl.): Boundary-Layer Theory. Sixth ed. McGraw-Hill Book Co., Inc., 1968.
6. Lapin, Yu. V.: The Turbulent Boundary Layer in Supersonic Gas Flows. NASA TT F-691, 1972.
7. Monin, A. S.; and Yaglom, A. M.: Statistical Fluid Mechanics: Mechanics of Turbulence. Volumes I and II. MIT Press, c.1971 and 1975.
8. Launder, B. E.; and Spalding, D. B.: Lectures in Mathematical Models of Turbulence. Academic Press, Inc., 1972.
9. Patankar, S. V.; and Spalding, D. B.: Heat and Mass Transfer in Boundary Layers. Second ed. Int. Textbook Co. Ltd. (London), c.1970.
10. Tennekes, H.; and Lumley, J. L.: A First Course in Turbulence. M.I.T. Press, c.1972.
11. Kutateladze, S. S.; and Leont'yev, A. I.: Heat-Mass Transfer and Friction in a Turbulent Boundary Layer. NASA TT F-805, 1974.
12. Cebeci, Tuncer; and Smith, A. M. O.: Analysis of Turbulent Boundary Layers. Academic Press, Inc., 1974.
13. Van Driest, E. R.: Turbulent Boundary Layer in Compressible Fluids. J. Aeronaut. Sci., vol. 18, no. 3, Mar. 1951, pp. 145-160, 216.
14. Kovásznay, Leslie S. G.: Turbulence in Supersonic Flow. J. Aeronaut. Sci., vol. 20, no. 10, Oct. 1953, pp. 657-674, 682.
15. Coles, D. E.: The Turbulent Boundary Layer in a Compressible Fluid. U.S. Air Force Proj. RAND Rep. R-403-PR (DDC Doc. No. AD 285 651), Rand Corp., Sept. 1962.
16. Hornung, H. G.: A Survey of Compressible Flow Boundary Layers - Theory and Experiment. Rep. ACA 67, Dep. Supply, Australian Aeronaut. Res. Comm., Feb. 1966.

17. Baronti, Paolo; Fox, Herbert; and Soll, David: A Survey of the Compressible Turbulent Boundary Layer With Mass Transfer. *Astronaut. Acta*, vol. 13, no. 3, May-June 1967, pp. 239-249.
18. Beckwith, Ivan E.: Recent Advances in Research on Compressible Turbulent Boundary Layers. *Analytic Methods in Aircraft Aerodynamics*, NASA SP-228, 1970, pp. 355-416.
19. Reynolds, W. C.: Computation of Turbulent Flows - State-of-the-Art, 1970. Rep. MD-27 (Grants NSF-GK-10034 and NASA-NgR-05-020-420), Dep. Mech. Eng., Stanford Univ., Oct. 1970. (Available as NASA CR-128372.)
20. Reynolds, W. C.: Computation of Turbulent Flows. Rep. No. TFC-4 (Grant NASA-NgR-05-020-622), Dep. Mech. Eng., Stanford Univ., Apr. 1975. (Available as NASA CR-143323.)
21. Harlow, Francis H., ed.: Turbulence Transport Modeling. Volume XIV of AIAA Selected Reprint Series, Feb. 1973.
22. Bradshaw, P.: The Understanding and Prediction of Turbulent Flow. *J. Roy. Aeronaut. Soc.*, vol. 76, no. 739, July 1972, pp. 403-418.
23. Leslie, D. C.: Review of Developments in Turbulence Theory. *Rep. Prog. Phys.*, vol. 36, no. 11, 1973, pp. 1365-1424.
24. Mellor, George L.; and Herring, H. James: A Survey of the Mean Turbulent Field Closure Models. *AIAA J.*, vol. 11, no. 5, May 1973, pp. 590-599.
25. Sandborn, V. A.: A Review of Turbulence Measurements in Compressible Flow. NASA TM X-62,337, 1974.
26. *The Mechanics of Turbulence*. Gordon & Breach, Sci. Pub., Inc., c.1964.
27. Recent Developments in Boundary Layer Research. AGARDograph 97, May 1965.
28. *Compressible Turbulent Boundary Layers*. NASA SP-216, 1969.
29. Boeing Symposium on Turbulence. *J. Fluid Mech.*, vol. 41, pt. 1, Mar. 26, 1970, pp. 1-240; vol. 41, pt. 2, Apr. 13, 1970, pp. 241-480.
30. Turbulent Shear Flows. AGARD-CP-93, Sept. 1971.
31. Sivasegaram, S.: A Review of the Literature Pertaining to Experimental Investigation of the Two-Dimensional, Compressible, Turbulent, Wall Boundary Layers. Rep. TWF/TN/44, Dep. Mech. Eng., Imperial Coll. Sci. & Technol., Apr. 1968.
32. Fernholz, H.: Departures From a Fully Developed Turbulent Velocity Profile on a Flat Plate in Compressible Boundary Layers. *Fluid Dyn. Trans.*, vol. 6, pt. II, 1972, pp. 161-177.

33. Jeromin, L. O. F.: The Status of Research in Turbulent Boundary Layers With Fluid Injection. Progress in Aeronautical Sciences, Volume 10, D. Küchemann, P. Carrière, B. Etkin, W. Fiszdon, N. Rott, Smolderen, I. Tani, and W. Wuest, eds., Pergamon Press, 1970, pp. 65-189.
34. Anderson, Larry W.; and Morse, Howard L.: A Turbulent Model Study for the Multicomponent Nonsimilar Turbulent Boundary Layer Program. AFWL-TR-71-57, U.S. Air Force, Oct. 1971. (Available from DDC as AD 734 752.)
35. Gopinath, R.; and East, R. A.: The Effect of Adverse Pressure Gradient on the Hypersonic Turbulent Boundary Layer on a Nozzle Wall at High Rates of Heat Transfer. A.A.S.U. Rep. No. 326, Dep. Aeronaut. & Astronaut., Univ. of Southampton, Apr. 1973.
36. Bradshaw, P.; and Ferriss, D. H.: Calculation of Boundary-Layer Development Using the Turbulent Energy Equation: Compressible Flow on Adiabatic Walls. J. Fluid Mech., vol. 46, pt. 1, Mar. 15, 1971, pp. 83-110.
37. Fernholz, H. H.; and Finley, P. J.: A Critical Compilation of Compressible Turbulent Boundary Layer Data. Compressible Turbulent Boundary Layers, Volume 1, Lecture Series 86, Von Kármán Inst. Fluid Dyn., Mar. 1976.
38. Callens, E. Eugene, Jr.: A Time-Dependent Approach to Fluid Mechanical Phenomenology. AIAA Paper No. 70-46, Jan. 1970.
39. Deissler, R. G.; and Loeffler, A. L., Jr.: Analysis of Turbulent Flow and Heat Transfer on a Flat Plate at High Mach Numbers With Variable Fluid Properties. NASA TR R-17, 1959. (Supersedes NACA TN 4262.)
40. Herring, H. James; and Mellor, George L.: A Method of Calculating Compressible Turbulent Boundary Layers. NASA CR-1144, 1968.
41. Rotta, J. C.: Introduction to Turbulent Boundary Layer Calculation. VKI Short Course on Turbulent Boundary Layers, Lect. Ser. 5 - Pt. 1, von Karman Inst. Fluid Dyn., Mar. 1968, pp. 1-67.
42. Favre, A.: Statistical Equations of Turbulent Gases. Problems of Hydrodynamics and Continuum Mechanics. Soc. Indust. & Appl. Math., 1969, pp. 231-266.
43. Rubesin, Morris W.; and Rose, William C.: The Turbulent Mean-Flow, Reynolds-Stress, and Heat-Flux Equations in Mass-Averaged Dependent Variables. NASA TM X-62248, 1973.
44. Morkovin, M. V.: Effects of High Acceleration on a Turbulent Supersonic Shear Layer. Proceedings of the 1955 Heat Transfer and Fluid Mechanics Institute, vol. 4, 1955, pp. 1-17.
45. Computation of Turbulent Boundary Layers - 1968 AFOSR-IFP-Stanford Conference, Volume 1, S. J. Kline, M. V. Morkovin, G. Sovran, and D. J. Cockrell, eds., Stanford Univ., c.1969.

46. Schofield, W. H.: The Effect of Sudden Discontinuities on Turbulent Boundary Layer Development. Rep. ARL/M.E. 139, Dep. Supply (Melbourne), Mar. 1973.
47. Fischer, Michael C.; Maddalon, Dal V.; Weinstein, Leonard M.; and Wagner, Richard D., Jr.: Boundary-Layer Surveys on a Nozzle Wall at $M_\infty \approx 20$ Including Hot-Wire Fluctuation Measurements. AIAA Paper No. 70-746, June-July 1970.
48. Beckwith, Ivan E.; Harvey, William D.; and Clark, Frank L. (Appendix A by Ivan E. Beckwith, William D. Harvey, and Christine M. Darden and appendix B by William D. Harvey, Lemuel E. Forrest, and Frank L. Clark): Comparisons of Turbulent-Boundary-Layer Measurements at Mach Number 19.5 With Theory and an Assessment of Probe Errors. NASA TN D-6192, 1971.
49. Harvey, William D.; Bushnell, Dennis M.; and Beckwith, Ivan E.: Fluctuating Properties of Turbulent Boundary Layers for Mach Numbers up to 9. NASA TN D-5496, 1969.
50. Kemp, Joseph H., Jr.; and Owen, F. Kevin: Experimental Study of Nozzle Wall Boundary Layers at Mach Numbers 20 to 47. NASA TN D-6965, 1972.
51. Finley, P. J.: Static Pressure Profiles for Turbulent Boundary Layers on the Walls of Contoured Hypersonic Nozzles. IC Aero Rep. 77-01, Dep. Aeronaut., Imperial Coll. Sci. & Technol., Jan. 1977.
52. Oh, Y. H.: Analysis of Two-Dimensional Free Turbulent Mixing. AIAA Paper No. 74-594, June 1974.
53. Bushnell, Dennis M.; and Beckwith, Ivan E.: Calculation of Nonequilibrium Hypersonic Turbulent Boundary Layers and Comparisons With Experimental Data. AIAA J., vol. 8, no. 8, Aug. 1970, pp. 1462-1469.
54. Fischer, Michael C.; and Weinstein, Leonard M.: Cone Transitional Boundary-Layer Structure at $M_e = 14$. AIAA J., vol. 10, no. 5, May 1972, pp. 699-701.
55. Demetriades, Anthony: Hypersonic Viscous Flow Over a Slender Cone. Part III: Laminar Instability and Transition. AIAA Paper No. 74-535, June 1974.
56. Owen, F. K.: Fluctuation Measurements in Compressible Boundary Layers. Rep. No. 1,076,69, Dep. Eng. Sci., Univ. Oxford, Mar. 1969.
57. Fischer, Michael C.: Spreading of a Turbulent Disturbance. AIAA J., vol. 10, no. 7, July 1972, pp. 957-959.
58. Bushnell, D. M.; and Alston, D. W.: Calculation of Transitional Boundary-Layer Flows. AIAA J., vol. 11, no. 4, Apr. 1973, pp. 554-556.
59. Owen, F. K.; and Horstman, C. C.: Hypersonic Transitional Boundary Layers. AIAA J., vol. 10, no. 6, June 1972, pp. 769-775.

60. Stainback, P. Calvin; Wagner, Richard D.; Owen, F. Kevin; and Horstman, Clifford C.: Experimental Studies of Hypersonic Boundary-Layer Transition and Effects of Wind-Tunnel Disturbances. NASA TN D-7453, 1974.
61. Stainback, P. Calvin: Use of Rouse's Stability Parameter in Determining the Critical Layer Height of a Laminar Boundary Layer. AIAA J., vol. 8, no. 1, Jan. 1970, pp. 173-175.
62. Laderman, A. J.; and Demetriades, A.: Mean and Fluctuating Flow Measurements in the Hypersonic Boundary Layer Over a Cooled Wall. J. Fluid Mech., vol. 63, pt. 1, Mar. 18, 1974, pp. 121-144.
63. Moon, Lamar Foster: Selected Statistical Properties of a High Velocity Turbulent Boundary Layer With Surface Mass Addition. Ph. D. Thesis, Univ. of Utah, 1973.
64. Watson, Ralph D.: Wall Cooling Effects on Hypersonic Transitional/Turbulent Boundary Layers at High Reynolds Numbers. AIAA Paper No. 75-834, June 1975.
65. Beckwith, I. E.: Development of a High Reynolds Number Quiet Tunnel for Transition Research. AIAA J., vol. 13, no. 3, Mar. 1975, pp. 300-306.
66. Owen, F. K.; and Horstman, C. C.: A Study of Turbulence Generation in a Hypersonic Boundary Layer. AIAA Paper No. 72-182, Jan. 1972.
67. Dorodnitsyn, A.: Boundary Layer in Compressible Gas. Appl. Math. & Mech., vol. 6, no. 6, 1942, pp. 449-486.
68. Mager, Artur: Transformation of the Compressible Turbulent Boundary Layer. J. Aeronaut. Sci., vol. 25, no. 5, May 1958, pp. 305-311.
69. Culick, Fred E. C.; and Hill, Jacques A. F.: A Turbulent Analog of the Stewartson-Illingworth Transformation. J. Aeronaut. Sci., vol. 25, no. 4, Apr. 1958, pp. 259-262.
70. Burggraf, O. R.: The Compressibility Transformation and the Turbulent-Boundary-Layer Equations. J. Aerosp. Sci., vol. 29, no. 4, Apr. 1962, pp. 434-439.
71. Monaghan, R. J.: On The Behavior of Boundary Layers at Supersonic Speeds. Fifth International Aeronautical Conference, Rita J. Turino and Caroline Taylor, eds., Inst. Aeronaut. Sci., Inc., June 1955, pp. 277-315.
72. Eckert, E. R. G.: Engineering Relations for Friction and Heat Transfer to Surfaces in High Velocity Flow. J. Aeronaut. Sci., vol. 22, no. 8, Aug. 1955, pp. 585-587.
73. Sommer, Simon C.; and Short, Barbara J.: Free-Flight Measurements of Turbulent-Boundary-Layer Skin Friction in the Presence of Severe Aerodynamic Heating at Mach Numbers From 2.8 to 7.0. NACA TN 3391, 1955.

74. Crocco, L.: Transformations of the Compressible Turbulent Boundary Layer With Heat Exchange. AIAA J., vol. 1, no. 12, Dec. 1963, pp. 2723-2731.
75. Baronti, Paolo O.; and Libby, Paul A.: Velocity Profiles in Turbulent Compressible Boundary Layers. AIAA J., vol. 4, no. 2, Feb. 1966, pp. 193-202.
76. Jeromin, L. O. F.: A Transformation for Compressible Turbulent Boundary Layers With Air Injection. J. Fluid Mech., vol. 31, pt. 1, Jan. 1968, pp. 65-94.
77. Lewis, John E.; Kubota, Toshi; and Webb, Wilmot H.: Transformation Theory for the Compressible Turbulent Boundary Layer With Arbitrary Pressure Gradient. AIAA Paper No. 69-160, Jan. 1969.
78. Economos, Constantino; and Boccio, John: An Investigation of the High Speed Turbulent Boundary Layer With Heat Transfer and Arbitrary Pressure Gradient. Part I - Summary Report. NASA CR-1679, 1970.
79. Maise, George; and McDonald, Henry: Mixing Length and Kinematic Eddy Viscosity in a Compressible Boundary Layer. AIAA J., vol. 6, no. 1, Jan. 1968, pp. 73-80.
80. Bertram, Mitchel H.; Cary, Aubrey M., Jr.; and Whitehead, Allen H. Jr.: Experiments With Hypersonic Turbulent Boundary Layers on Flat Plates and Delta Wings. Paper presented at AGARD Specialists' Meeting on Hypersonic Boundary Layers and Flow Fields (London, England), May 1968.
81. Spalding, D. B.; and Chi, S. W.: The Drag of a Compressible Turbulent Boundary Layer on a Smooth Flat Plate With and Without Heat Transfer. J. Fluid Mech., vol. 18, pt. 1, Jan. 1964, pp. 117-143.
82. Cary, Aubrey M., Jr.; and Bertram, Mitchel H.: Engineering Prediction of Turbulent Skin Friction and Heat Transfer in High-Speed Flow. NASA TN D-7507, 1974.
83. Winter, K. G.; Rotta, J. C.; and Smith, K. G. (Francesca Neffgen, transl.): Turbulent Boundary Layer Studies on a "Waisted" Body of Revolution in Subsonic and Supersonic Flow. B-533, Boeing Co., Apr. 1969.
84. White, F. M.; and Christoph, G. H.: A Simple New Analysis of Compressible Turbulent Two-Dimensional Skin Friction Under Arbitrary Conditions. AFFDL-TR-70-133, U.S. Air Force, Feb. 1971.
85. Kutateladze, S. S.; and Leont'ev, A. I.: Drag Law in a Turbulent Flow of a Compressible Gas and the Method of Calculating Friction and Heat Exchange. TIL/T.5258, British Minist. Aviat., Dec. 1961.
86. Wilson, Robert E.: Turbulent Boundary-Layer Characteristics at Supersonic Speeds - Theory and Experiment. J. Aeronaut. Sci., vol. 17, no. 9, Sept. 1950, pp. 585-594.

87. Van Driest, E. R.: The Problem of Aerodynamic Heating. *Aeronaut. Eng. Rev.*, vol. 15, no. 10, Oct. 1956, pp. 26-41.
88. Harkness, John L.: The Effect of Heat Transfer on Turbulent Boundary Layer Skin Friction. DRL-436, CM-940 (Contract NOrd-16498), Univ. of Texas, 1959.
89. Moore, Dave R.: Velocity Similarity in the Compressible Turbulent Boundary Layer With Heat Transfer. Ph. D. Thesis, Univ. of Texas, 1962.
90. Li, T. Y.; and Nagamatsu, H. T.: Effects of Density Fluctuations on the Turbulent Skin Friction of an Insulated Flat Plate at High Supersonic Speeds. *J. Aeronaut. Sci.*, vol. 18, no. 10, Oct. 1951, pp. 696-697.
91. Kosterin, S. I.; and Koshmarov, Yu. A.: The Turbulent Boundary Layer on a Flat Plate in a Uniform Stream of a Compressible Fluid. *Soviet Phys. - Tech. Phys.*, vol. 4, no. 7, Jan. 1960, pp. 819-828.
92. Cope, W. F.: The Turbulent Boundary Layer in Compressible Flow. R. & M. No. 2840, Brit. A.R.C., 1953.
93. Monaghan, R. J.: Comparison Between Experimental Measurements and a Suggested Formula for the Variation of Turbulent Skin-Friction in Compressible Flow. C.P. No. 45, British A.R.C., 1951.
94. Peterson, John B., Jr.: A Comparison of Experimental and Theoretical Results for the Compressible Turbulent-Boundary-Layer Skin Friction With Zero Pressure Gradient. NASA TN D-1795, 1963.
95. Bertram, Mitchel H.; and Neal, Luther, Jr.: Recent Experiments in Hypersonic Turbulent Boundary Layers. Presented at the AGARD Specialists' Meeting on Recent Developments in Boundary-Layer Research (Naples, Italy), May 1965. (Also available as NASA TM X-56335.)
96. Zoby, Ernest V.; and Sullivan, Edward M.: Correlation of Free-Flight Turbulent Heat-Transfer Data From Axisymmetric Bodies With Compressible Flat-Plate Relationships. NASA TN D-3802, 1967.
97. Pearce, Blaine: A Comparison of Four Simple Calculation Methods for the Compressible Turbulent Boundary Layer on a Flat Plate. Rep. No. TOR-0066(5758-02)-3 (Contract No. F04701-69-C-0066), Syst. Eng. Oper., Aerosp. Corp., Mar. 16, 1970. (Available from DDC as AD 708 147.)
98. Hopkins, Edward J.; and Inouye, Mamoru: An Evaluation of Theories for Predicting Turbulent Skin Friction and Heat Transfer on Flat Plates at Supersonic and Hypersonic Mach Numbers. *AIAA J.*, vol. 9, no. 6, June 1971, pp. 993-1003.
99. Saltzman, Edwin J.; and Fisher, David F.: Some Turbulent Boundary-Layer Measurements Obtained From the Forebody of an Airplane at Mach Numbers up to 1.72. NASA TN D-5838, 1970.

100. Erlich, Émile: Probing in Flight the Boundary-Layer of the Supersonic Airplane Mirage IV. *Rech. Aérop.*, no. 122, Jan.-Feb. 1968, pp. 11-19.
101. Fisher, David F.; and Saltzman, Edwin J.: Local Skin Friction Coefficients and Boundary-Layer Profiles Obtained in Flight From the XB-70-1 Airplane at Mach Numbers up to 2.5. NASA TN D-7220, 1973.
102. Colburn, Allan P.: A Method for Correlating Forced Convection Heat Transfer Data and a Comparison With Fluid Friction. *Trans. Amer. Inst. Chem. Eng.*, vol. XXIX, 1933, pp. 174-211.
103. Van Driest, E. R.: Turbulent Boundary Layer on a Cone in a Supersonic Flow at Zero Angle of Attack. *J. Aeronaut. Sci.*, vol. 19, no. 1, Jan. 1952, pp. 55-57, 72.
104. Coles, Donald: The Law of the Wake in the Turbulent Boundary Layer. *J. Fluid Mech.*, vol. 1, pt. 2, July 1956, pp. 191-226.
105. Spalding, D. B.: A Single Formula for the "Law of the Wall." *Trans. ASME, Ser. E: J. Appl. Mech.*, vol. 28, no. 3, Sept. 1961, pp. 455-457.
106. Kleinstein, Gdalia: Generalized Law of the Wall and Eddy-Viscosity Model for Wall Boundary Layers. *AIAA J.*, vol. 5, no. 8, Aug. 1967, pp. 1402-1407.
107. Hama, Francis R.: Boundary-Layer Characteristics for Smooth and Rough Surfaces. *Trans. Soc. Nav. Architects & Mar. Eng.*, vol. 62, 1954, pp. 333-358.
108. Stevenson, T. N.: A Law of the Wall for Turbulent Boundary Layers With Suction or Injection. Rep. No. 166, Coll. of Aeronaut., Cranfield (England), July 1963.
109. Fernholz, H.: Geschwindigkeitsprofile, Temperaturprofile und halbempirische Gesetze in kompressiblen turbulenten Grenzschichten bei konstantem Druck. *Ing.-Arch.*, Bd. 38, Heft 4-5, Sept. 1969, pp. 311-328.
110. Mathews, Douglas C.; Childs, Morris E.; and Paynter, Gerald C.: Use of Coles' Universal Wake Function for Compressible Turbulent Boundary Layers. *J. Aircr.*, vol. 7, no. 2, Mar.-Apr. 1970, pp. 137-140.
111. Sun, Chen-Chih; and Childs, Morris E.: A Modified Wall Wake Velocity Profile for Turbulent Compressible Boundary Layers. *J. Aircr.*, vol. 10, no. 6, June 1973, pp. 381-383.
112. Kane, T. J.: A Velocity Profile Correlation and Prediction Procedure for Compressible Turbulent Boundary Layers Including Effects of Heat and Mass Transfer. Rep. H072, McDonnell Douglas Corp., Mar. 21, 1969.

113. Kane, T. J.: A Velocity Profile Correlation and Prediction Procedure for Compressible Turbulent Boundary Layers Including Effects of Heat and Mass Transfer. Rep. H072, Addendum No. 1, McConnell Douglas Corp., Jan. 30, 1970.
114. Squire, L. C.: A Law of the Wall for Compressible Turbulent Boundary Layers With Air Injection. J. Fluid Mech., vol. 37, pt. 3, 1969, pp. 449-456.
115. Chen, Karl K.: Compressible Turbulent Boundary-Layer Heat Transfer to Rough Surfaces in Pressure Gradient. AIAA J., vol. 10, no. 5, May 1972, pp. 623-629.
116. White, F. M.; and Christoph, G. H.: A Simple Theory for the Two-Dimensional Compressible Turbulent Boundary Layer. Trans. ASME, Ser. D: J. Basic Eng., vol. 94, no. 3, Sept. 1972, pp. 636-642.
117. Danberg, James E.: A Re-Evaluation of Zero Pressure Gradient Compressible Turbulent Boundary Layer Measurements. BRL Rep. No. 1642, U.S. Army, Apr. 1973. (Available from DDC as AD 762 152.)
118. Gran, R. L.; Lewis, J. E.; and Kubota, T.: The Effect of Wall Cooling on a Compressible Turbulent Boundary Layer. J. Fluid Mech., vol. 66, pt. 3, Nov. 25, 1974, pp. 507-528.
119. Reshotko, Eli; and Tucker, Maurice: Approximate Calculation of the Compressible Turbulent Boundary Layer With Heat Transfer and Arbitrary Pressure Gradient. NACA TN 4154, 1957.
120. Englert, Gerald W.: Estimation of Compressible Boundary-Layer Growth Over Insulated Surfaces With Pressure Gradient. NACA TN 4022, 1957.
121. Spence, D. A.: The Growth of Compressible Turbulent Boundary Layers on Isothermal and Adiabatic Walls. R & M No. 3191, British A.R.C., 1961.
122. Sasman, Philip K.; and Cresci, Robert J.: Compressible Turbulent Boundary Layer With Pressure Gradient and Heat Transfer. AIAA J., vol. 4, no. 1, Jan. 1966, pp. 19-25.
123. Camarata, F. J.; and McDonald, H.: A Procedure for Predicting Characteristics of Compressible Turbulent Boundary Layers Which Includes the Treatment of Upstream History. Rep. G212238-3, Res. Lab., United Aircraft Corp., Aug. 1968.
124. Flaherty, R. J.: A Method for Estimating Turbulent Boundary Layers and Heat Transfer in an Arbitrary Pressure Gradient. Rep. UAR-G51, United Aircraft Corp., Aug. 1968.
125. Zwarts, Frank J.: The Compressible Turbulent Boundary Layer in a Pressure Gradient. Ph. D. Thesis, McGill Univ., 1970.

126. Head, M. R.: Entrainment in a Turbulent Boundary Layer. R & M No. 3152, British A.R.C., 1960.
127. Standen, N. M.: A Concept of Mass Entrainment Applied to Compressible Turbulent Boundary Layers in Adverse Pressure Gradients. Proceedings of the 4th Congress of the International Council of the Aeronautical Sciences, Robert R. Dexter, ed., Spartan Books, Inc., 1965, pp. 1101-1125.
128. So, Ronald M. C.: An Extension of a Turbulent Incompressible Boundary Layer Theory to Compressible Boundary Layers. Tech. Note 65-6, Mech. Eng. Res. Lab., McGill Univ., Dec. 1965.
129. Green, J. E.: The Prediction of Turbulent Boundary Layer Development in Compressible Flow. J. Fluid Mech., vol. 31, pt. 4, Mar. 18, 1968, pp. 753-778.
130. Miller, Leonard D.: Predicting Turbulent Compressible Boundary Layers in Strong Adverse Pressure Gradients. J. Spacecr. & Rockets, vol. 5, no. 8, Aug. 1968, pp. 959-963.
131. Michel, Roger; Quémard, Claude; and Cousteix, Jean: Practical Method for Prediction of Two- and Three-Dimensional Turbulent Boundary Layers. Rech. Aérop., no. 1, Jan.-Feb. 1972, pp. 1-14.
132. Johnson, Charles B.; and Boney, Lillian R.: A Simple Integral Method for the Calculation of Real-Gas Turbulent Boundary Layers With Variable Edge Entropy. NASA TN D-6217, 1971.
133. Pinckney, S. Z.: Method for Predicting Compressible Turbulent Boundary Layers in Adverse Pressure Gradients. NASA TM X-2302, 1971.
134. Green, J. E.: Application of Head's Entrainment Method to the Prediction of Turbulent Boundary Layers and Wakes in Compressible Flow. Tech. Rep. 72079, British R.A.E., June 1972.
135. Green, J. E.; Weeks, D. J.; and Brooman, J. W. F.: Prediction of Turbulent Boundary Layers and Wakes in Compressible Flow by a Lag-Entrainment Method. Tech. Rep. 72231, British R.A.E., Jan. 1973.
136. Stewartson, K.: Correlated Incompressible and Compressible Boundary Layers. Proc. Roy. Soc. (London), ser. A, vol. 200, no. A1060, Dec. 22, 1949, pp. 84-100.
137. Ludwig, H.; and Tillmann, W.: Investigations of the Wall-Shearing Stress in Turbulent Boundary Layers. NACA TM 1285, 1950.
138. Pasiuk, Lionel; Hastings, Samuel M.; and Chatham, Rodney: Experimental Reynolds Analogy Factor for a Compressible Turbulent Boundary Layer With a Pressure Gradient. NOL TR 64-200, U.S. Naval Ordnance Lab. (White Oak, Md.), Nov. 27, 1964.

139. Lewis, J. E.; Gran, R. L.; and Kubota, T.: An Experiment on the Adiabatic Compressible Turbulent Boundary Layer in Adverse and Favourable Pressure Gradients. *J. Fluid Mech.*, vol. 51, pt. 4, Feb. 22, 1972, pp. 657-672.
140. Von Kármán, Th.: The Analogy Between Fluid Friction and Heat Transfer. *ASME Trans.*, vol. 61, no. 8, Nov. 1939, pp. 705-710.
141. Stroud, John F.; and Miller, Leonard D.: An Experimental and Analytical Investigation of Hypersonic Inlet Boundary Layers. Volume I. AFFDL-TR-65-123, Vol. I, U.S. Air Force, Aug. 1965. (Available from DDC as AD 621 343.)
142. Harris, Julius E.: Numerical Solution of the Equations for Compressible Laminar, Transitional, and Turbulent Boundary Layers and Comparisons With Experimental Data. NASA TR R-368, 1971.
143. Carr, Lawrence W.; and Fox, Herbert: Numerical Solution of the Turbulent Boundary Layer. ARL 68-0215, U.S. Air Force, Dec. 1968. (Available from DDC as AD 685 240.)
144. Martellucci, A.; Rie, H.; and Sontowski, J. F.: Evaluation of Several Eddy Viscosity Models Through Comparison With Measurements in Hypersonic Flows. AIAA Paper No. 69-688, June 1969.
145. Sontowski, J. F.: An Eddy Viscosity Model for Compressible Turbulent Boundary Layers. Tech. Inform. Ser. No. 69SD241, Re-Entry Systems, General Electric Co., July 1969.
146. Miner, E. W.; Anderson, E. C.; and Lewis, Clark H.: A Computer Program for Two-Dimensional and Axisymmetric Nonreacting Perfect Gas and Equilibrium Chemically Reacting Laminar, Transitional and/or Turbulent Boundary Layer Flows. VPI-E-71-8, May 1971. (Available as NASA CR-132601.)
147. Shang, J. S.: Computation of Hypersonic Turbulent Boundary Layers With Heat Transfer. AIAA Paper No. 73-699, July 1973.
148. Omori, Satoaki: Calculation of Eddy Viscosity in a Compressible Turbulent Boundary Layer With Mass Injection and Chemical Reaction. Volumes I and II. NASA CR-129019, 1973.
149. Levine, Jay N.: Transpiration and Film Cooling Boundary Layer Computer Program. Volume I - Numerical Solutions of the Turbulent Boundary Layer Equations With Equilibrium Chemistry. NASA CR-125683, 1971.
150. Gloss, Roger J.: Transpiration and Film Cooling Boundary Layer Computer Program. Volume II - Computer Program and User's Manual. NASA CR-126728, 1971.
151. Fivel, H. J.; Masek, R. V.; and Mockapetris, L. J.: Analytical Comparison of Hypersonic Flight and Wind Tunnel Viscous/Inviscid Flow Fields. NASA CR-2489, 1975.

152. Dwyer, H. A.; Doss, E. D.; and Goldman, A. L.: A Computer Program for the Calculation of Laminar and Turbulent Boundary Layer Flows. NASA CR-114366, [1972].
153. Waiter, S. A.; and LeBlanc, L. P.: Solution of the Equations of the Compressible Boundary Layer (Laminar, Transition, Turbulent) by an Implicit Finite Difference Technique. Rep. No. SD 69-484, Space Div., North American Rockwell Corp., Sept. 1969.
154. Adams, John C., Jr.: Eddy Viscosity-Intermittency Factor Approach to Numerical Calculation of Transitional Heating on Sharp Cones in Hypersonic Flow. AEDC-TR-70-210, U.S. Air Force, Nov. 1970.
155. Chan, Y. Y.: Turbulent Boundary-Layer Computations Based on an Extended Mixing Length Approach. AIAA J., vol. 8, no. 10, Oct. 1970, pp. 1873-1875.
156. Donaldson, Coleman duP.; and Sullivan, Roger D.: An Invariant Second-Order Closure Model of the Compressible Turbulent Boundary Layer on a Flat Plate. Contract No. NASW-2224, Aeronaut. Res. Assoc. Princeton, Inc., June 1972. (Available as NASA CR-128172.)
157. Cebeci, Tuncer; Smith, A. M. O.; and Mosinskis, G.: Calculation of Compressible Adiabatic Turbulent Boundary Layers. AIAA J., vol. 8, no. 11, Nov. 1970, pp. 1974-1982.
158. Pletcher, R. H.: Calculation Method for Compressible Turbulent Boundary Flows With Heat Transfer. AIAA J., vol. 10, no. 3, Mar. 1972, pp. 245-246.
159. Shamroth, S. J.; and McDonald, H.: Assessment of a Transitional Boundary Layer Theory at Low Hypersonic Mach Numbers. NASA CR-2131, 1972.
160. Albers, James A.; and Gregg, John L.: Computer Program for Calculating Laminar, Transitional, and Turbulent Boundary Layers for a Compressible Axisymmetric Flow. NASA TN D-7521, 1974.
161. Keller, Herbert B.; and Cebeci, Tuncer: Accurate Numerical Methods for Boundary-Layer Flows. II: Two-Dimensional Turbulent Flows. AIAA J., vol. 10, no. 9, Sept. 1972, pp. 1193-1199.
162. Wortman, Andrzej: Three-Dimensional Turbulent Boundary Layer Calculations - Exact and Simplified Solutions. AIAA Paper No. 75-854, June 1975.
163. Kendall, Robert M.; Anderson, Larry W.; and Aungier, Ronald H.: Nonsimilar Solution for Laminar and Turbulent Boundary-Layer Flows Over Ablating Surfaces. AIAA J., vol. 10, no. 9, Sept. 1972, pp. 1230-1236.
164. Kuhn, Gary D.: Calculation of Compressible, Nonadiabatic Boundary Layers in Laminar, Transitional and Turbulent Flow by the Method of Integral Relations. NASA CR-1797, 1970.

165. Deboy, Gail R.; and Abbott, Douglas E.: Examination of Turbulent Shear Models and the Prediction of Compressible Turbulent Boundary Layers by the Method of Weighted Residuals. Tech. Rep. FMTR-71-1 (NASA Grant No. NGT 15-005-005), School Mech. Eng., Purdue Univ., Jan. 1971. (Available as NASA CR-118079.)
166. Baker, A. J.: Finite Element Computational Theory for Three-Dimensional Boundary Layer Flow. AIAA Paper No. 72-108, Jan. 1972.
167. Bushnell, D. M.; and Alston, D. W.: Calculation of Compressible Adverse Pressure Gradient Turbulent Boundary Layers. AIAA J., vol. 10, no. 2, Feb. 1972, pp. 229-230.
168. Harris, Julius E.; and Morris, Dana J.: Solution of the Three-Dimensional Compressible, Laminar, and Turbulent Boundary-Layer Equations With Comparisons to Experimental Data. Proceedings of the Fourth International Conference on Numerical Methods in Fluid Dynamics, Volume 35 of Lecture Notes in Physics, Robert D. Richtmyer, ed., Springer-Verlag, 1975, pp. 204-211.
169. Cebeci, Tuncer; Smith, A. M. O.; and Wang, L. C.: A Finite-Difference Method for Calculating Compressible Laminar and Turbulent Boundary Layers. Part I. Rep. No. DAC-67131, McDonald Douglas Aircraft Co., Inc., Mar. 1969.
170. Shang, J. S.; Hankey, W. L., Jr.; and Dwoyer, D. L.: Numerical Analysis of Eddy Viscosity Models in Supersonic Turbulent Boundary Layers. AIAA J., vol. 11, no. 12, Dec. 1973, pp. 1677-1683.
171. Launder, B. E.; and Priddin, C. H.: A Comparison of Some Proposals for the Mixing Length Near a Wall. Int. J. Heat & Mass Transfer, vol. 16, no. 3, Mar. 1972, pp. 700-702.
172. Bradshaw, P. (appendix by V. C. Patel): The Strategy of Calculation Methods for Complex Turbulent Flows. I.C. Aero Rep. 73-05, Aeronaut. Dep., Imperial Coll. Sci. & Technol., Aug. 1973.
173. Jones, W. P.; and Renz, U.: Condensation From a Turbulent Stream Onto a Vertical Surface. Int. J. Heat & Mass Transfer, vol. 17, no. 9, Sept. 1974, pp. 1019-1028.
174. Van Driest, E. R.: On Turbulent Flow Near a Wall. J. Aeronaut. Sci., vol. 23, no. 11, Nov. 1956, pp. 1007-1011.
175. McDonald, H.: Mixing Length and Kinematic Eddy Viscosity in a Low Reynolds Number Boundary Layer. Rep. J214453-1, Res. Lab., United Aircraft Corp., Sept. 1970.
176. Bushnell, Dennis M.; and Morris, Dana J.: Shear-Stress, Eddy-Viscosity, and Mixing-Length Distributions in Hypersonic Turbulent Boundary Layers. NASA TM X-2310, 1971.

177. Horstman, C. C.; and Owen, F. K.: Turbulent Properties of a Compressible Boundary Layer. AIAA J., vol. 10, no. 11, Nov. 1972, pp. 1418-1424.
178. Michel, Roger; Quémard, Claude; and Durant, Roland: Application of a Mixing Length Scheme to the Study of Equilibrium Turbulent Boundary Layers. NASA TT F-13,463, 1971.
179. Huffman, G. David; and Bradshaw, Peter: A Note on von Kármán's Constant in Low Reynolds Number Turbulent Flows. J. Fluid Mech., vol. 53, pt. 1, May 9, 1972, pp. 45-60.
180. Cebeci, Tuncer: Variation of the Van Driest Damping Parameter With Mass Transfer. AIAA J., vol. 11, no. 2, Feb. 1973, pp. 237-238.
181. Kays, W. M.: Heat Transfer to the Transpired Turbulent Boundary Layer. Int. J. Heat & Mass Transfer, vol. 15, no. 5, May 1972, pp. 1023-1044.
182. McDonald, H.; and Fish, R. W.: Practical Calculations of Transitional Boundary Layers. Boundary Layer Effects in Turbomachines, J. Surugue, ed., AGARD-AG-164, Dec. 1972, pp. 29-53.
183. Launder, B. E.; and Jones, W. P.: On the Prediction of Laminarisation. C.P. No. 1036, British A.R.C., 1969.
184. Squire, L. C.: A Law of the Wall for Compressible Turbulent Boundary Layers With Air Injection. J. Fluid Mech., vol. 37, pt. 3, 1969, pp. 449-456.
185. Cebeci, Tuncer: Kinematic Eddy Viscosity at Low Reynolds Numbers. AIAA J., vol. 11, no. 1, Jan. 1973, pp. 102-104.
186. Baker, R. J.; and Launder, B. E.: The Turbulent Boundary Layer With Foreign Gas Injection: II - Predictions and Measurements in Severe Streamwise Pressure Gradients. Rep. No. BL/TN/A/59, Dep. Mech. Eng., Imperial Coll. Sci. & Technol., Jan. 1973.
187. Antonia, R. A.; and Luxton, R. E.: The Response of a Turbulent Boundary Layer to a Step Change in Surface Roughness. Part I. Smooth to Rough. J. Fluid Mech., vol. 48, pt. 4, Aug. 27, 1971, pp. 721-761.
188. Glowacki, W. J.; and Chi, S. W.: A Study of the Effect of Pressure Gradient on the Eddy Viscosity and Mixing Length for Incompressible Equilibrium Turbulent Boundary Layers. NOLTR-74-105, U.S. Navy, May 1974. (Available from DDC as AD 783 942.)
189. Bushnell, D. M.; Cary, A. M., Jr.; and Holley, B. B.: Mixing Length in Low Reynolds Number Compressible Turbulent Boundary Layers. AIAA J., vol. 13, no. 8, Aug. 1975, pp. 1119-1121.
190. Johnson, Charles B.; and Bushnell, Dennis M.: Power-Law Velocity-Profile-Exponent Variations With Reynolds Number, Wall Cooling, and Mach Number in a Turbulent Boundary Layer. NASA TN D-5753, 1970.

191. Escudier, M. P.: The Distribution of the Mixing Length in Turbulent Flows Near Walls. Rep. No. TWF/TN/1, Mech. Eng. Dep., Imperial Coll. Sci. & Technol., Mar. 1965.
192. Chan, Y. Y.: A Note on the Effect of Turbulent Prandtl Number Distribution on Compressible Turbulent Boundary Layers. C.A.S.I. Trans., vol. 6, no. 2, Sept. 1973, pp. 102-104.
193. Meier, H. U.; and Rotta, J. C.: Experimental and Theoretical Investigations of Temperature Distributions in Supersonic Boundary Layers. AIAA Paper No. 70-744, June-July 1970.
194. Blom, J.: Experimental Determination of the Turbulent Prandtl Number in a Developing Temperature Boundary Layer. Heat Transfer 1970, Volume II - Forced Convection, Elsevier Pub. Co. (Amsterdam), 1970.
195. Meier, H. U.; Voisinet, R. L. P.; and Gates, D. F.: Temperature Distributions Using the Law of the Wall for Compressible Flow With Variable Turbulent Prandtl Numbers. AIAA Paper No. 74-596, June 1974.
196. Simpson, R. L.; Whitten, D. G.; and Moffat, R. J.: An Experimental Study of the Turbulent Prandtl Number of Air With Injection and Suction. Int. J. Heat & Mass Transfer, vol. 13, no. 1, Jan. 1970, pp. 125-143.
197. Hopkins, Edward J.; Rubesin, Morris W.; Inouye, Mamoru; Keener, Earl R.; Mateer, George C.; and Polek, Thomas E.: Summary and Correlation of Skin-Friction and Heat-Transfer Data for a Hypersonic Turbulent Boundary Layer on Simple Shapes. NASA TN D-5089, 1969.
198. Hopkins, Edward J.; Keener, Earl R.; Polek, Thomas E.; and Dwyer, Harry A.: Hypersonic Turbulent Skin-Friction and Boundary-Layer Profiles on Nonadiabatic Flat Plates. AIAA J., vol. 10, no. 1, Jan. 1972, pp. 40-48.
199. Hironimus, G. A.: Hypersonic Shock Tunnel Experiments on the W7 Flat Plate Model - Expansion Side, Turbulent Flow and Leading Edge Transpiration Data. CAL Rep. No. AA-1952-Y-2 (Contract No. AF 33(615)-1847), U.S. Air Force, Feb. 1966.
200. Wallace, J. E.: Hypersonic Turbulent Boundary-Layer Studies at Cold Wall Conditions. Proceedings of the 1967 Heat Transfer and Fluid Mechanics Institute, Paul A. Libby, Daniel B. Olfe, and Charles W. Van Atta, eds., Stanford Univ. Press, c.1967, pp. 427-451.
201. Holden, Michael S.: An Experimental Investigation of Turbulent Boundary Layers at High Mach Number and Reynolds Numbers. NASA CR-112147, 1972.
202. Glushko, G. S.: Turbulent Boundary Layer on a Flat Plate in an Incompressible Fluid. NASA TT F-10,080, 1966.
203. Baker, R. J.; and Launder, B. E.: The Turbulent Boundary Layer With Foreign Gas Injection - I. Measurements in Zero Pressure Gradient. Int. J. Heat & Mass Transfer, vol. 17, no. 2, Feb. 1974, pp. 275-291.

204. Blackwell, B. F.; Kays, W. M.; and Moffat, R. J.: The Turbulent Boundary Layer on a Porous Plate: An Experimental Study of the Heat Transfer Behavior With Adverse Pressure Gradients. Rep. No. HMT-16 (NASA Grant NgL-05-020-134), Dep. Mech. Eng., Stanford Univ., Aug. 1972. (Also available as NASA CR-130291.)
205. Hopkins, Edward J.; and Keener, Earl R.: Pressure-Gradient Effects on Hypersonic Turbulent Skin-Friction and Boundary-Layer Profiles. AIAA J., vol. 10, no. 9, Sept. 1972, pp. 1141-1142.
206. Fiedler, H.; and Head, M. R.: Intermittency Measurements in the Turbulent Boundary Layer. J. Fluid Mech., vol. 25, pt. 4, Aug. 1966, pp. 719-735.
207. Kline, S. J.: Some Remarks on Turbulent Shear Flows. Proc. Inst. Mech. Eng. (London), vol. 180, pt. 3J, 1965-1966, pp. 222-244.
208. Fischer, M. C.; and Wagner, R. D.: Transition and Hot-Wire Measurements in Hypersonic Helium Flow. AIAA J., vol. 10, no. 10, Oct. 1972, pp. 1326-1332.
209. Bushnell, Dennis M.; Johnson, Charles B.; Harvey, William D.; and Feller, William V.: Comparison of Prediction Methods and Studies of Relaxation in Hypersonic Turbulent Nozzle-Wall Boundary Layers. NASA TN D-5433, 1969.
210. Lee, Roland E.: Evaluation of the Turbulent Transport Terms for a Two-Dimensional Nozzle Wall Boundary Layer Flow at Mach Number Five and With Pressure Gradient, Heat Transfer and Upstream Effects. Ph. D. Thesis, Catholic Univ. of America, 1973.
211. Gates, David F.: An Experimental Investigation of the Effect of Upstream Conditions on the Downstream Characteristics of Compressible Turbulent Boundary Layers. Ph. D. Thesis, Univ. of Maryland, 1973.
212. Back, L. H.; and Cuffel, R. F.: Relationship Between Temperature and Velocity Profiles in a Turbulent Boundary Layer Along a Supersonic Nozzle With Heat Transfer. AIAA J., vol. 8, no. 11, Nov. 1970, pp. 2066-2069.
213. Squire, L. C.; and Verma, V. K.: The Calculation of Compressible Turbulent Boundary Layers With Fluid Injection. C.P. No. 1265, British A.R.C., 1973.
214. Landis, Raymond B.: The Prediction of Compressible Turbulent Boundary-Layers Flows With Mass Addition. Paper No. 72-HT-58, American Soc. Mech. Eng., Aug. 1972.
215. Rubesin, Morris W.: The Influence of Surface Injection on Heat Transfer and Skin Friction Associated With the High-Speed Turbulent Boundary Layer. NACA RM A55L13, 1956.

216. Danberg, James E.: Characteristics of the Turbulent Boundary Layer With Heat and Mass Transfer at $M = 6.7$. NOL TR 64-99, U.S. Navy, Oct. 19, 1964. (Available from DDC as AD 452 471.)
217. Bushnell, D. M.; Watson, R. D.; and Holley, B. B.: Mach Number and Reynolds Number Effects on Skin Friction Reduction by Injection. J. Spacecr. & Rockets, vol. 12, no. 8, Aug. 1975, pp. 506-508.
218. Dhawan, S.; and Narasimha, R.: Some Properties of Boundary Layer Flow During the Transition From Laminar to Turbulent Motion. J. Fluid Mech., vol. 3, pt. 4, Jan. 1958, pp. 418-436.
219. Masaki, M.; and Yakura, J. K.: Transitional Boundary Layer Considerations for the Heating Analyses of Lifting Reentry Vehicles. AIAA Paper No. 68-1155, Dec. 1968.
220. Morkovin, Mark V.: Critical Evaluation of Transition From Laminar to Turbulent Shear Layers With Emphasis on Hypersonically Traveling Bodies. AFFDL-TR-68-149, U.S. Air Force, Mar. 1969. (Available from DDC as AD 686 178.)
221. Mayne, Arloe W., Jr.; and Dyer, D. F.: Comparisons of Theory and Experiment for Turbulent Boundary Layers on Simple Shapes at Hypersonic Conditions. Proceedings of the 1970 Heat Transfer and Fluid Mechanics Institute, Turgut Sarpkaya, ed., Stanford Univ. Press, 1970, pp. 168-188.
222. Bradshaw, P.: Effects of Streamline Curvature on Turbulent Flow. AGARDograph No. 169, Aug. 1973.
223. Mayne, Arloe W., Jr.: A Method for Computing Boundary-Layer Flows, Including Normal Pressure Gradient and Longitudinal Curvature Effects. AEDC-TR-75-21, U.S. Air Force, Apr. 1975. (Available from DDC as AD A008 739.)
224. Sturek, Walter B.: Compressible Turbulent Boundary Layer Computations for Flow With Longitudinal Curvature. BRL Mem. Rep. No. 2457, U.S. Army, Mar. 1975. (Available from DDC as AD A009 703.)
225. Meroney, R. N.: Measurements of Turbulent Boundary Layer Growth Over a Longitudinally Curved Surface. Proj. THEMIS Tech. Rep. No. 25, U.S. Navy, Jan. 1974. (Available from DDC as AD 777 455.)
226. Bradshaw, P.: The Effect of Mean Compression or Dilatation on the Turbulence Structure of Supersonic Boundary Layers. J. Fluid Mech., vol. 63, pt. 3, Apr. 29, 1974, pp. 449-464.
227. Dvorak, F. A.: Calculation of Turbulent Boundary Layers and Wall Jets Over Curved Surfaces. AIAA J., vol. 11, no. 4, Apr. 1973, pp. 517-524.
228. Baldwin, B. S.; and Rose, W. C.: Calculation of Shock-Separated Turbulent Boundary Layers. Aerodynamic Analyses Requiring Advanced Computers - Part I, NASA SP-347, 1975, pp. 401-417.

229. Wolfshtein, M.; Naot, D.; and Lin, A.: Models of Turbulence. Rep. ME-746(N), Ben-Gurion Univ. Negev (Israel), June 1974.
230. Rotta, J. C.: Effect of Streamwise Wall Curvature on Compressible Turbulent Boundary Layers. Phys. Fluids Suppl., vol. 10, pt. II, no. 9, Sept. 1967, pp. S174-S180.
231. Wilcox, D. C.; and Alber, I. E.: A Turbulence Model for High Speed Flows. Proceedings of 23rd Heat Transfer and Fluid Mechanics Institute, Stanford Univ. Press, June 1972, pp. 231-252.
232. Osborne, C.: User's Guide to the Gibson-Spalding and Green Programs for the Calculation of Compressible Turbulent Boundary Layers With Pressure Gradient and Heat Transfer. I.C. Aero Rep. 73-01, Dep. Aeronaut., Imperial Coll. Sci. & Technol., Mar. 1973.
233. Huffman, G. David; Zimmerman, D. R.; and Bennett, W. A.: The Effect of Free-Stream Turbulence Level on Turbulent Boundary Layer Behavior. Boundary Layer Effects in Turbomachines, J. Surugue, ed., AGARD-AG-164, Dec. 1972, pp. 89-115.
234. Rose, William C.; and Murphy, John D.: Ratio of Reynolds Shear Stress to Turbulence Kinetic Energy in a Boundary Layer. Phys. Fluids, vol. 16, no. 6, June 1973, pp. 935-937.
235. Blottner, F. G.: Computational Techniques for Boundary Layers. Paper for AGARD Lecture Series 73 on Computational Methods for Inviscid and Viscous Two- and Three-Dimensional Flow Fields (Von Kármán Inst.), Feb. 17-22, 1975.
236. Flügge-Lotz, I.; and Blottner, F. G.: Computation of the Compressible Laminar Boundary-Layer Flow Including Displacement-Thickness Interaction Using Finite-Difference Methods. AFOSR 2206, U.S. Air Force, Jan. 1962.
237. Davis, R. T.; and Flügge-Lotz, I.: Laminar Compressible Flow Past Axisymmetric Blunt Bodies (Results of a Second-Order Theory). Tech. Rep. No. 143 (Grants AF-AFOSR-62-242 and AF-AFOSR-235-63), Div. Eng. Mech., Stanford Univ., Dec. 1963.
238. Kendall, Robert M.; and Bartlett, Eugene P.: Nonsimilar Solution of the Multicomponent Laminar Boundary Layer by an Integral-Matrix Method. AIAA J., vol. 6, no. 6, June 1968, pp. 1089-1097.
239. Kendall, Robert M.: An Analysis of the Coupled Chemically Reacting Boundary Layer and Charring Ablator. Part V - A General Approach to the Thermochemical Solution of Mixed Equilibrium-Nonequilibrium, Homogeneous or Heterogeneous Systems. NASA CR-1064, 1968.
240. Price, Joseph M.; and Harris, Julius E.: Computer Program for Solving Compressible Nonsimilar-Boundary-Layer Equations for Laminar, Transitional, or Turbulent Flows of a Perfect Gas. NASA TM X-2458, 1972.

241. Hixon, Barbara A.; Beckwith, Ivan E.; and Bushnell, Dennis M.: Computer Program for Compressible Laminar or Turbulent Nonsimilar Boundary Layers. NASA TM X-2140, 1971.
242. Blottner, F. G.: Finite Difference Methods of Solution of the Boundary-Layer Equations. AIAA J., vol. 18, no. 2, Feb. 1970, pp. 193-205.
243. Hunt, James L.; Bushnell, Dennis M.; and Beckwith, Ivan E.: The Compressible Turbulent Boundary Layer on a Blunt Swept Slab With and Without Leading-Edge Blowing. NASA TN D-6203, 1971.
244. Cebeci, Tuncer; Kaups, Kalle; Ramsey, Judy; and Moser, Alfred: Calculation of Three-Dimensional Compressible Laminar and Turbulent Boundary Layers - Calculation of Three-Dimensional Compressible Boundary Layers on Arbitrary Wings. Aerodynamic Analyses Requiring Advanced Computers - Part I, NASA SP-347, 1975, pp. 41-76.
245. Kendall, Robert M.; Bonnett, William S.; Nardo, Charles T.; and Abbett, Michael J.: Calculation of Three-Dimensional Compressible Laminar and Turbulent Boundary Flows - Three-Dimensional Compressible Boundary Layers of Reacting Gases Over Realistic Configurations. Aerodynamic Analyses Requiring Advanced Computers - Part I, NASA SP-347, 1975, pp. 77-99.
246. Marconi, Frank; Yaeger, Larry; and Hamilton, H. Harris: Computation of High-Speed Inviscid Flows About Real Configurations. Aerodynamic Analyses Requiring Advanced Computers - Part II, NASA SP-347, 1975, pp. 1411-1455.
247. Frieders, Michael C.; and Lewis, Clark H.: Effects of Mass Transfer Into Laminar and Turbulent Boundary Layers Over Cones at Angle of Attack. AEDC-TR-75-55, U.S. Air Force, Aug. 1975. (Available from DDC as AD A013 813.)
248. Raetz, G. S.: A Method of Calculating Three-Dimensional Laminar Boundary Layers of Steady Compressible Flows. Rep. No. NAI-58-73, Northrop Aircraft, Inc., Dec. 1957.
249. Der, Joe, Jr.: A Study of General Three-Dimensional Boundary Layer Problems by an Exact Numerical Method. AIAA Paper No. 69-138, Jan. 1969.
250. Wang, K. C.: Three-Dimensional Boundary Layer Near the Plane of Symmetry of a Spheroid at Incidence. J. Fluid Mech., vol. 43, pt. 1, Aug. 17, 1970, pp. 187-209.
251. Wang, K. C.: Three-Dimensional Laminar Boundary Layer Over Body of Revolution at Incidence. Part VI. General Methods and Results of the Case of High Incidence. AFOSR-TR-73-1045, U.S. Air Force, May 1973. (Available from DDC as AD 763 831.)
252. Dwyer, H. A.; and Sanders, B. R.: Magnus Forces on Spinning Supersonic Cones - Part I: The Boundary Layer. AIAA Paper 75-193, Jan. 1975.

253. Fannelöp, T. K.; and Humphreys, D. A.: The Solution of the Laminar and Turbulent Threedimensional Boundary Layer Equations With a Simple Finite Difference Technique. FFA Rep. 126, Aeronaut. Res. Inst. of Sweden, 1975.
254. Kitchens, Clarence W., Jr.; Gerber, Nathan; and Sedney, Raymond: Computational Implications of the Zone of Dependence Concept for Three-Dimensional Boundary Layers on a Spinning Body. BRL Rep. No. 1774, U.S. Army, Apr. 1975.
255. Mayne, Arloe Wesley, Jr.: Analysis of Laminar Boundary Layers on Right Circular Cones at Angle of Attack, Including Streamline-Swallowing Effects. Ph. D. Thesis, Univ. of Tennessee, 1972.
256. Wang, K. C.: On the Determination of the Zones of Influence and Dependence for Three-Dimensional Boundary-Layer Equations. J. Fluid Mech., vol. 48, pt. 2, July 28, 1971, pp. 397-404.
257. Kitchens, C. W., Jr.; Sedney, R.; and Gerber, N.: The Role of the Zone of Dependence Concept in Three-Dimensional Boundary-Layer Calculations. AIAA 2nd Computational Fluid Dynamics Conference, June 1975, pp. 102-112.
258. Popinski, Zenon; and Davis, R. T.: Three-Dimensional Compressible Laminar Boundary Layers on Sharp and Blunt Circular Cones at Angle of Attack. NASA CR-112316, 1973..
259. Ting, Lu: On the Initial Conditions for Boundary Layer Equations. J. Math. & Phys., vol. XLIV, no. 4, Dec. 1965, pp. 353-367.
260. Cebeci, Tuncer; Kaups, Kalle; Mosinskis, G. J.; and Rehn, J. A.: Some Problems of the Calculation of Three-Dimensional Boundary-Layer Flows on General Configurations. NASA CR-2285, 1973.
261. Blottner, F. G.; and Ellis, Molly: Three-Dimensional, Incompressible Boundary Layer on Blunt Bodies. Part I: Analysis and Results. SLA-73-0366, Sandia Corp., Apr. 1973.
262. McGowan, J. J., III; and Davis, R. T.: Development of a Numerical Method To Solve the Three-Dimensional Compressible Laminar Boundary-Layer Equations With Application to Elliptical Cones at Angle of Attack. ARL 70-0341, U.S. Air Force, Dec. 1970.
263. Vatsa, Veer Narain; and Davis, R. T.: The Use of Levy-Lees Variables in Three-Dimensional Boundary-Layer Flows. NASA CR-112315, 1973.
264. Kline, S. J.; Reynolds, W. C.; Schraub, F. A.; and Runstadler, P. W.: The Structure of Turbulent Boundary Layers. J. Fluid Mech., vol. 30, pt. 4, Dec. 22, 1967, pp. 741-773.

265. Van den Berg, B.; Elsenaar, A.; Lindhout, J. P. F.; and Wesseling, P.: Measurements in an Incompressible Three-Dimensional Turbulent Boundary Layer, Under Infinite Swept Wing Conditions, and Comparison With Theory. *J. Fluid Mech.*, vol. 70, pt. 1, July 15, 1975, pp. 127-148.
266. European Research Programme on Viscous Flows - Eurovisc Annual Report 1974. B. van den Berg, L. F. East, T. K. Fannelop, E. H. Hirschel, and R. Michel, eds., Rep. SP-74001, Natl. Aerosp. Lab. (Amsterdam), Aug. 1974.
267. Nash, John F.; and Patel, Virendra C.: Three-Dimensional Turbulent Boundary Layers. *Sci. & Business Consultants, Inc.*, 1972.
268. Hanjalić, K.; and Launder, B. E.: A Reynolds Stress Model of Turbulence and Its Application to Thin Shear Flows. *J. Fluid Mech.*, vol. 52, pt. 4, Apr. 25, 1972, pp. 609-638.
269. Bradshaw, P.: Anomalous Effects of Pressure Gradient on Supersonic Turbulent Boundary Layers. Rep. No. 72-21, Aeronaut. Dep., Imperial Coll. *Sci. & Technol.*, Nov. 1972.
270. Fiedler, H.: Intermittency Distributions in Turbulent Wall Boundary Layers With and Without Pressure Gradients. NASA TT F-11,326, 1967.
271. Harris, Julius E.: Calculation of Three-Dimensional Compressible Laminar and Turbulent Boundary Layers - An Implicit Finite-Difference Procedure for Solving the Three-Dimensional Compressible Laminar, Transitional, and Turbulent Boundary-Layer Equations. *Aerodynamic Analyses Requiring Advanced Computers - Part I*, NASA SP-347, 1975, pp. 19-40.
272. Klebanoff, P. S.: Characteristics of Turbulence in a Boundary Layer With Zero Pressure Gradient. NACA Rep. 1247, 1955. (Supersedes NACA TN 3178.)
273. Rotta, J. C.: Temperaturverteilungen in der turbulenten Grenzschicht and der ebenen Platte. *Int. J. of Heat & Mass Transfer.*, vol. 7, no. 2, Feb. 1964, pp. 215-228.
274. Shang, J. S.: A Parametric Study of Hypersonic Turbulent Boundary Layers With Heat Transfer. ARL TR 74-0003, U.S. Air Force, Jan. 1974. (Available from DDC as AD 778 430.)
275. Cebeci, Tuncer: A Model for Eddy-Conductivity and Turbulent Prandtl Number. Rep. No. MDC-J0747/01, McDonnell Douglas Corp., May 1970.
276. Rainbird, William John: Turbulent Boundary-Layer Growth and Separation on a Yawed Cone. *AIAA J.*, vol. 6, no. 12, Dec. 1968, pp. 2410-2416.
277. Adams, John C., Jr.: Analysis of the Three-Dimensional Compressible Turbulent Boundary Layer on a Sharp Cone at Incidence in Supersonic and Hypersonic Flow. AEDC-TR-72-66, U.S. Air Force, June 1972. (Available from DDC as AD 743 003.)

278. Bradshaw, P.: Calculation of Three-Dimensional Turbulent Boundary Layers. *J. Fluid Mech.*, vol. 46, pt. 3, Apr. 13, 1971, pp. 417-445.
279. Cooke, J. C.; and Hall, M. G.: Boundary Layers in Three Dimensions. *Boundary Layer Problems*. Vol. 2 of *Progress in Aeronautical Sciences*, Antonio Ferri, D. Küchemann, and L. H. G. Sterne, eds., Macmillan Co., c.1962, pp. 221-282.
280. Stewartson, K.: *The Theory of Laminar Boundary Layers in Compressible Fluids*. Oxford Univ. Press, Inc., 1964.
281. Crabtree, L. F.; Küchemann, D.; and Sowerby, L.: Three-Dimensional Boundary Layers. *Laminar Boundary Layers*, L. Rosenhead, ed., Oxford Univ. Press, Inc., 1963, pp. 409-491.
282. Mager, A.: Three-Dimensional Laminar Boundary Layers. *Theory of Laminar Flows*, F. K. Moore, ed., Princeton Univ. Press, 1964, pp. 286-394.
283. Hansen, Arthur G.: Compressible, Three-Dimensional, Laminar Boundary Layers - A Survey of Current Methods of Analysis. Douglas Paper 3105, Douglas Aircraft Co., Inc., Sept. 28, 1964.
284. East, Lionel F.: Computation of Three-Dimensional Turbulent Boundary Layers. FFA TN AE-1211, Aeronaut. Res. Inst. of Sweden, Sept. 1975.
285. Bordner, G. L.; and Davis, R. T.: Compressible Three-Dimensional Laminar Boundary Layers on Cones at Incidence to Shear and Axisymmetric Wake Flows. ARL 71-0262, U.S. Air Force, Nov. 1971. (Available from DDC as AD 736 828.)
286. Davis, R. T.: The Use of Crocco Type Variables in the Solution of Boundary Layer Problems. ARL TR 74-0059, U.S. Air Force, June 1974.
287. Dwyer, Harry A.: Solution of a Three-Dimensional Boundary-Layer Flow With Separation. *AIAA J.*, vol. 6, no. 7, July 1968, pp. 1336-1342.
288. Krause, Egon: Comment on "Solution of a Three-Dimensional Boundary-Layer Flow With Separation." *AIAA J.*, vol. 7, no. 3, Mar. 1969, pp. 575-576.
289. Keller, Herbert B.: A New Difference Scheme for Parabolic Problems. *Numerical Solution of Partial Differential Equations - II*, Bert Hubbard, ed., Academic Press Inc., 1971, pp. 327-350.
290. Keller, Herbert B.; and Cebeci, Tuncer: Accurate Numerical Methods for Boundary Layer Flows. I. Two Dimensional Laminar Flows. *Proceedings of the Second International Conference on Numerical Methods in Fluid Dynamics*. Volume 8 of *Lecture Notes in Physics*, Maurice Holt, ed., Springer-Verlag, 1971, pp. 92-100.
291. East, L. F.; and Hoxey, R. P.: Low-Speed Three-Dimensional Turbulent Boundary-Layer Data. Parts 1 and 2. R. & M. No. 3653, British A.R.C., 1971.

292. Tracy, Richard R.: Hypersonic Flow Over a Yawed Circular Cone. Hypersonic Res. Proj. Mem. No. 69 (Contract No. DA-31-124-ARO(D)-33), Graduate Aeronaut. Lab., California Inst. Technol., Aug. 1973.
293. Adams, John C., Jr.: Implicit Finite-Difference Analysis of Compressible Laminar, Transitional, and Turbulent Boundary Layers Along the Windward Streamline of a Sharp Cone at Incidence. AEDC-TR-71-235, U.S. Air Force, Dec. 1971.
294. Anderson, E. C.; and Lewis, C. H.: Laminar or Turbulent Boundary-Layer Flows of Perfect Gases or Reacting Gas Mixtures in Chemical Equilibrium. NASA CR-1893, 1971.
295. Orzechowski, J. A.; and Baker, A. J.: COMOC: Three-Dimensional Boundary Region Variant. Programmer's Manual. NASA CR-132449, 1974.
296. Baker, A. J.; and Zelazny, S. W.: COMOC: Three Dimensional Boundary Region Variant. Theoretical Manual and User's Guide. NASA CR-132450, 1974.
297. Bradshaw, P.; and Ferriss, D. H.: Application of a General Method of Calculating Turbulent Shear Layers. Trans. ASME, Ser. D: J. Basic Eng., vol. 94, no. 2, June 1972, pp. 345-352.
298. Bradshaw, P.; and Unsworth, K.: An Improved Fortran Program for the Bradshaw-Ferriss-Atwell Method of Calculating Turbulent Shear Layers. I.C. Aero Rep. 74-02, Dep. Aeronaut., Imperial Coll. Sci. & Technol., Feb. 1974.
299. Beckwith, Ivan E.; and Bushnell, Dennis M.: Calculation by a Finite-Difference Method of Supersonic Turbulent Boundary Layers With Tangential Slot Injection. NASA TN D-6221, 1971.
300. Chan, Y. Y.: Compressible Turbulent Boundary Layer Computations Based on Extended Mixing Length Approach. C.A.S.I. Trans., vol. 5, no. 1, Mar. 1972, pp. 21-27.
301. Crawford, M. E.; and Kays, W. M.: STAN5 - A Program for Numerical Computation of Two-Dimensional Internal/External Boundary Layer Flows. Rep. No. HMT-23 ([Contracts] NSF GK534 and GK2201 and NASA NGR-05-020-134 and NAS 3-14336), Dep. Mech. Eng., Stanford Univ., Dec. 1975.
302. Sullivan, Roger D.: A Program To Compute the Turbulent Boundary Layer on a Rotating Cone. Working Paper No. 76-2 (Contract No. NAS 2-8014), Aeronaut. Res. Assoc. Princeton, Inc., Aug. 1976. (Available as NASA CR-151981.)
303. Fivel, H. J.; and Masek, R. V.: Analytical Comparison of Hypersonic Flight and Wind Tunnel Viscous/Inviscid Flow Fields. Check Case and Users Manual. NASA CR-132359, 1973.

304. Anderson, Larry W.; and Kendall, Robert M.: A Nonsimilar Solution for Multicomponent Reacting Laminar and Turbulent Boundary Layer Flows Including Transverse Curvature. AFWL-TR-69-106, U.S. Air Force, Mar. 1970. (Available from DDC as AD 867 904.)
305. Evans, R. Michael: Boundary Layer Integral Matrix Procedure for JANNAF Rocket Engine Performance Evaluation Methodology. BLIMP-J User's Manual. Aerotherm UM-75-64 (Contract NAS8-3093), Acurex Corp., July 1975. (Available as NASA CR-144046.)
306. Kuhn, Gary D.: FORTRAN Program for Computing Compressible Laminar, Transitional and Turbulent Boundary Layers With Arbitrary Pressure Gradients and Heat Transfer. NEAR TR 27 (Contract NAS1-9429), Nielsen Eng. & Res., Inc., Oct. 1970. (Available as NASA CR-145184.)
307. McDonald, Henry; and Fish, R. W.: Practical Calculations of Transition Boundary Layers. Int. J. Heat & Mass Transfer, vol. 16, no. 9, Sept. 1973, pp. 1729-1744.
308. Bronfin, B. R.; Cohen, L. S.; Coulter, L. J.; McDonald, H.; and Shamroth, S.: Development of Chemical Laser Computer Models. Volume 5, Parts 1 and 2: User's Manual for the MARBL Code. AFWL-TR-73-48-VOL-5-PTS-1 & 2, U.S. Air Force, July 1973. (Available from DDC as AD 912 363L and AD 912 465L.)
309. Reyhner, T. A.: A Computer Program for Finite-Difference Calculation of Compressible Turbulent Boundary Layers. Doc. No. D6-23236, Boeing Co., 1970.
310. Rie, H.: The GE-RESD Equilibrium Non-Similar Boundary Layer Program (ENSBL). Tech. Inform. Ser. No. 71SD212, General Electric Co., Feb. 1971.
311. Verma, V. K.: A Method of Calculation for Two-Dimensional and Axisymmetric Boundary Layers. CUED/A-Aero/TR3, Dep. Eng., Univ. of Cambridge, 1971.
312. Waiter, S. A.; and LeBlanc, Loyd P.: Solution of the Equations of the Compressible Boundary Layer (Laminar, Transition, Turbulent) by an Implicit Finite Difference Technique. Astronaut. Acta, vol. 16, no. 5, Nov. 1971, pp. 265-275.
313. Wilcox, David C.: Turbulence-Model Transition Predictions for Blunt-Body Flows. AFOSR-TR-74-1714, U.S. Air Force, July 1974. (Available from DDC as AD A000 575.)
314. Wortman, Andrew: Mass Transfer in Self-Similar Laminar Boundary-Layer Flows. Ph. D. Thesis, Univ. of California at Los Angeles, 1969.
315. Adams, J. C., Jr.: The Calculation of Subsonic and Transonic Turbulent Boundary Layers on an Infinite Yawed Airfoil. AIAA Paper No. 74-557, June 1974.

316. Adams, J. C., Jr.: Numerical Calculation of the Subsonic and Transonic Turbulent Boundary Layer on an Infinite Yawed Airfoil. AEDC-TR-73-112, U.S. Air Force, July 1973.
317. Baker, A. J.; Rogers, R. Clayton; and Zelazny, S. W.: Analytical Study of Mixing and Reacting Three-Dimensional Supersonic Combustor Flow Fields. Aerodynamic Analyses Requiring Advanced Computers - Part I, NASA SP-347, 1975, pp. 251-315.
318. Baker, A. J.; and Zelazny, S. W.: A Theoretical Study of Mixing Downstream of Transverse Injection Into a Supersonic Boundary Layer. NASA CR-112254, 1972.
319. Patankar, S. V.; and Spalding, D. B.: Numerical Prediction of Three-Dimensional Flows. Rep. EF/TN/A/46, Dep. Mech. Eng., Imperial Coll. Sci. & Technol., June 1972.
320. Caretto, L. S.; Curr, R. M.; and Spalding, D. B.: Two Numerical Methods for Three-Dimensional Boundary-Layers. Comput. Methods Appl. Mech. & Eng., vol. 1, no. 1, June 1972, pp. 39-57.
321. Krause, E.; Hirschel, E. H.; and Kordulla, W.: Fourth Order "Mehrestellen"-Integration for Three-Dimensional Turbulent Boundary Layers. AIAA Computational Fluid Dynamics Conference, July 1973, pp. 92-102.

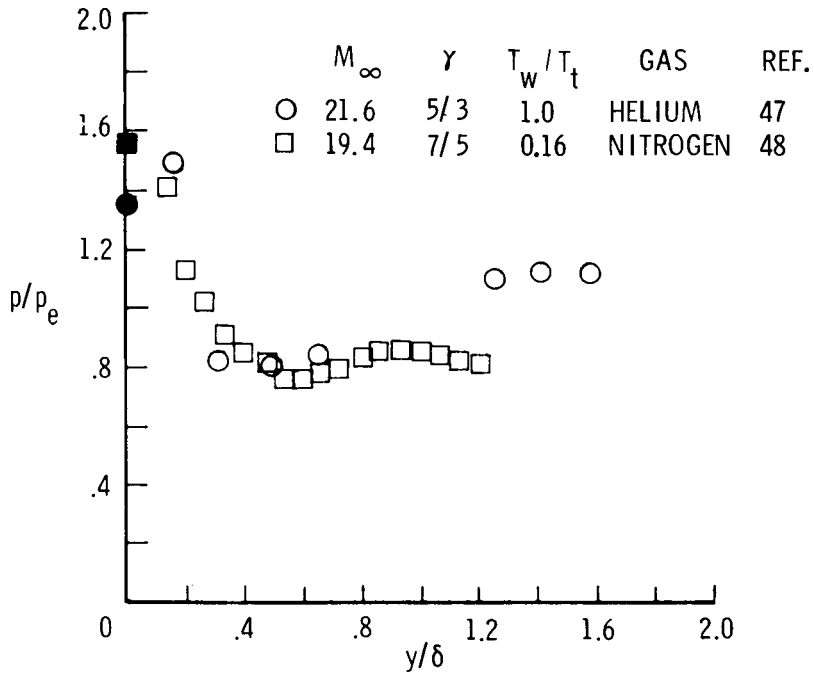


Figure 1.- Typical distribution of p with y at high Mach number.

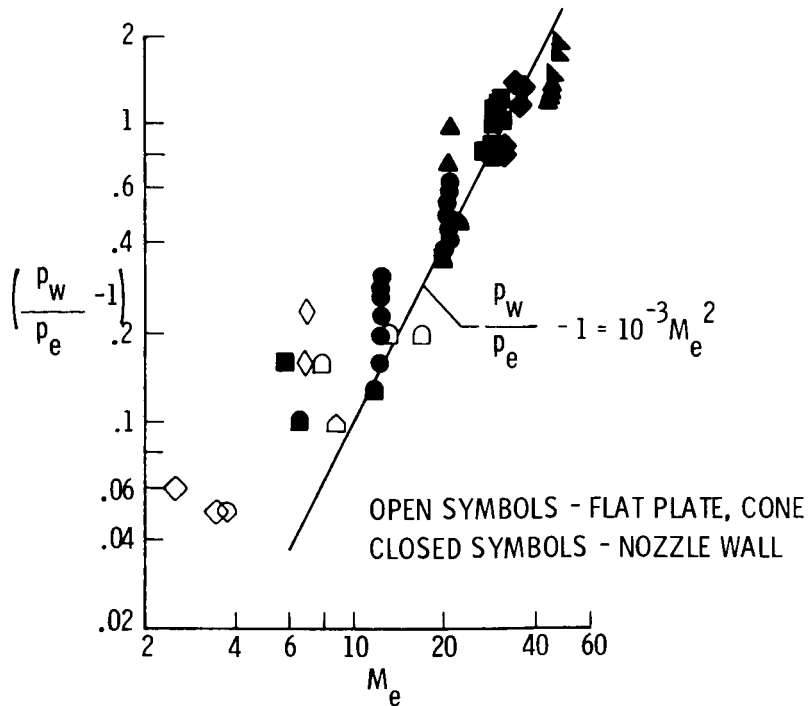


Figure 2.- Wall pressure increase at high Mach number (from ref. 50).

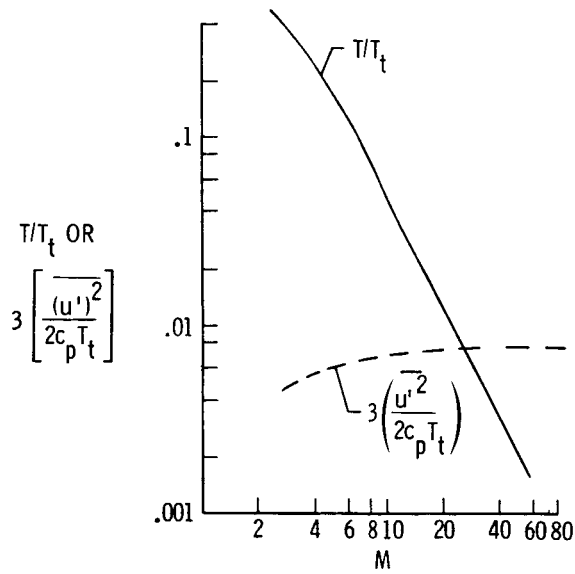
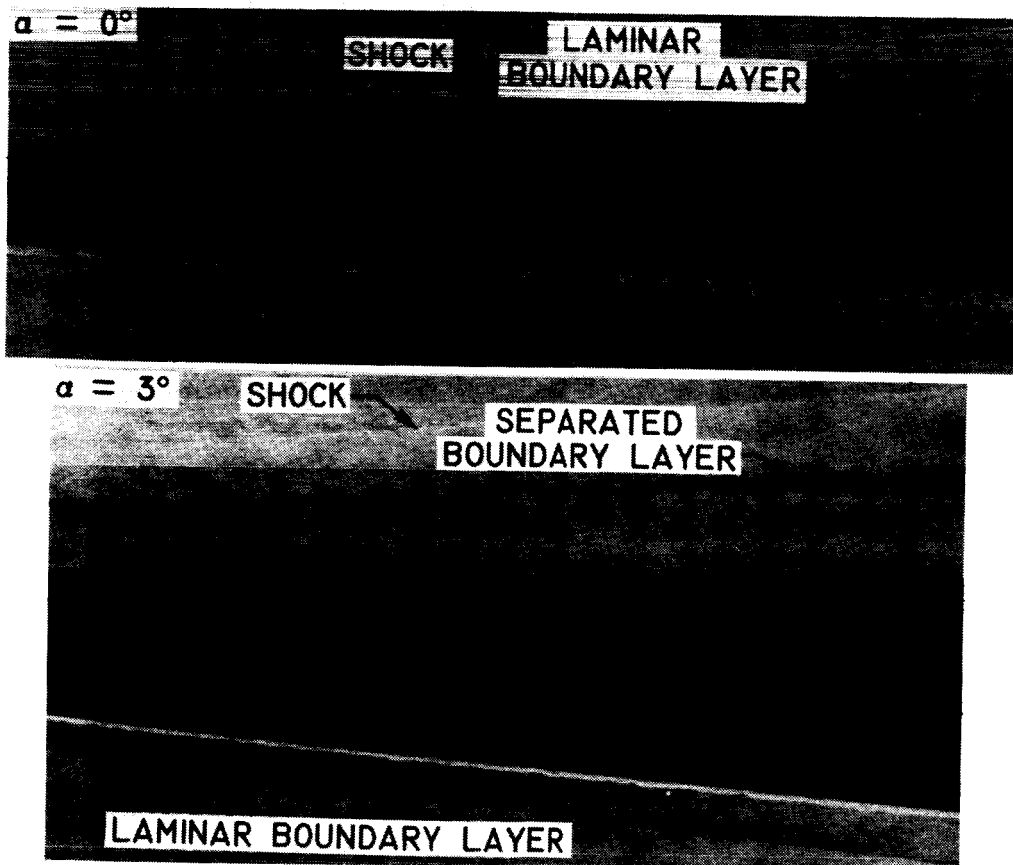


Figure 3.- Comparison of \bar{T}_{static} with $\overline{u'^2}/2c_p$ at high Mach numbers.
 $\sqrt{\overline{u'^2}}/u_e = 0.05$; $T_w/T_t \approx 1$; $\gamma = 1.4$.



L-77-169

Figure 4.- Illustration of disturbances upstream of transition.

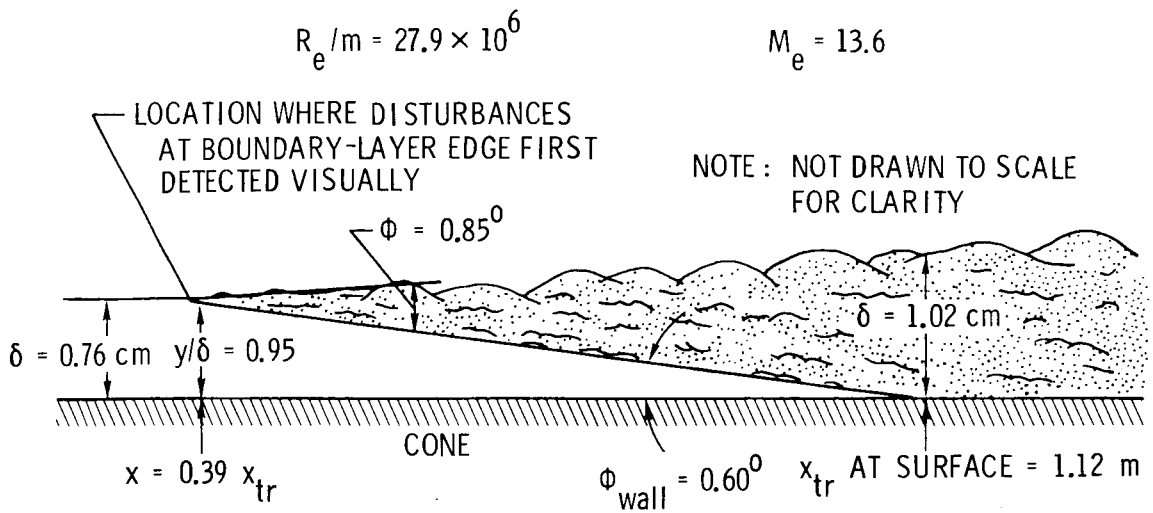
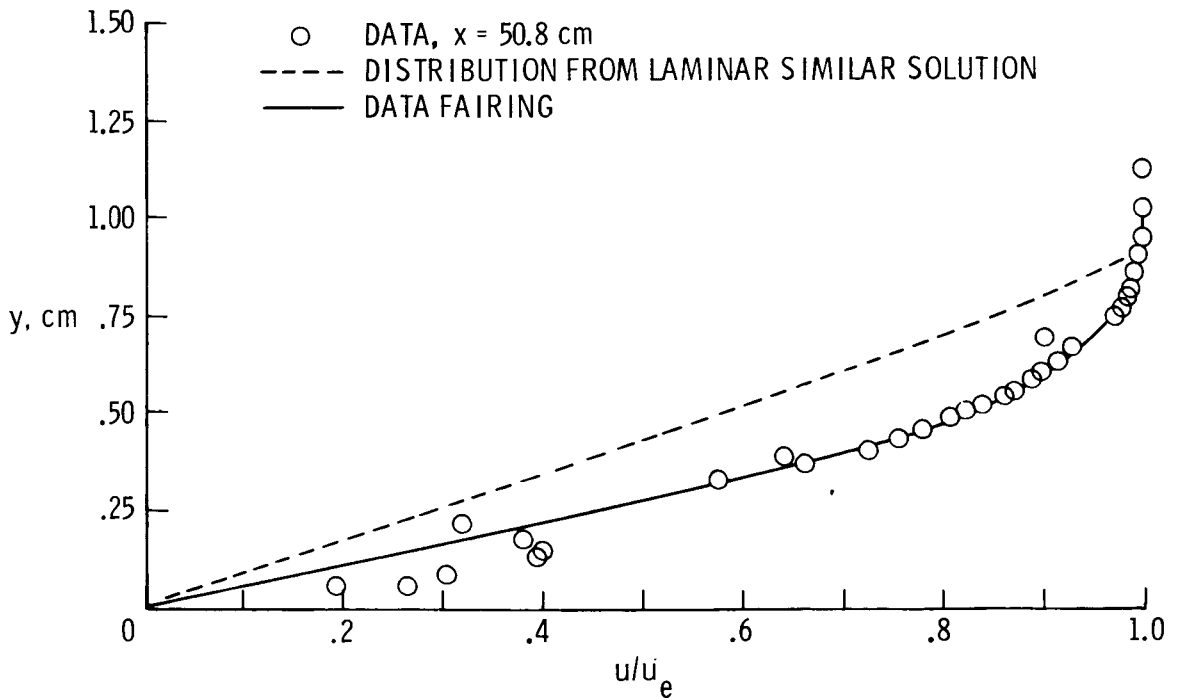


Figure 5.- Flow field schematic of precursor transition for Mach 18 cone experiments (taken from ref. 57).



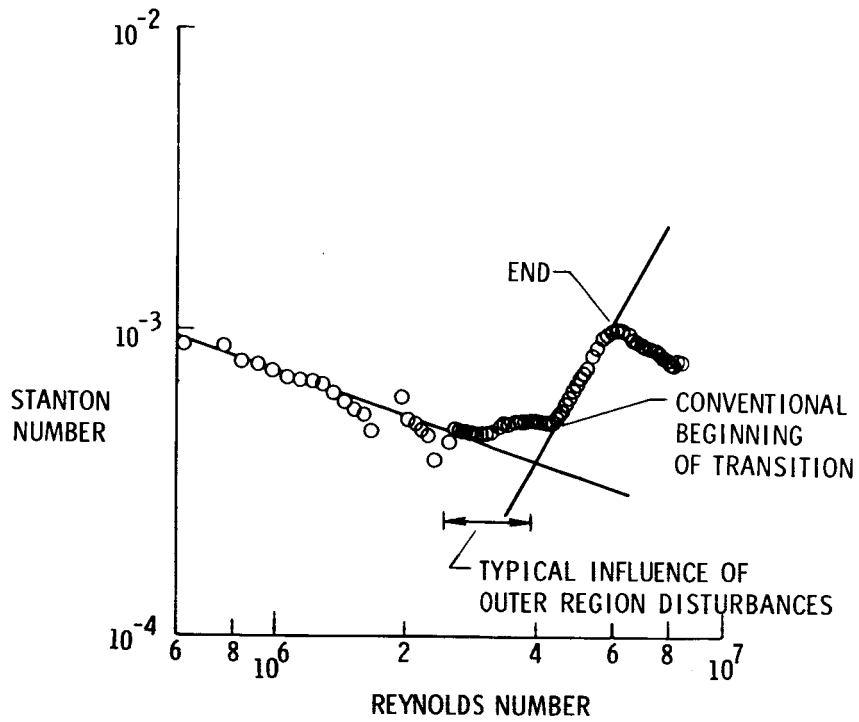


Figure 7.- Influence of precursor transition effect on wall heating (from ref. 60).

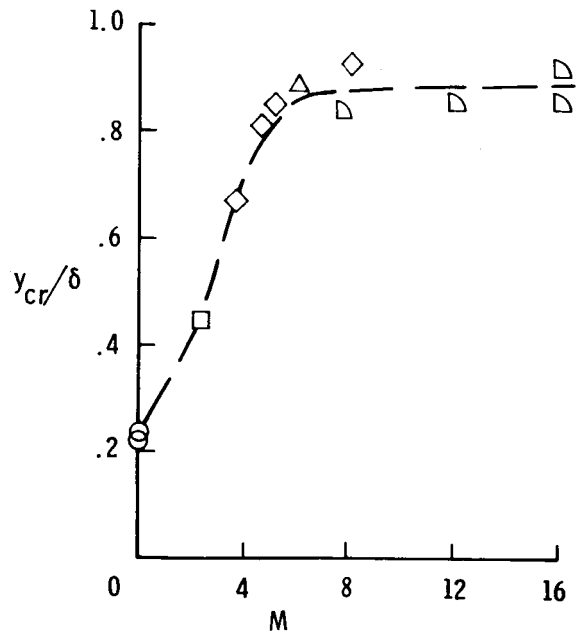


Figure 8.- Height of critical layer as function of Mach number (from ref. 62).

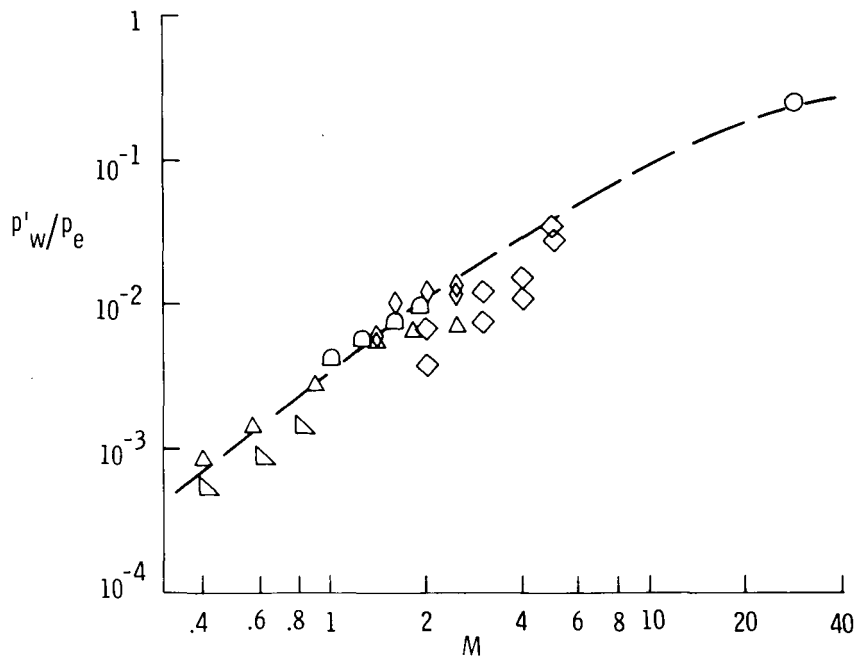


Figure 9.- Influence of Mach number on fluctuating wall pressure levels for turbulent boundary-layer flow (from ref. 47).

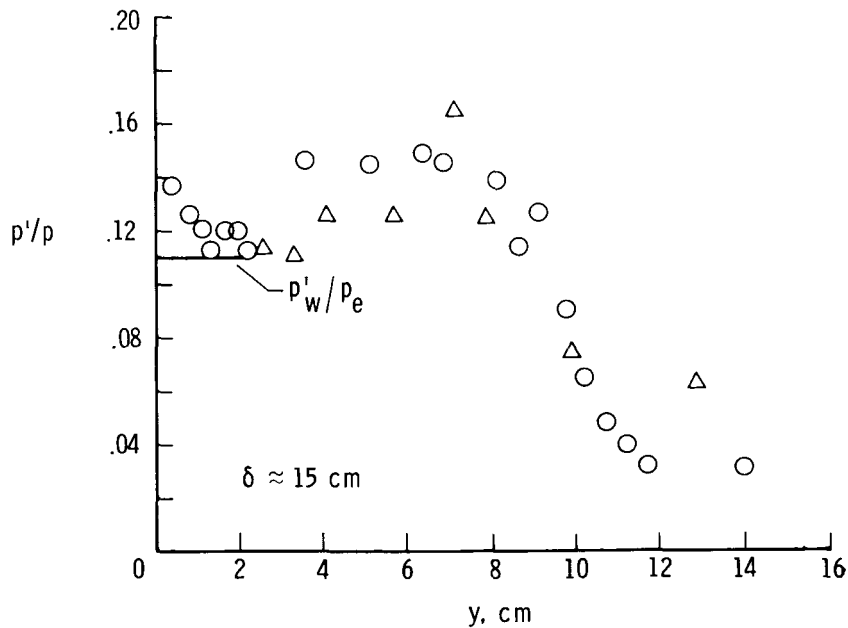


Figure 10.- Distribution of fluctuating static pressure through a turbulent boundary layer in high Mach number flow. $M_e = 9.4$; $Re_{\theta} = 36\,800$; $T_w/T_t = 0.38$. (Reprinted from ref. 62 with permission from Cambridge University Press.)

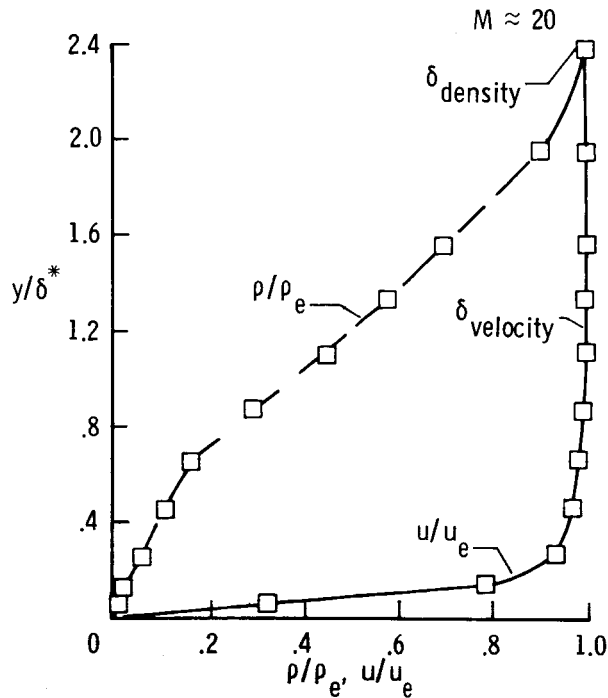
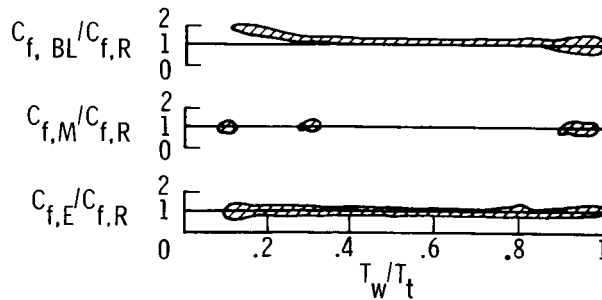


Figure 11.- Illustration of difference between pitot (or density) and velocity boundary-layer thicknesses at high Mach number (from ref. 47). δ_{density} is y-location where $\rho/\rho_e = 0.995$ and δ_{velocity} is y-location where $u/u_e = 0.995$.



$dp/dx = 0$
 $M = 2 \text{ TO } 20$
 $C_{f, BL}$ AND $C_{f, E}$ DERIVED
 FROM EXPERIMENTAL
 VELOCITY PROFILES

BL = BARONTI-LIBBY
 E = ECONOMOS-BOCCIO
 M = MEASURED/BALANCE
 R = REFERENCE

Figure 12.- Prediction of flat-plate skin friction by transformation methods of Baronti and Libby (ref. 75) and Economos and Boccio (ref. 78).

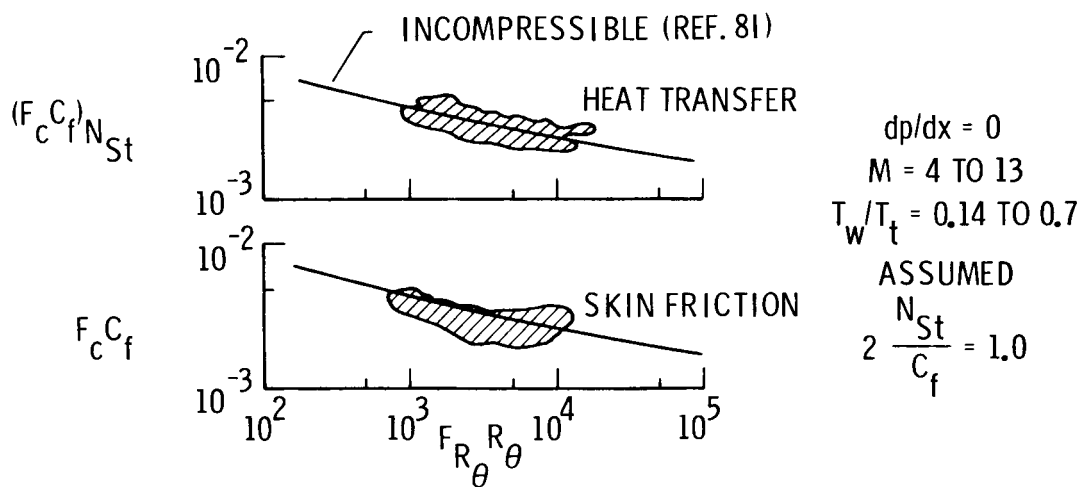
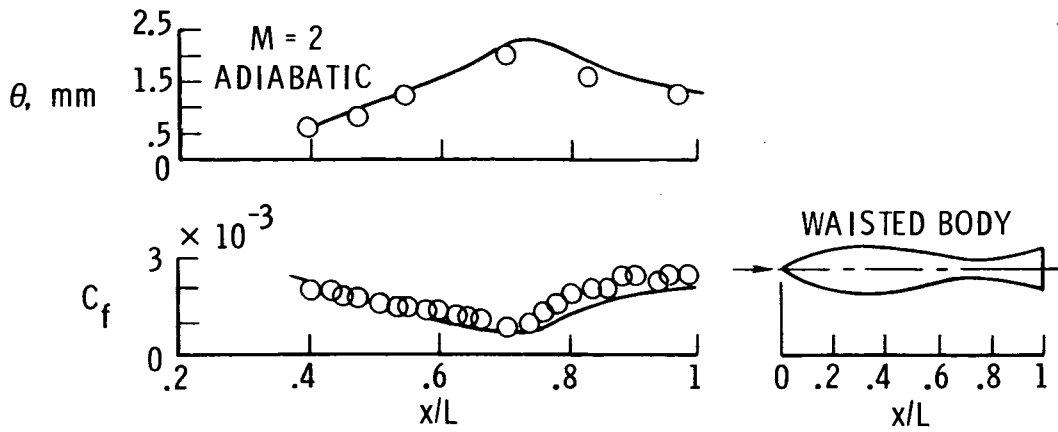
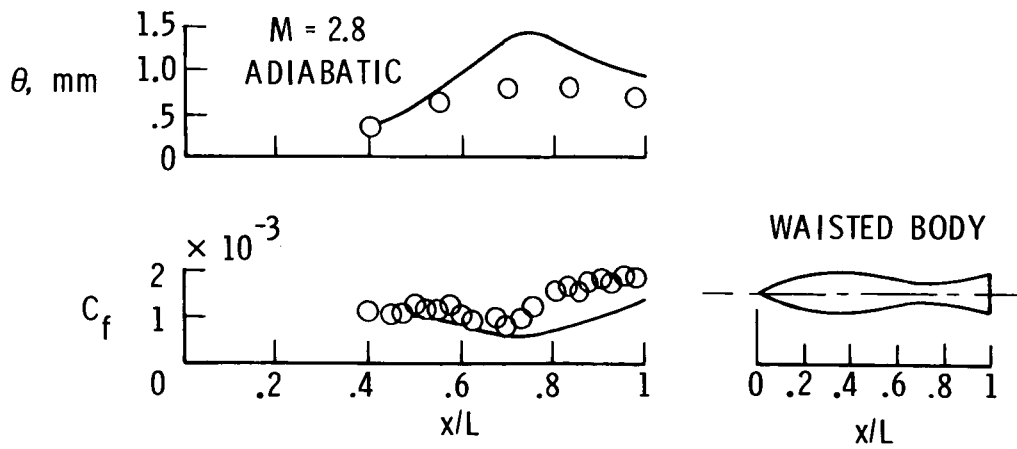


Figure 13.- Prediction of flat-plate skin friction and heating by transformation method of Coles (ref. 15).



(a) Economos and Boccio (ref. 78).



(b) Lewis et al. (ref. 77).

Figure 14.- Prediction of boundary-layer characteristics on a body of revolution (data from ref. 83).

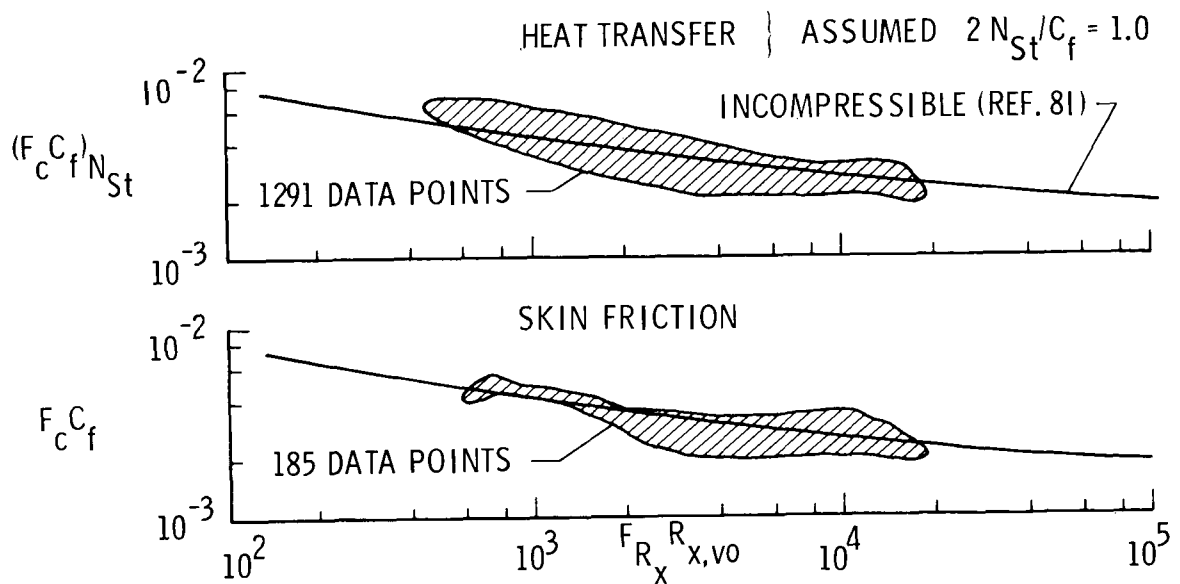


Figure 15.- Prediction of flat-plate skin friction and heating by correlation method of Van Driest (ref. 87). $M = 0$ to 10 ; $T_w/T_t = 0.14$ to 0.7 .

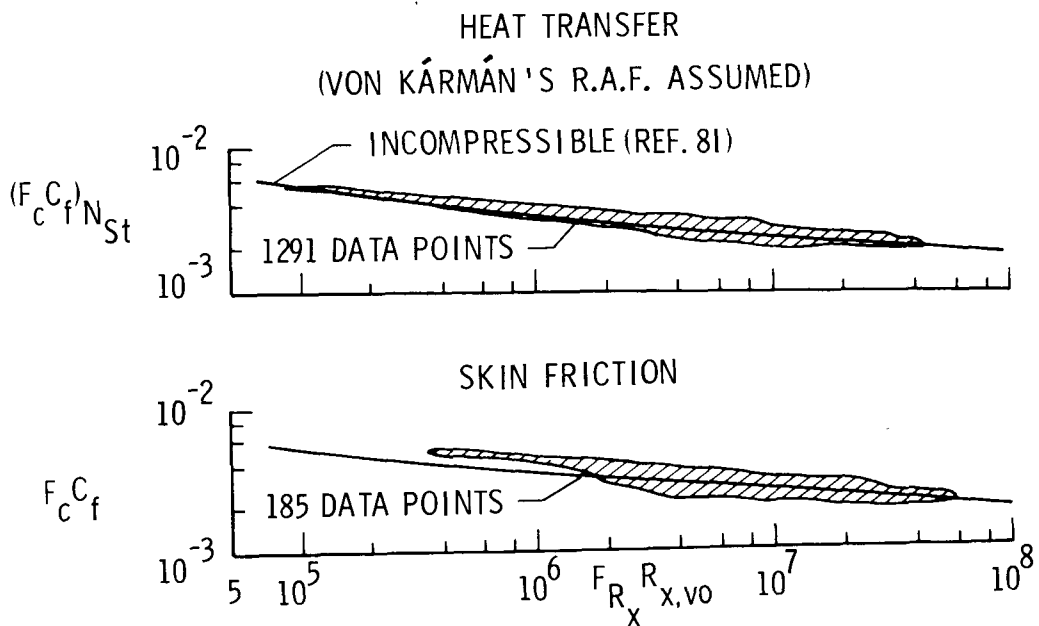


Figure 16.- Prediction of flat-plate skin friction and heating by correlation method of Spalding and Chi (ref. 81). $M = 0$ to 10 ; $T_w/T_t = 0.14$ to 0.7 . (R.A.F., Reynolds analogy factor.)

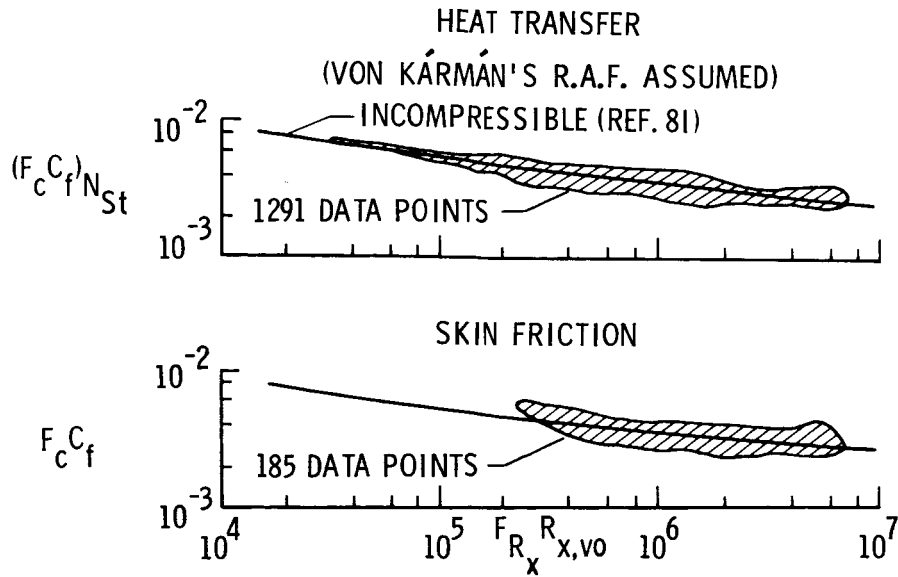


Figure 17.- Prediction of flat-plate skin friction and heating by correlation method of Eckert (ref. 72). $M = 0$ to 10 ; $T_w/T_t = 0.14$ to 0.7 . (R.A.F., Reynolds analogy factor.)

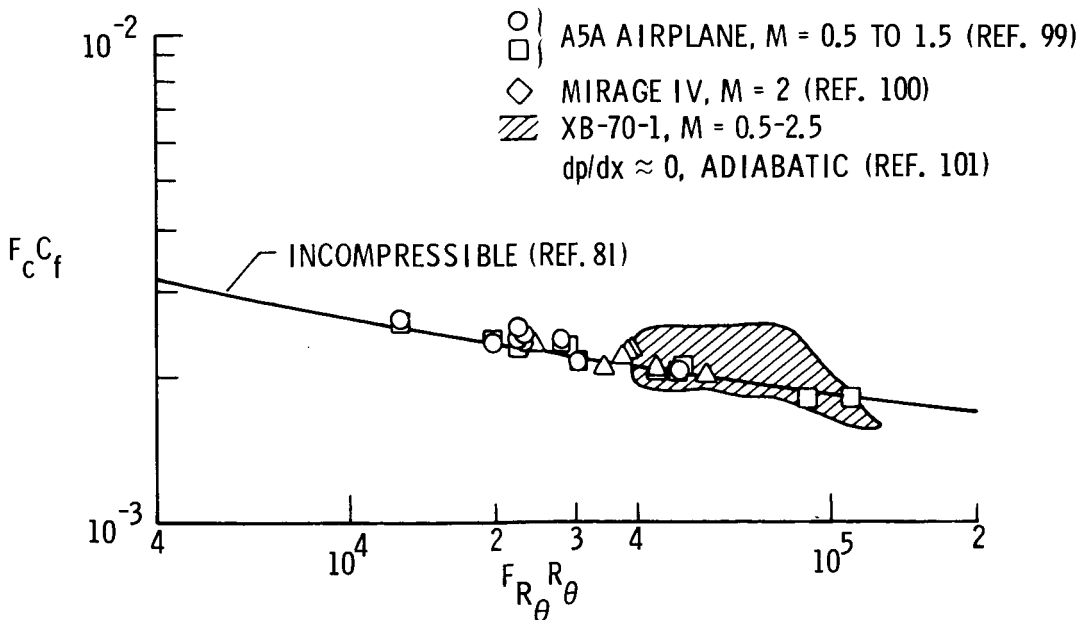


Figure 18.- Prediction of turbulent skin friction on conventional flight vehicles by Eckert's method (ref. 72).

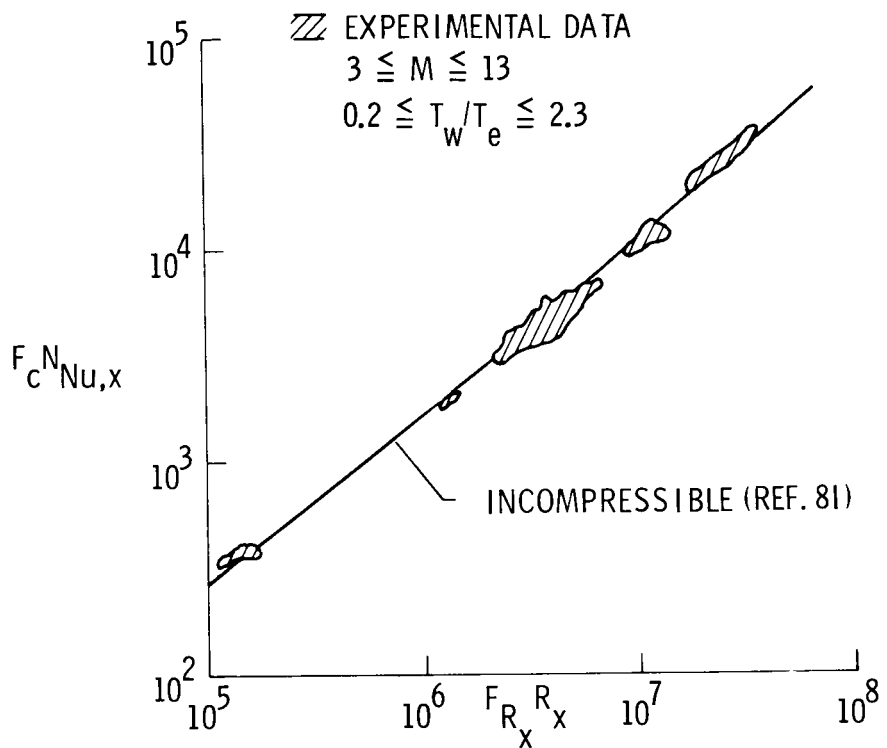
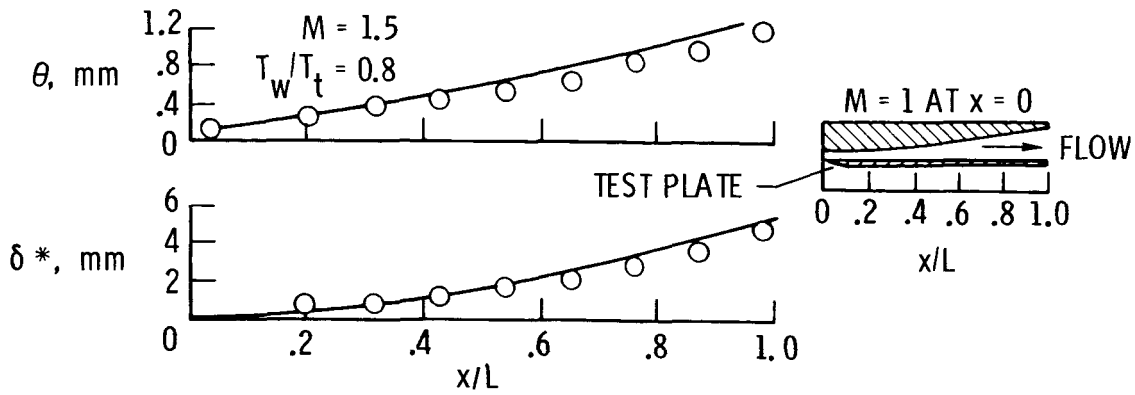
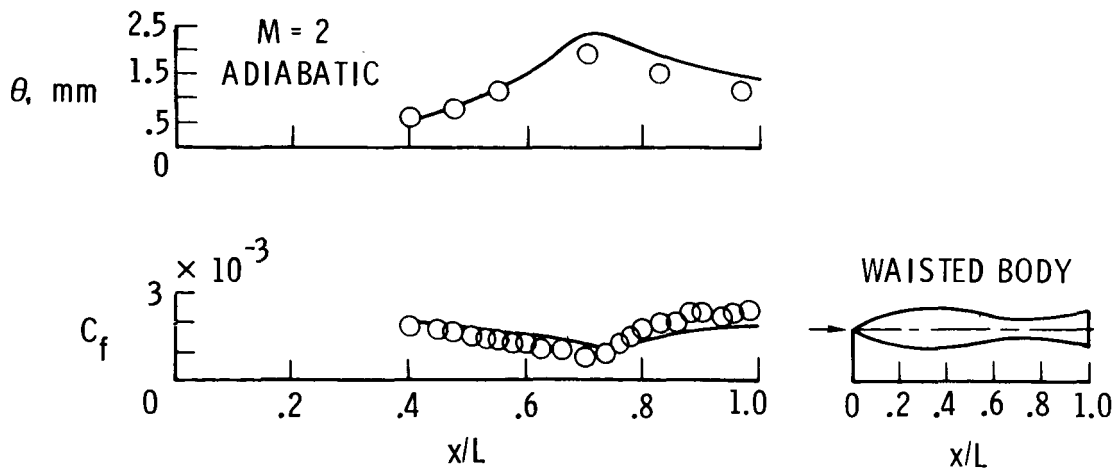


Figure 19.- Prediction of turbulent heating on sharp and blunt tipped axisymmetric bodies in flight by Eckert's method (ref. 72); data from reference 96.

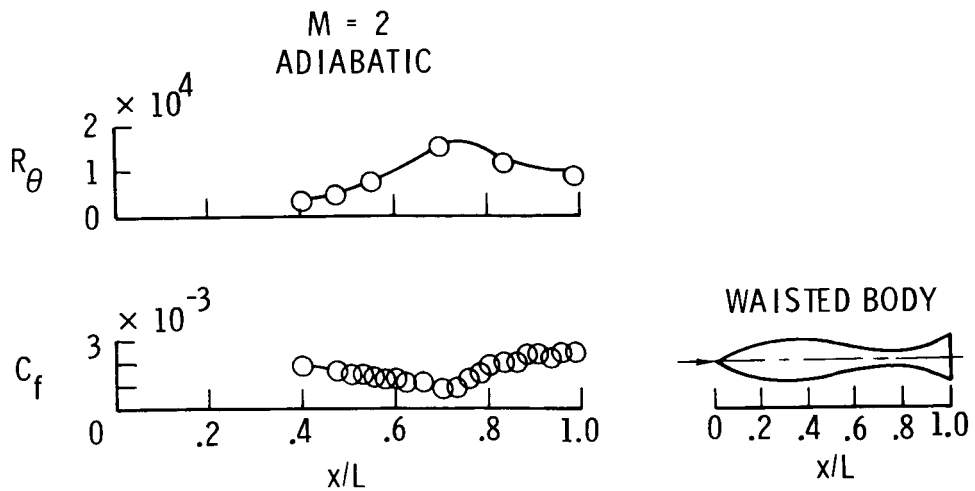


(a) Flat plate with favorable pressure gradient (experimental data from ref. 138).

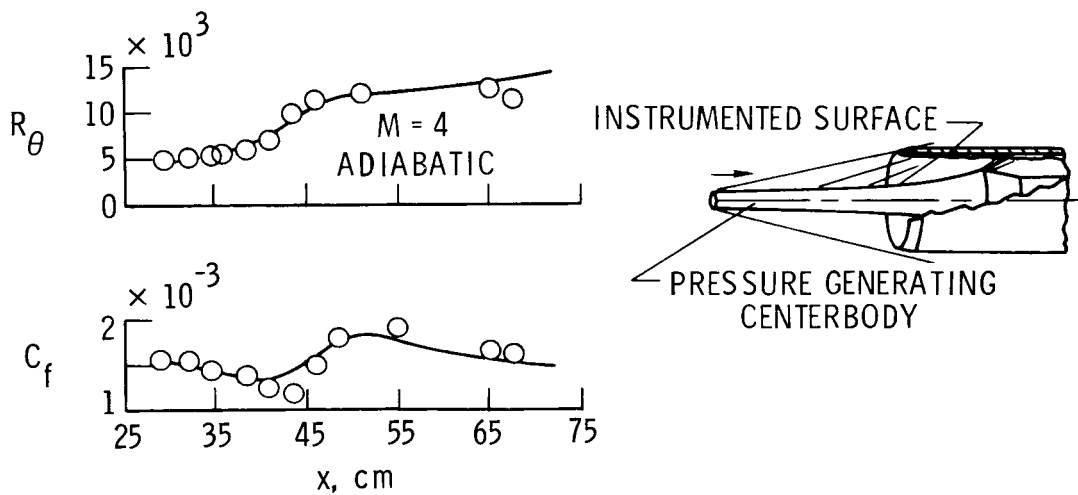


(b) Waisted body of revolution (experimental data from ref. 83).

Figure 20.- Prediction of boundary layer properties for turbulent flows with pressure gradient by Flaherty's integral method (ref. 124).



(a) Waisted body of revolution (experimental data from ref. 83).



(b) Flat cylinder (experimental data from ref. 139).

Figure 21.- Prediction of boundary-layer properties for flows with pressure gradients by Green's integral method (ref. 135).

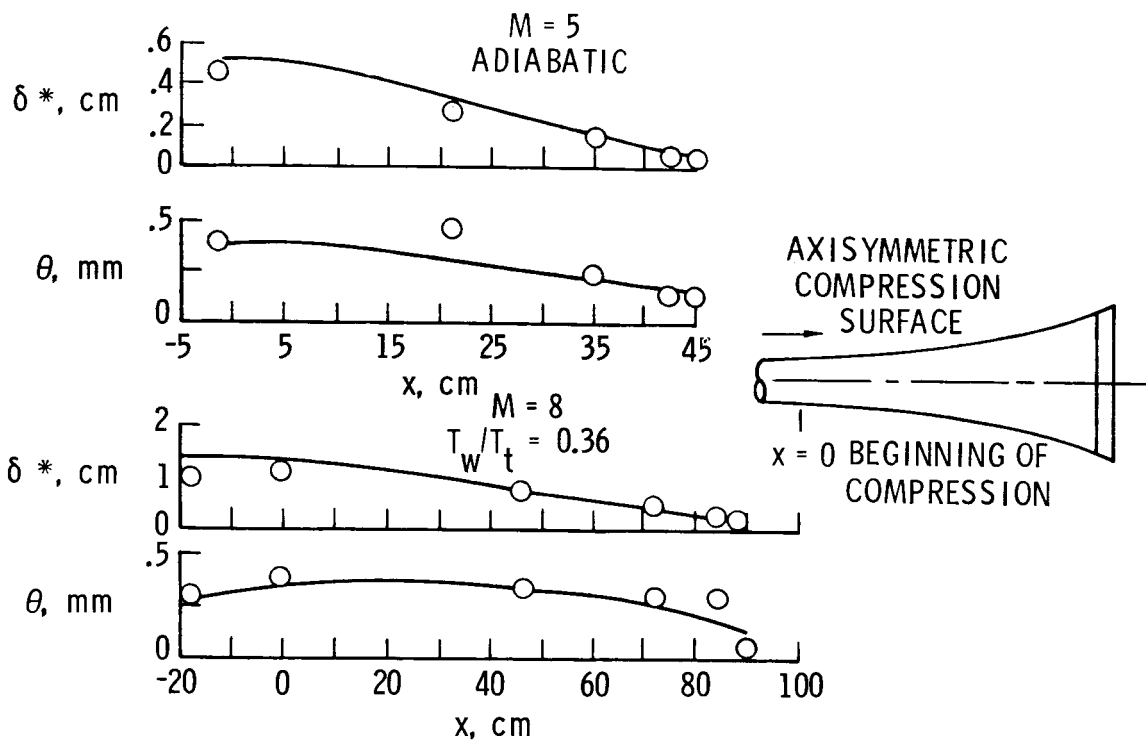
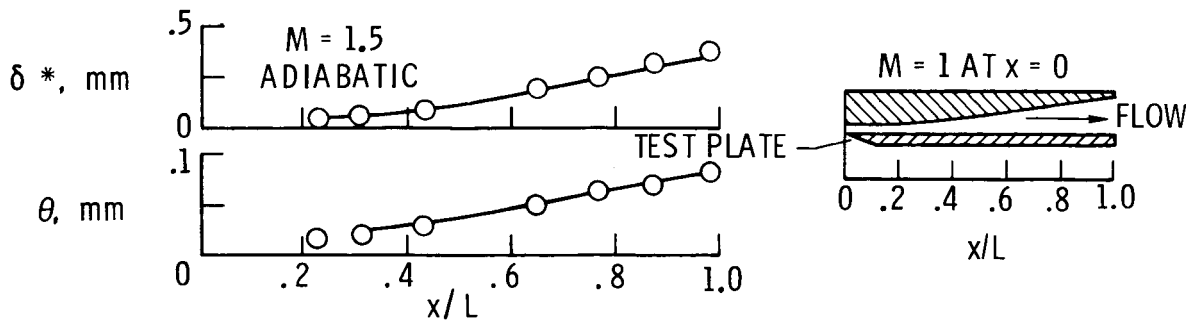
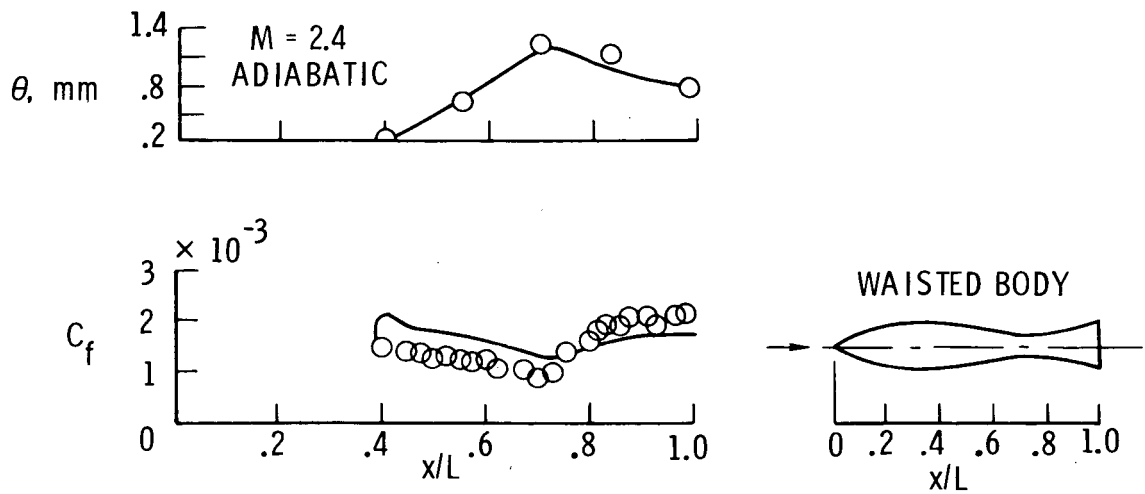


Figure 22.- Prediction of boundary-layer development on a concave surface by Pinckney's integral method (ref. 133). Experimental data from reference 141.



(a) Flat plate with favorable pressure gradient (experimental data from ref. 138).



(b) Waisted body of revolution (experimental data from ref. 83).

Figure 23.- Prediction of boundary-layer properties for flows with pressure gradient using Reeves' integral method (ref. 30, pp. 6-1 - 6-A2-2).

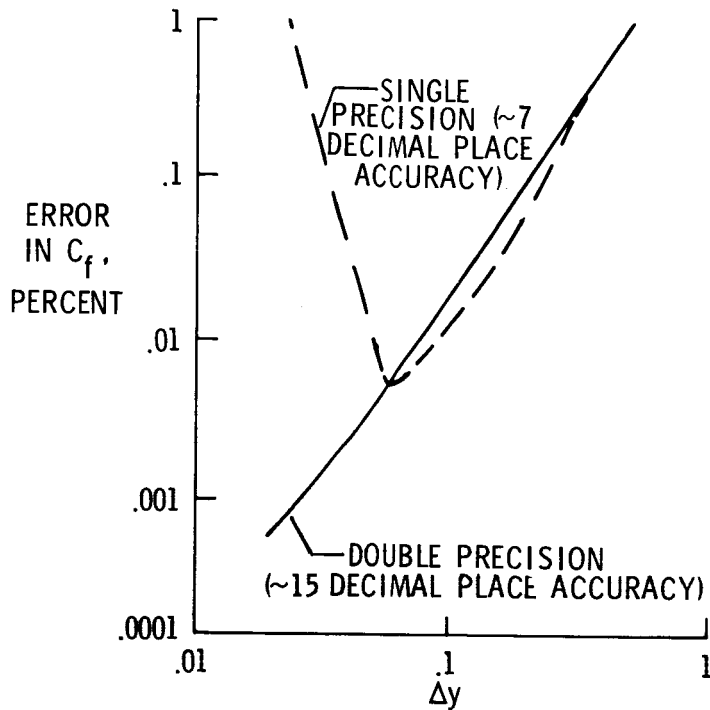


Figure 24.- Effect of grid spacing on computational error (from ref. 169).

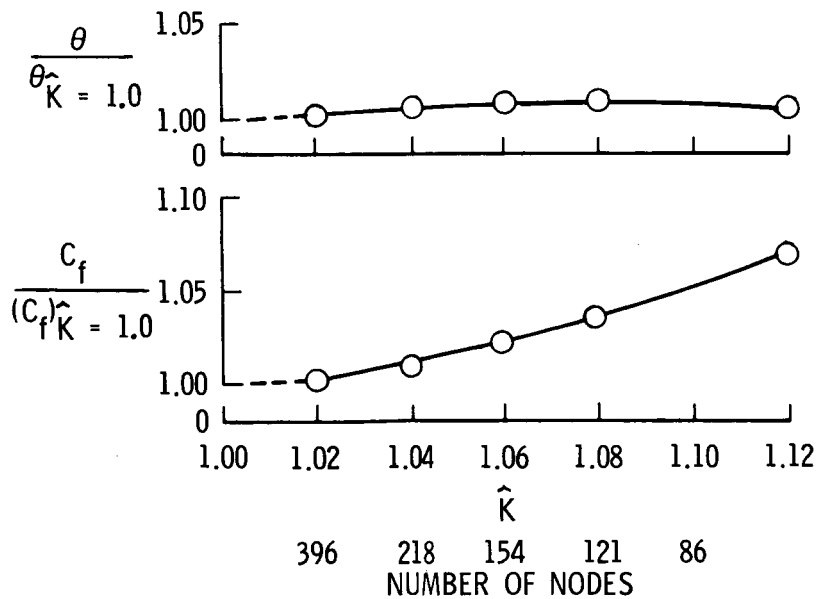


Figure 25.- Effect of variable grid spacing on calculated momentum thickness and skin friction. (Reprinted from ref. 170 with permission from the American Institute of Aeronautics and Astronautics.)

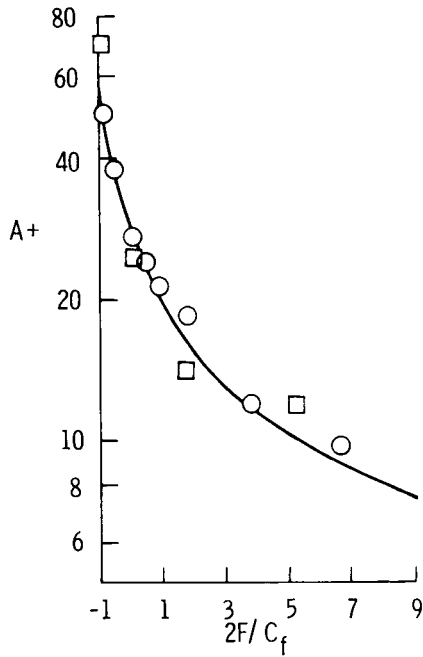


Figure 26.- Effect of wall blowing on wall damping parameter (from ref. 53).

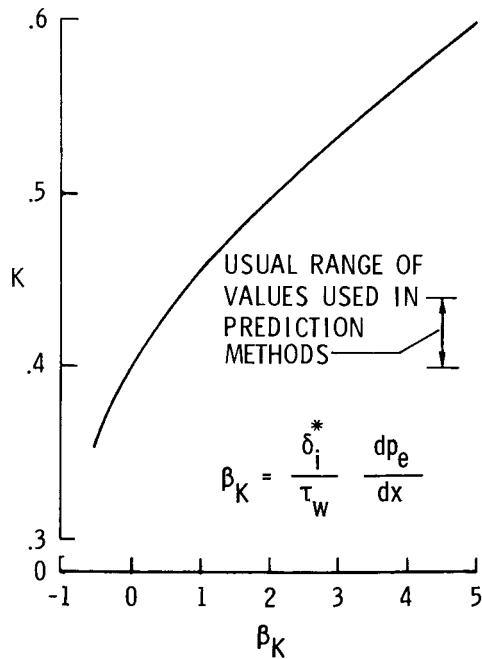


Figure 27.- Effect of dp/dx on K (from ref. 188).

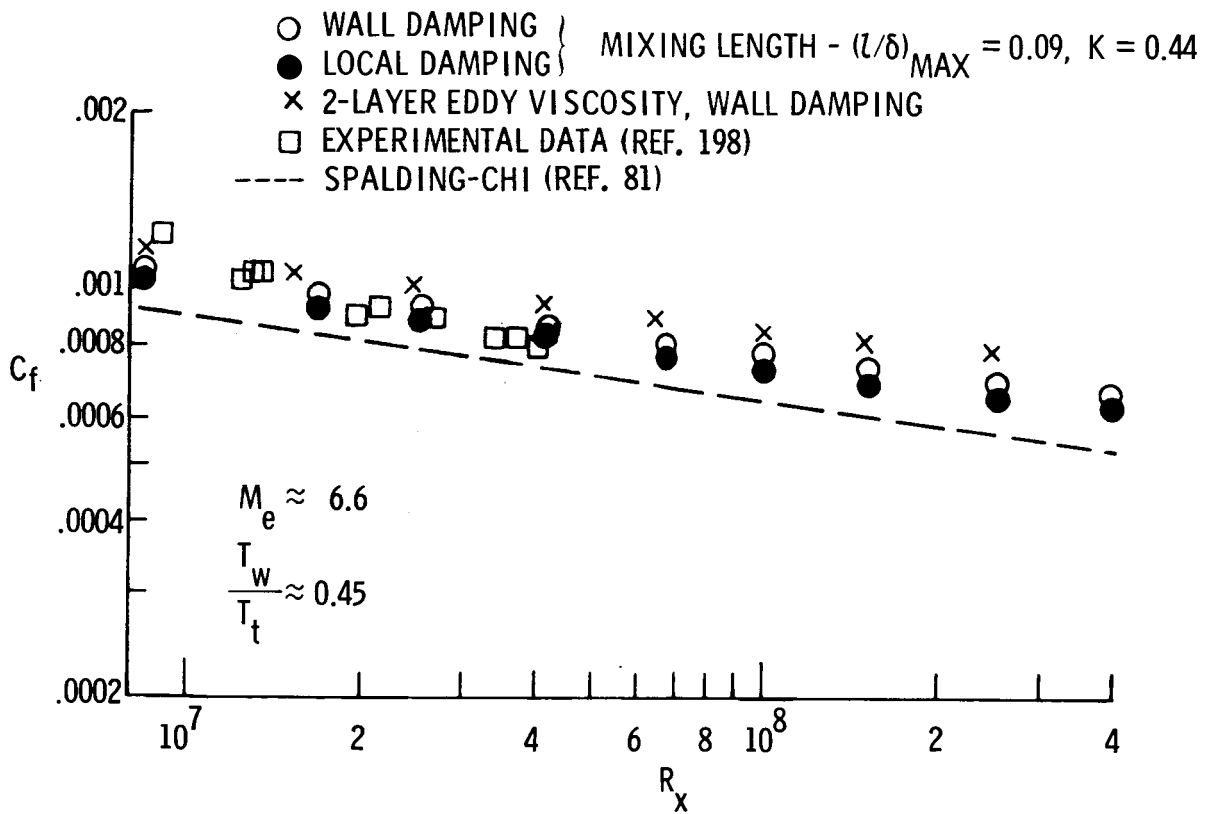
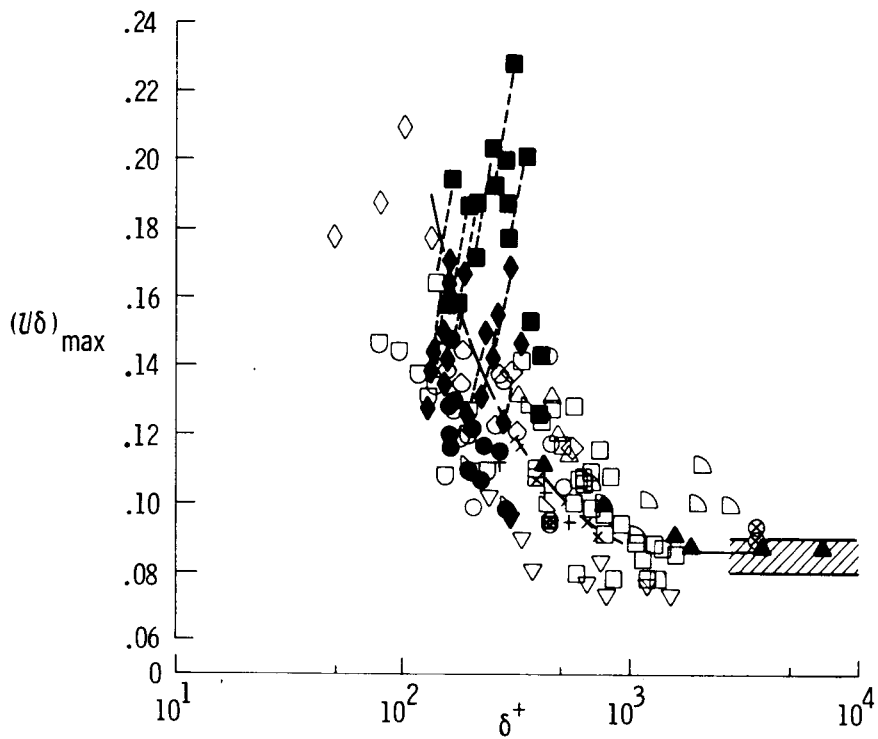
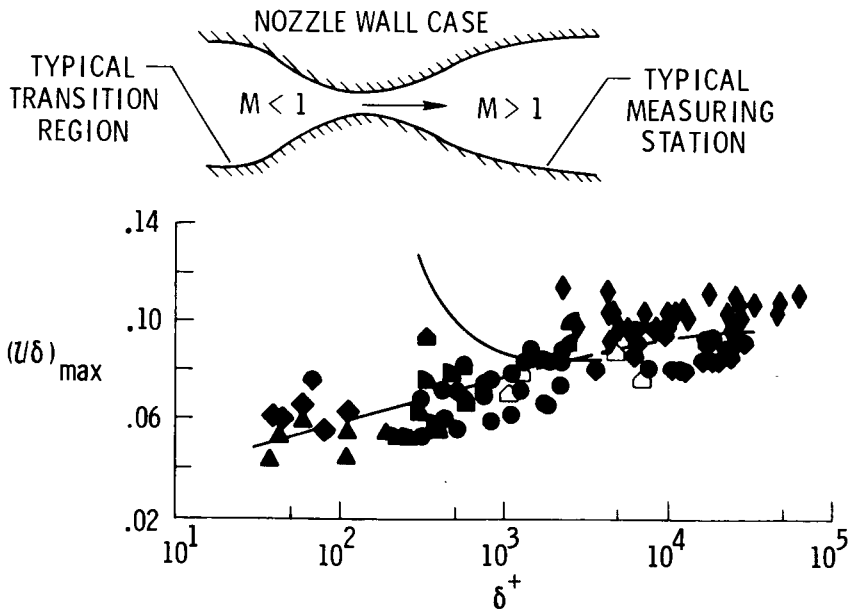


Figure 28.- Comparison of mixing length and Clauser form of eddy viscosity.



(a) Flow over plates, cones, and cylinders.



(b) Nozzle wall flow.

Figure 29.- Variation of $(u/\delta)_{\max}$ with δ^+ for various types of flow (from ref. 189).

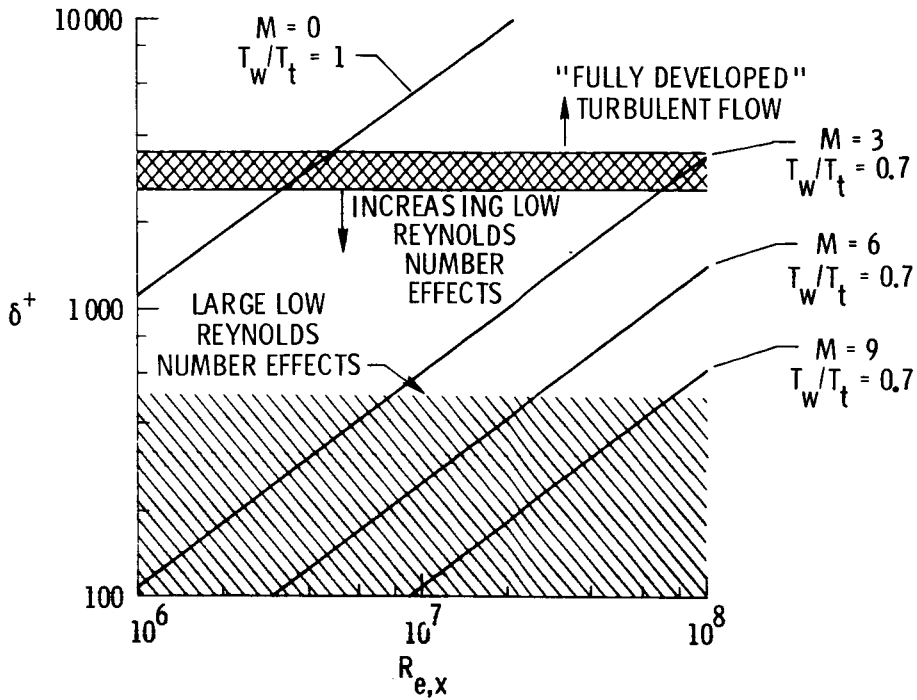


Figure 30.- Illustration of increasing importance of low Reynolds number effects at high Mach number.

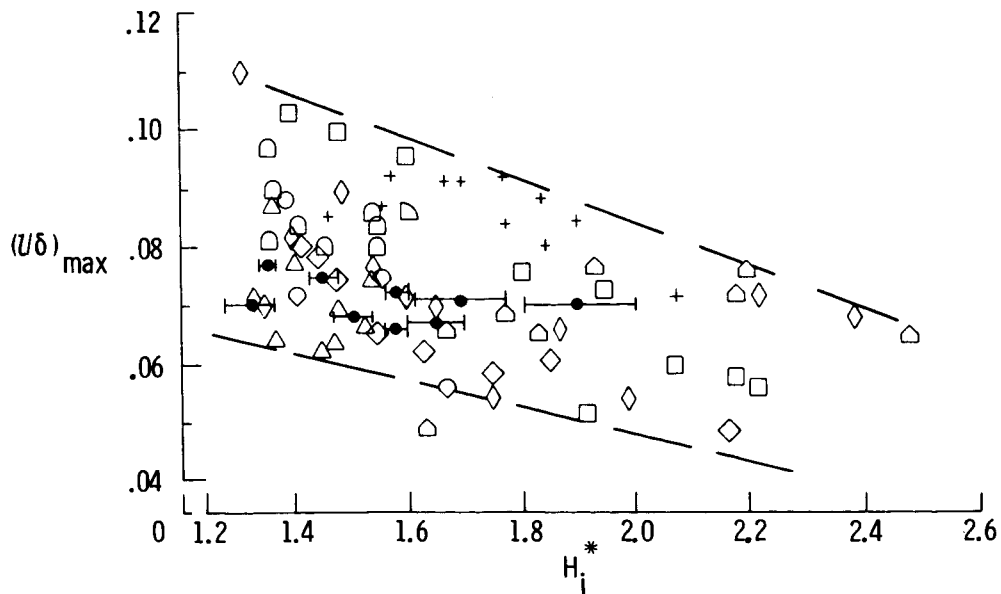


Figure 31.- Effect of wall injection and positive pressure gradient on $(1/\delta)_{\max}$ (from ref. 53).

- I MEIER AND ROTTA (REF. 193)
- II KAYS (REF. 181)
- III BLOM (REF. 194)
- IV MEIER, VOISINET, AND GATES (REF. 195)
- V SIMPSON, WHITTEN, AND MOFFAT (REF. 196)

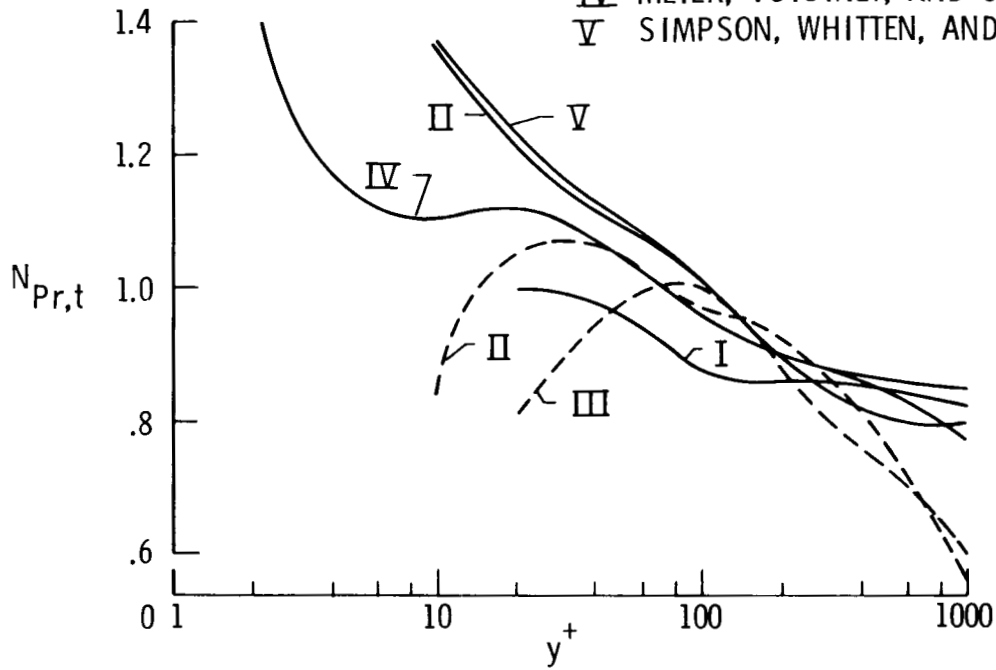


Figure 32.- Variation of turbulent Prandtl number with y^+ .

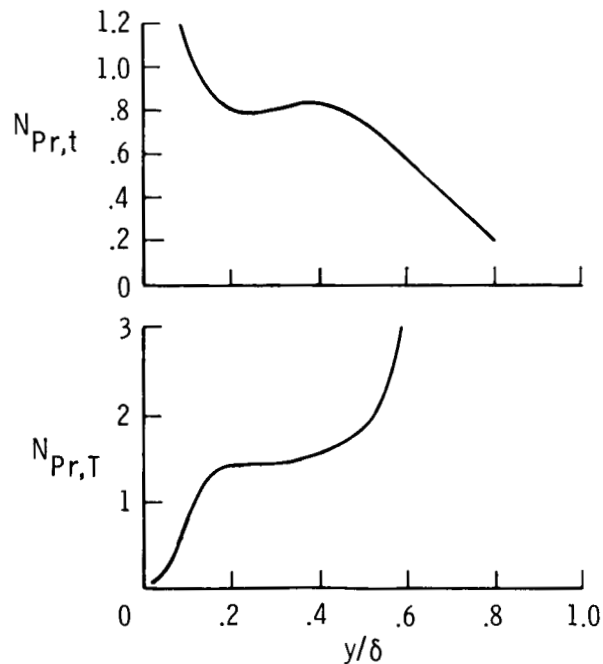


Figure 33.- Comparison of static with total turbulent Prandtl number at Mach 7.2. (Reprinted from ref. 177 with permission from the American Institute of Aeronautics and Astronautics.)

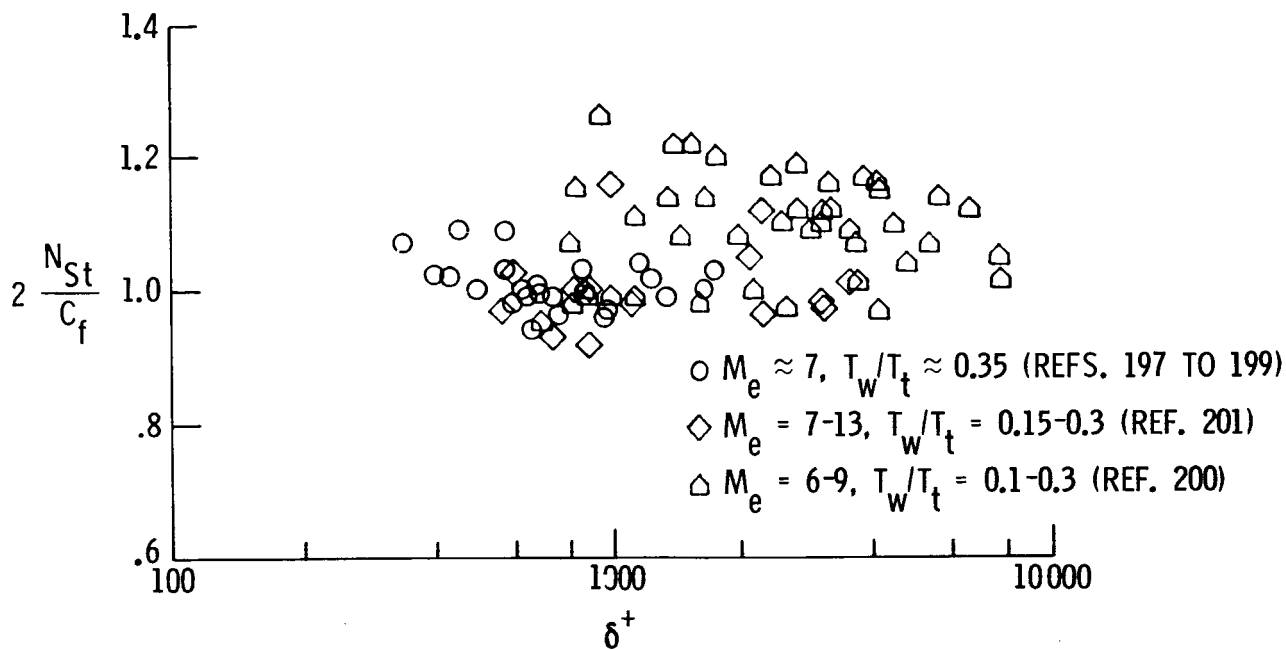


Figure 34.- Variation of Reynolds analogy factor with δ^+ .

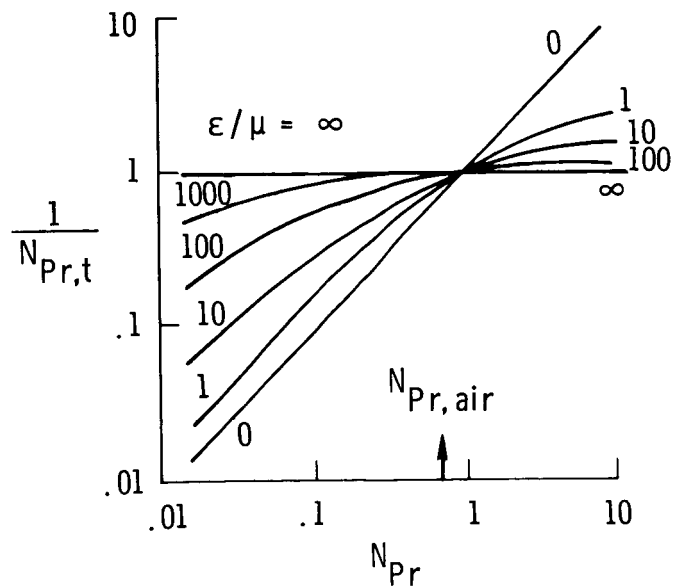


Figure 35.- Theoretical variation of turbulent Prandtl number with ϵ/μ . (Reprinted with permission from ref. 12.)

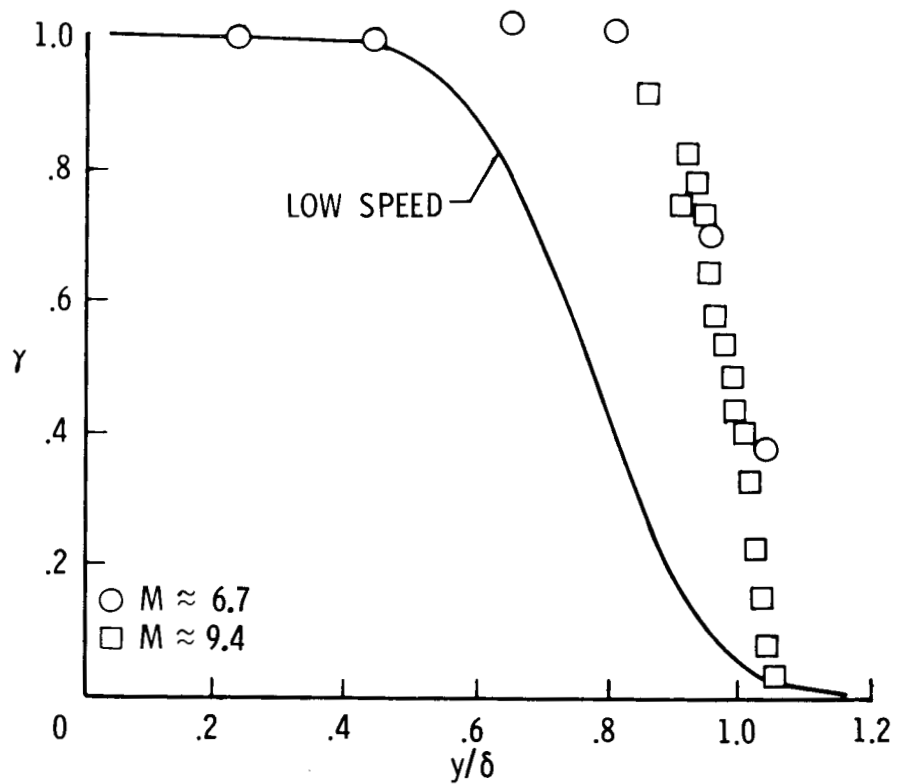


Figure 36.- Variation of normal intermittency through turbulent boundary layer up to Mach 9.4 (from ref. 25).

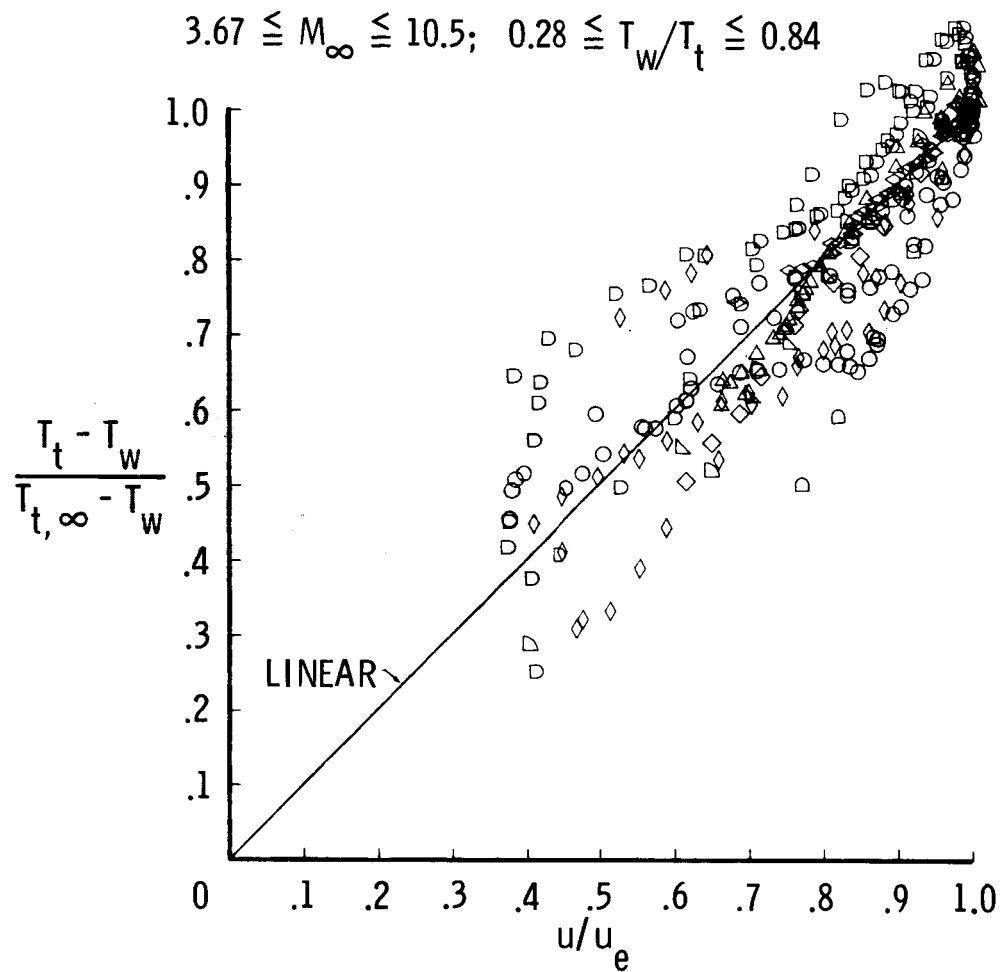


Figure 37.- Total temperature-velocity profiles for flat-plate type turbulent flow (from ref. 209).

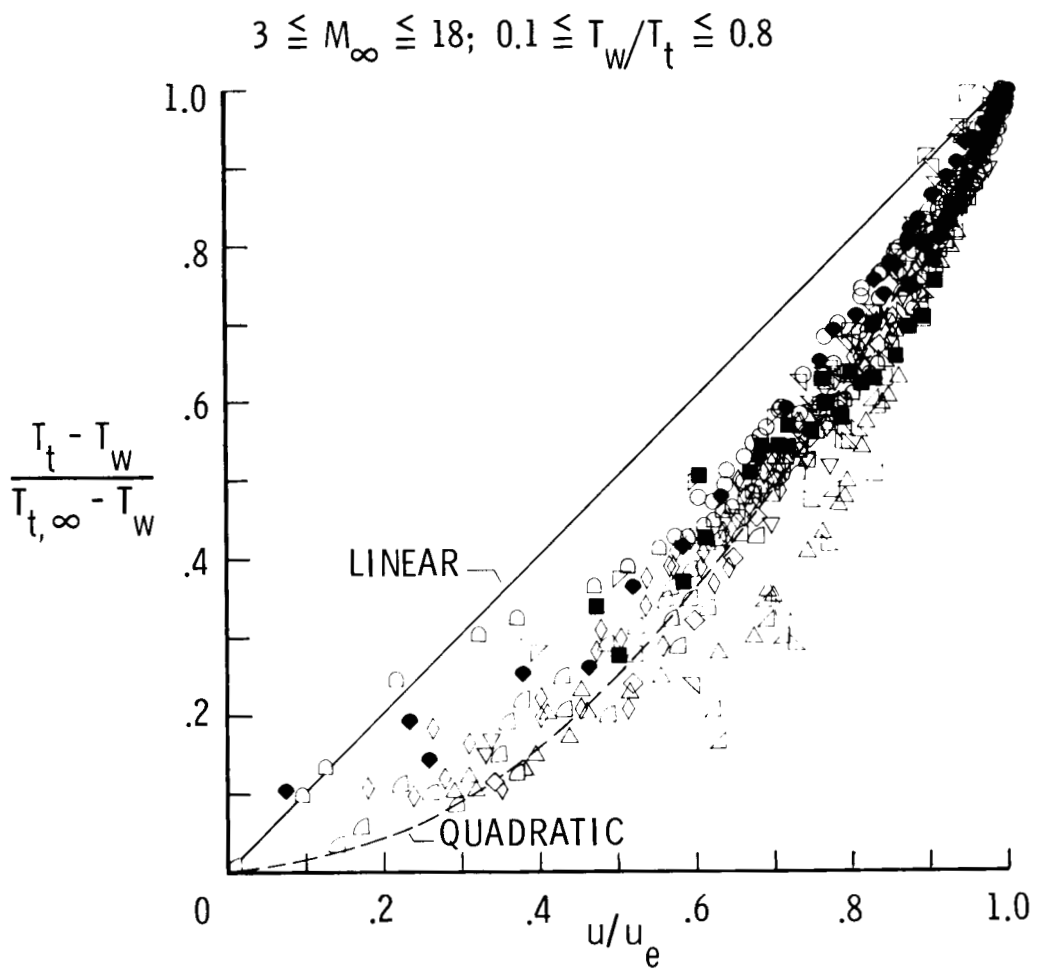


Figure 38.- Total temperature-velocity profiles for nozzle wall-type turbulent flow (from ref. 209).

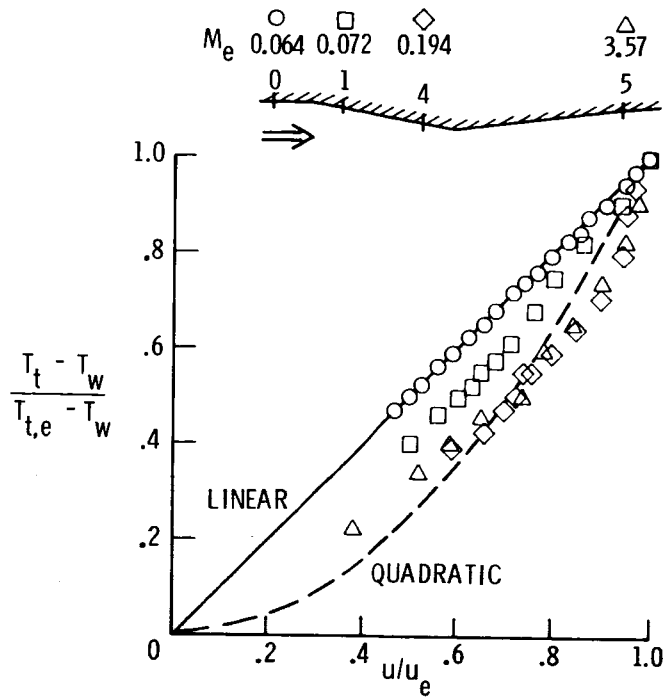


Figure 39.- Development of total temperature-velocity profile along a nozzle wall (data from ref. 212).

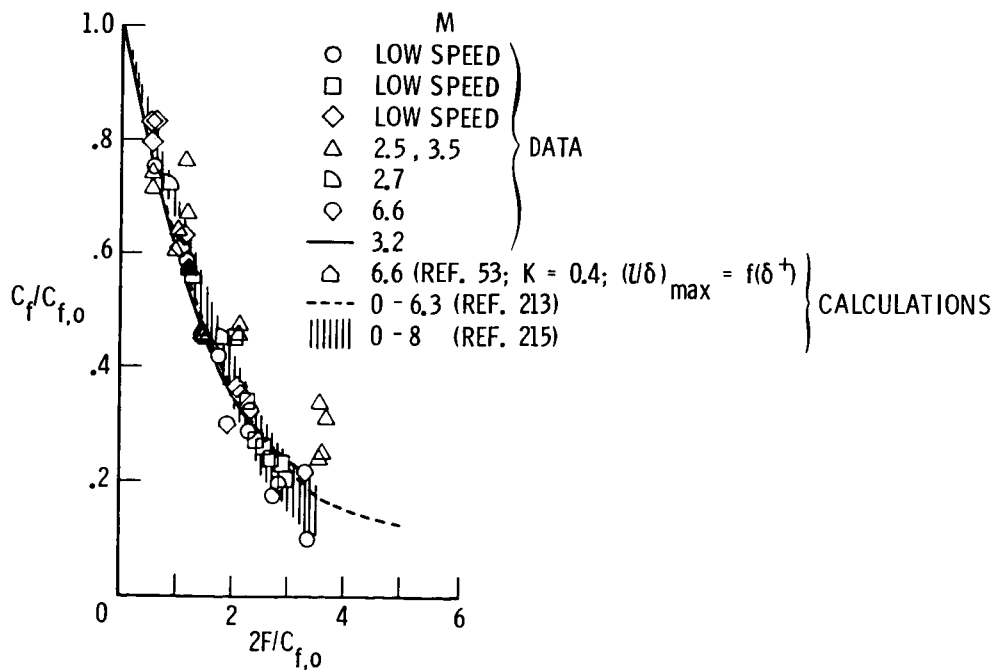


Figure 40.- Influence of wall blowing on turbulent skin friction (from ref. 217).

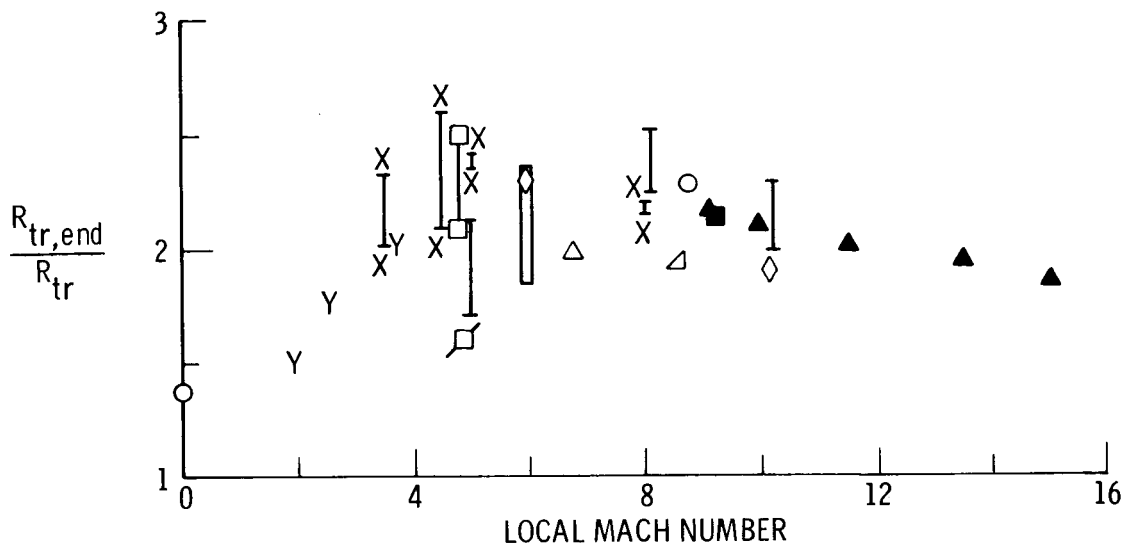


Figure 41.- Extent of transition zone in high speed flow. (Reprinted from ref. 219 with permission from the American Institute of Aeronautics and Astronautics.)

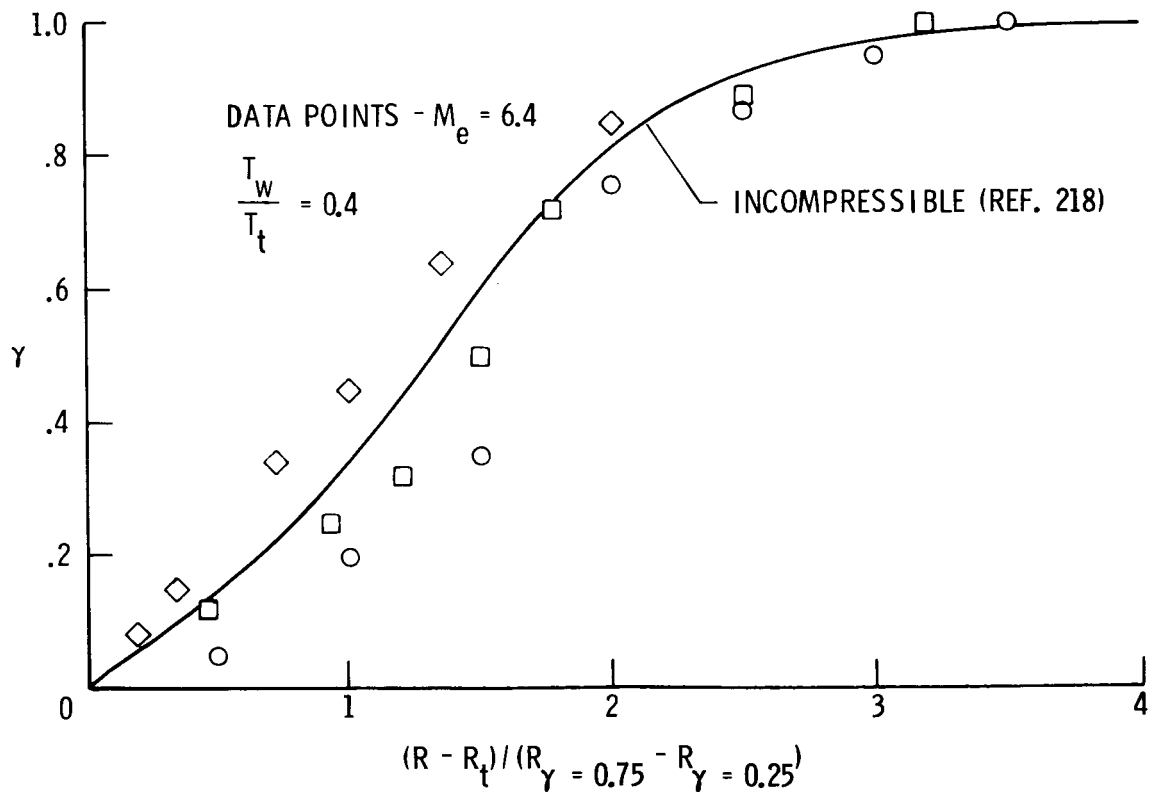


Figure 42.- Effect of Mach number on streamwise intermittency. (Reprinted from ref. 59 with permission from the American Institute of Aeronautics and Astronautics.)

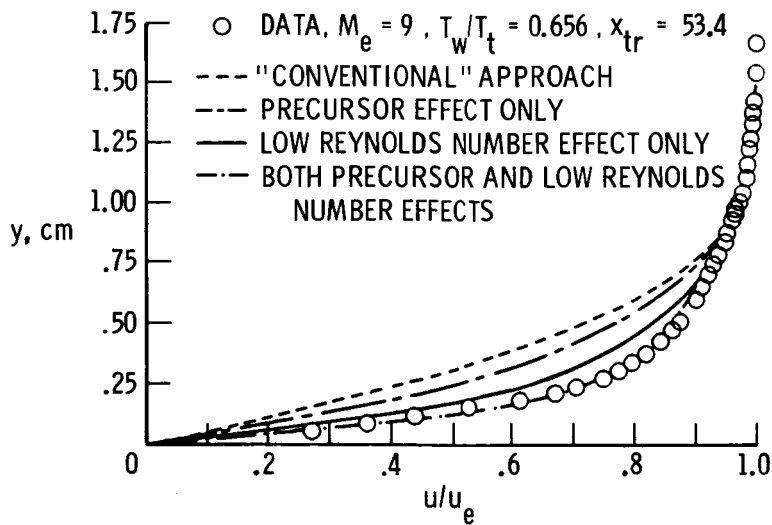


Figure 43.- Comparison of transitional calculations including precursor and low Reynolds number effects with data (from ref. 58). The profile is near center of transition region ($x = 78.7$ cm).

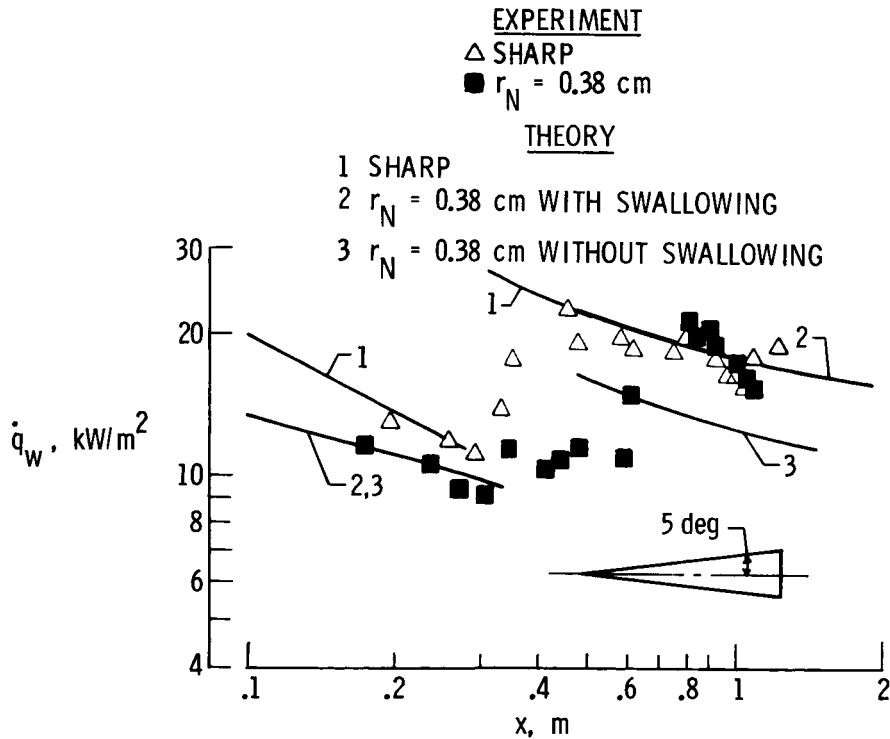


Figure 44.- Effects of variable entropy on wall heating data and calculations (from ref. 221). $M = 10$; $T_t = 1111$ K; $T_w = 294$ K; $A^+ = 26$; $K = 0.435$; $(1/\delta)_{max} = 0.09$; $N_{Pr,t} = 0.9$.

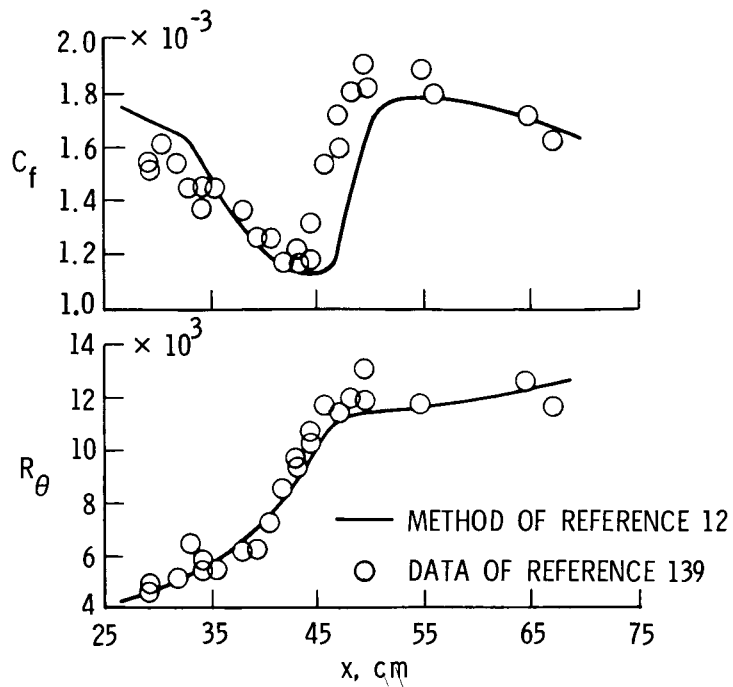


Figure 45.- Application of mean field closure for turbulent boundary-layer flow with pressure gradient. $K = 0.4$; $\alpha = 0.016$; $A^+ = f(p^+)$. (Reprinted with permission from ref. 12.)

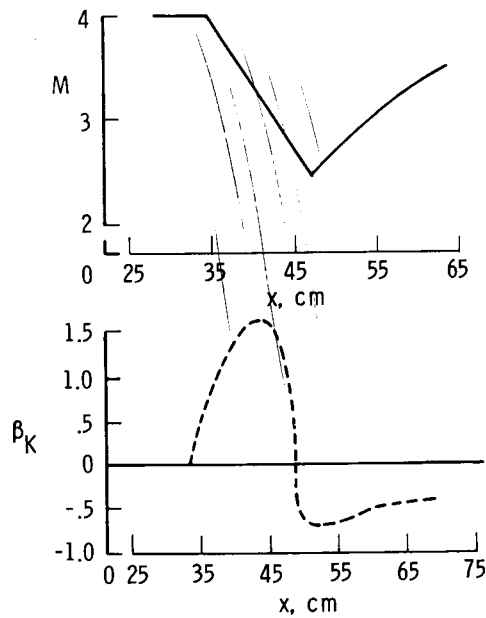


Figure 46.- Flow conditions for data in figure 45.

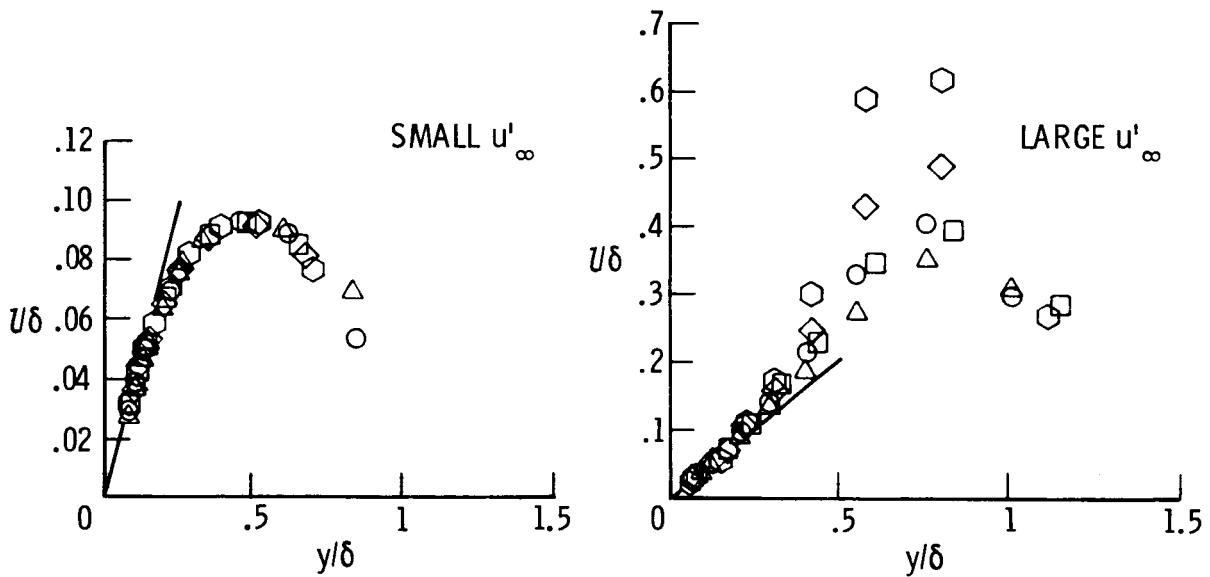


Figure 47.- Effect of fluctuating stream velocity on mixing length (from ref. 233).

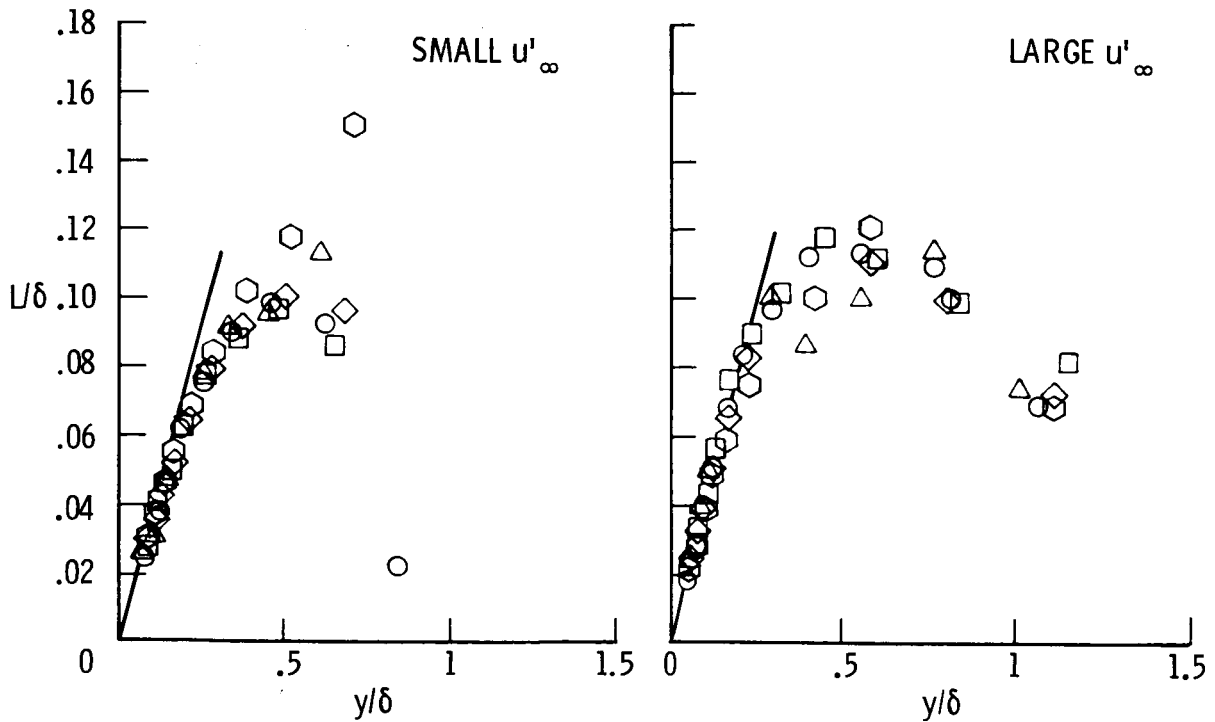


Figure 48.- Effect of fluctuating stream velocity on Bradshaw scale (from ref. 233).

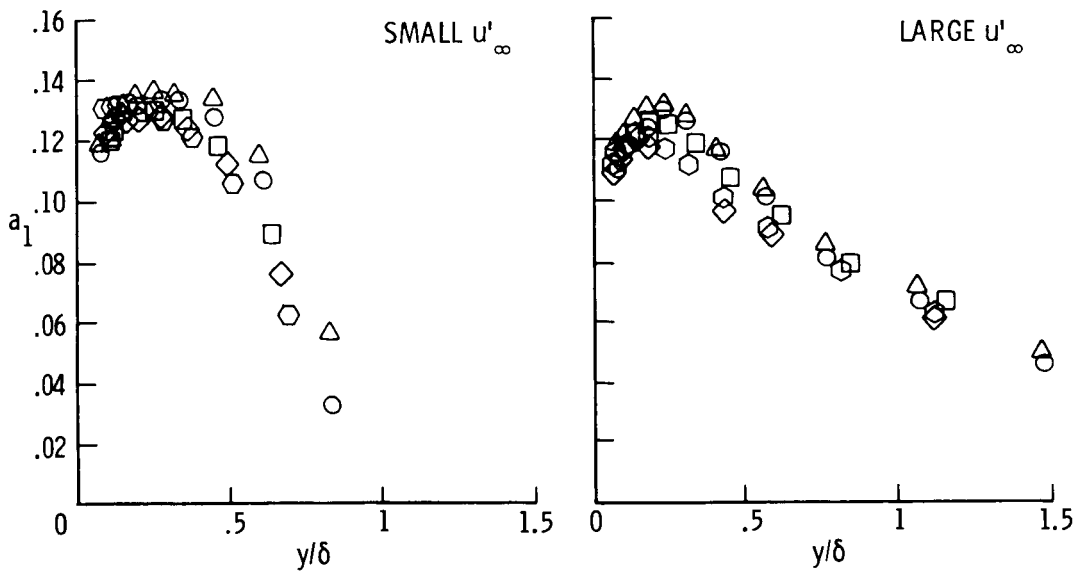


Figure 49.- Effect of fluctuating stream velocity on a_1 (from ref. 233).

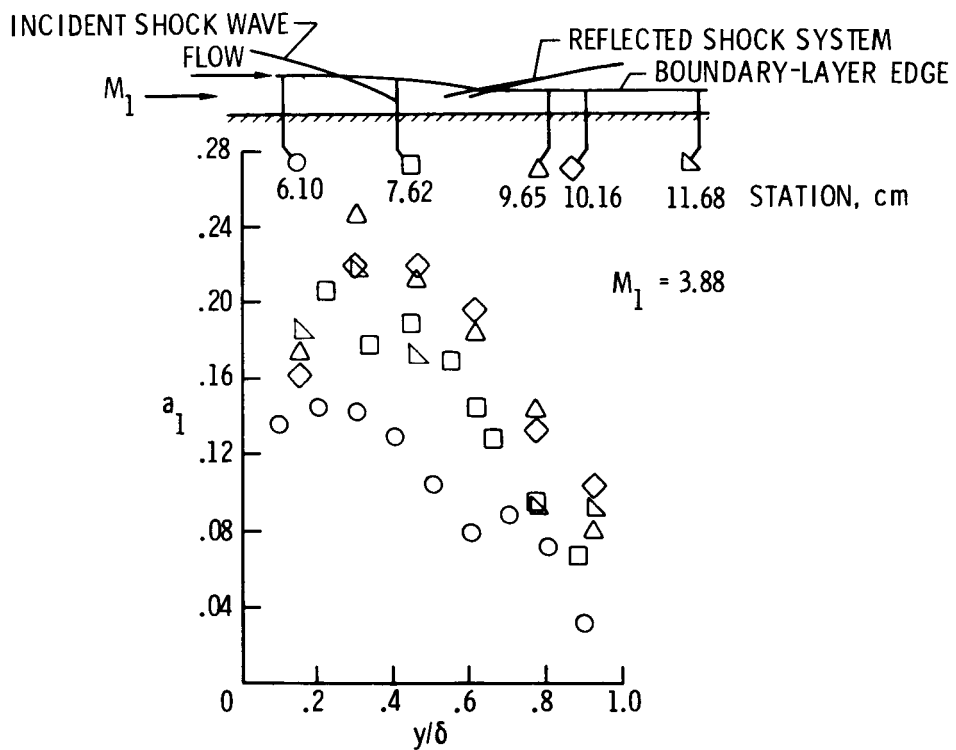


Figure 50.- Values of a_1 through a shock-boundary-layer interaction at Mach 3.88 (from ref. 234).

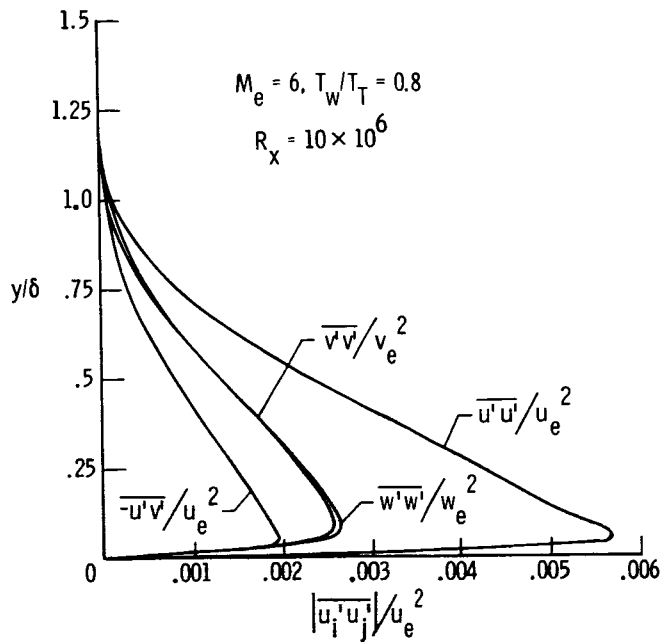


Figure 51.- Calculation of $\overline{u_i u_j}$ with a turbulent boundary layer using nonequilibrium turbulence modeling (from ref. 156).

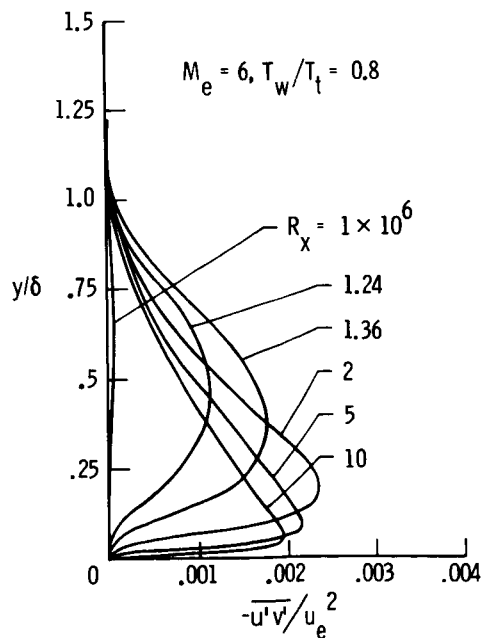


Figure 52.- Calculation of $\overline{u'v'}$ with a turbulent boundary layer using nonequilibrium turbulence modeling (from ref. 156).

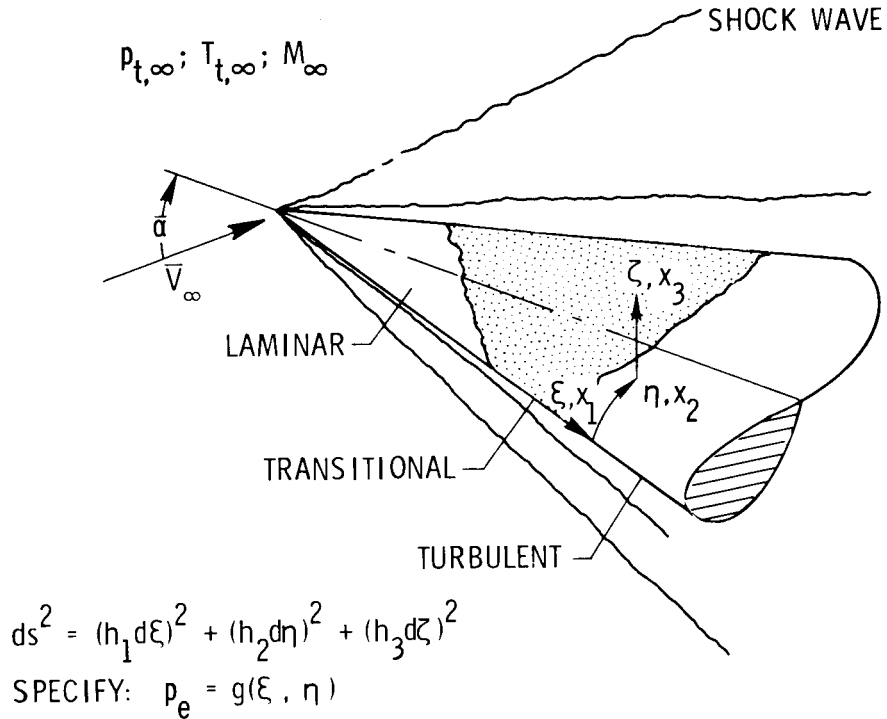


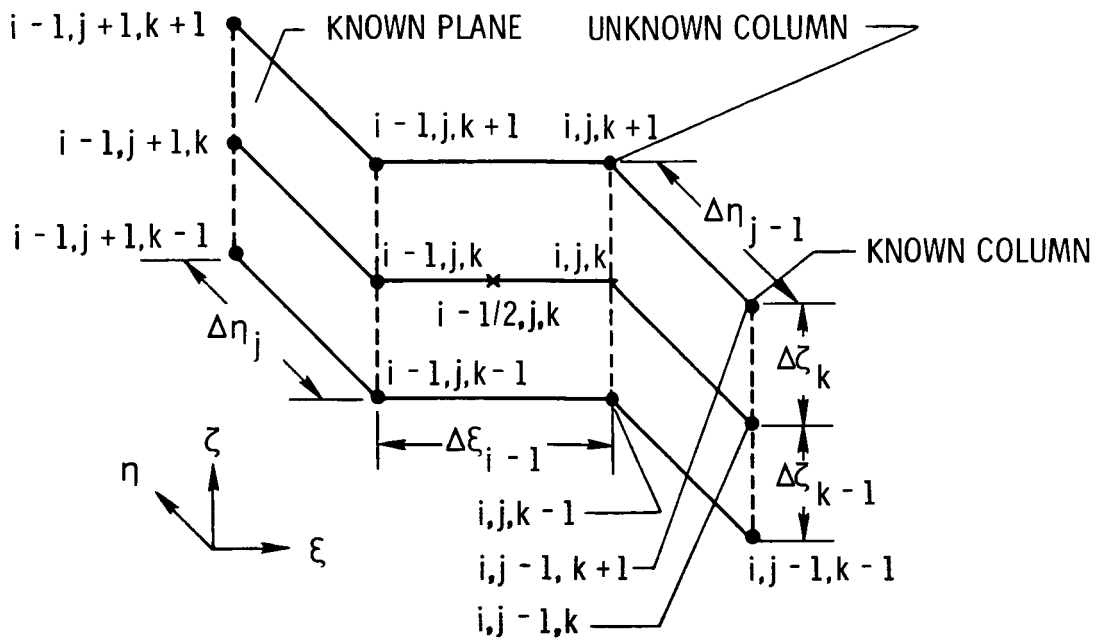
Figure 53.- Schematic of geometry and flow field.

$$\tau_{x1} = \rho l^2 \left[\left(\frac{\partial u_1}{\partial x_3} \right)^2 + \left(\frac{\partial u_2}{\partial x_3} \right)^2 \right]^{1/2} \frac{\partial u_1}{\partial x_3}$$

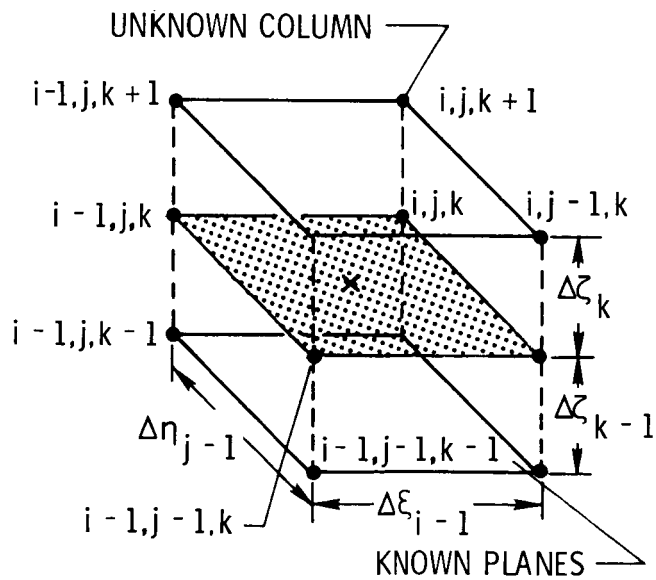
$$\tau_{x2} = \rho l^2 \left[\left(\frac{\partial u_1}{\partial x_3} \right)^2 + \left(\frac{\partial u_2}{\partial x_3} \right)^2 \right]^{1/2} \frac{\partial u_2}{\partial x_3}$$

$$\epsilon = \epsilon_{x1} = \epsilon_{x2} = \rho l^2 \left[\left(\frac{\partial u_1}{\partial x_3} \right)^2 + \left(\frac{\partial u_2}{\partial x_3} \right)^2 \right]^{1/2}$$

Figure 54.- Invariant turbulence concept (from ref. 243).



(a) Krause scheme (ref. 288).



(b) Crank-Nicolson scheme (ref. 261).

Figure 55.- Illustration of finite-difference grid schemes.

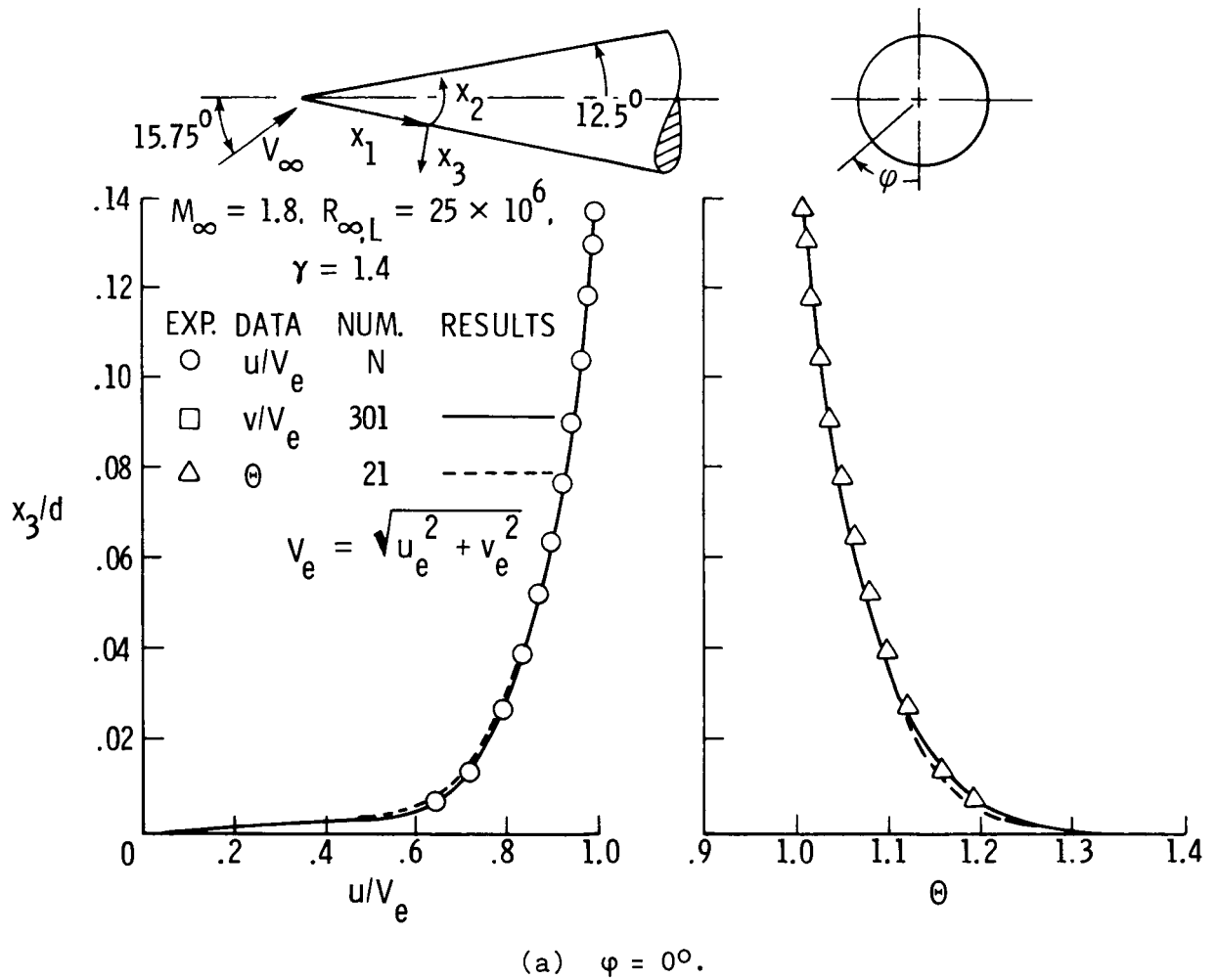
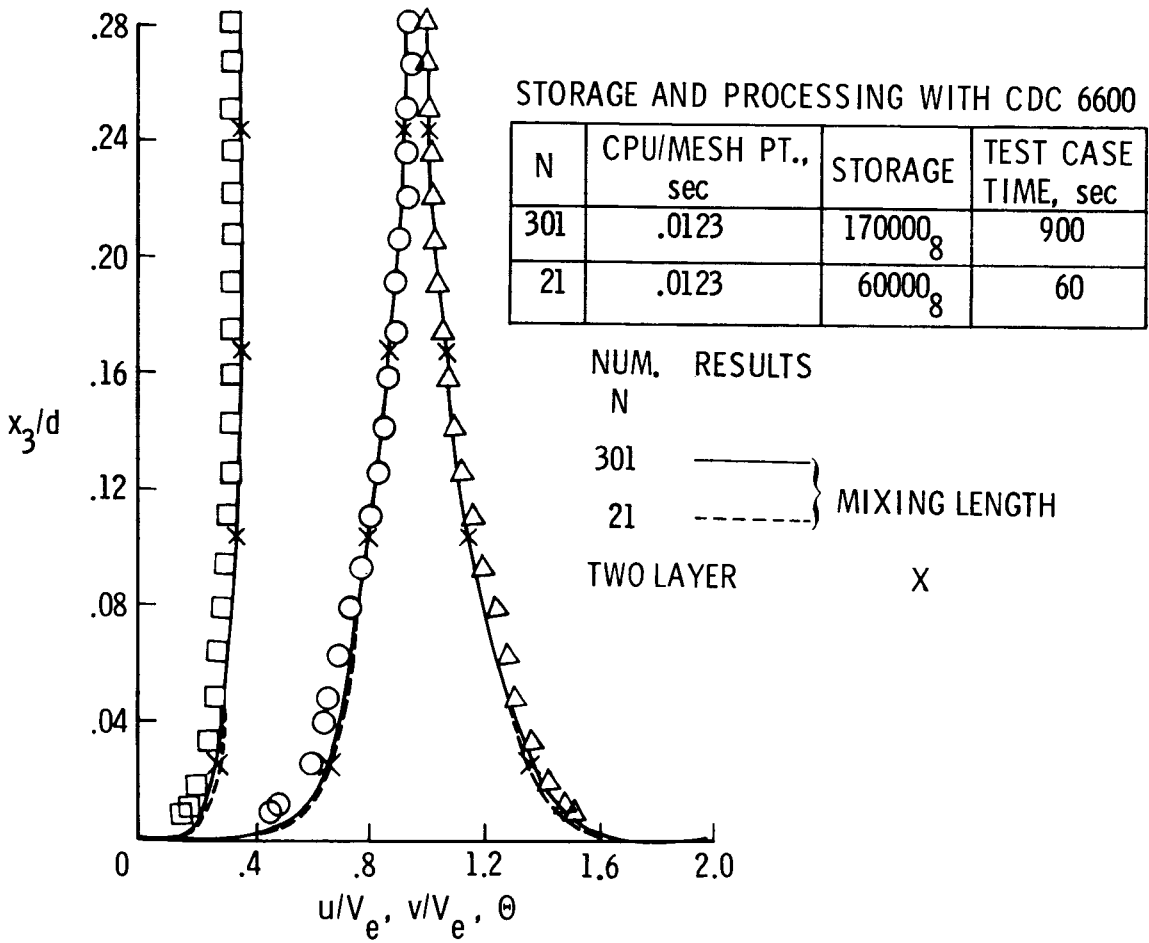


Figure 56.- Comparison of three-dimensional prediction scheme with data (from ref. 276) for a cone at angle of attack in a supersonic stream ($d = 2.54$ cm).



(b) $\varphi = 135^\circ$.

Figure 56.- Concluded.

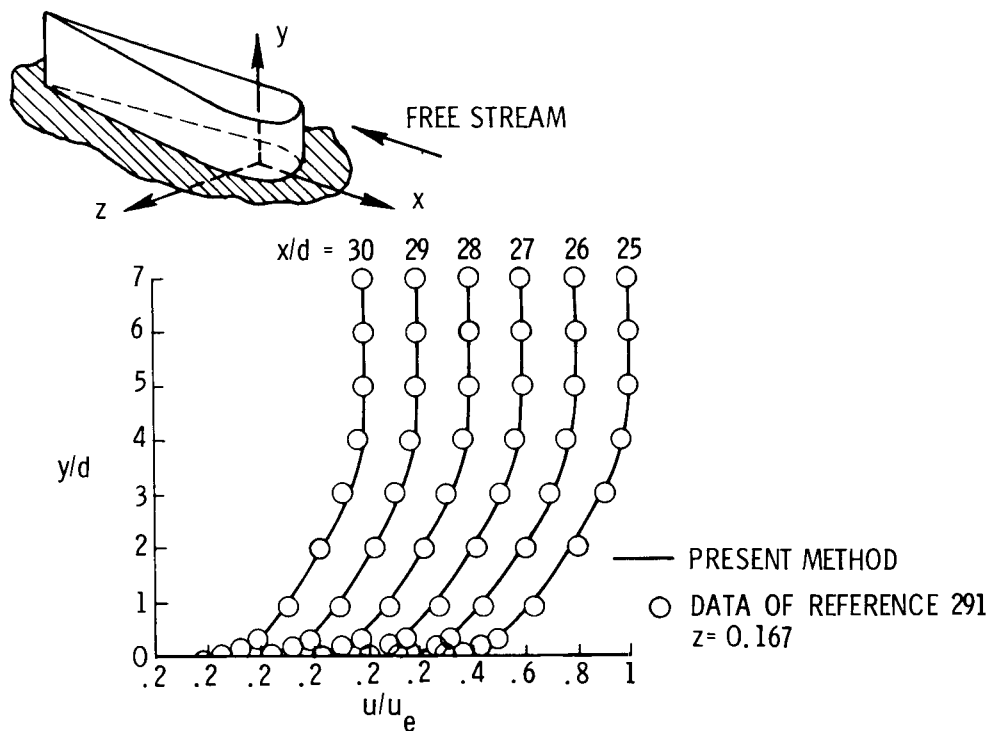


Figure 57.- Comparison of numerical results with experimental data
($d = 2.54$ cm).

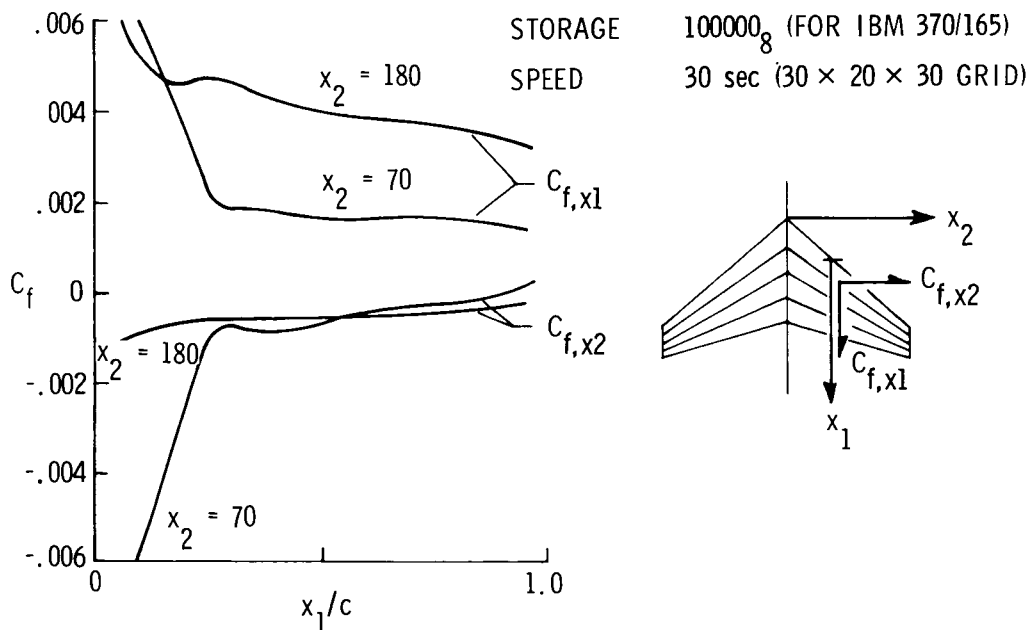


Figure 58.- Numerical results for supercritical wing.
 $M_\infty = 0.5$; $R_\infty = 1.5 \times 10^6$.

BOUNDARY LAYER IS COVERED BY A NODAL NETWORK

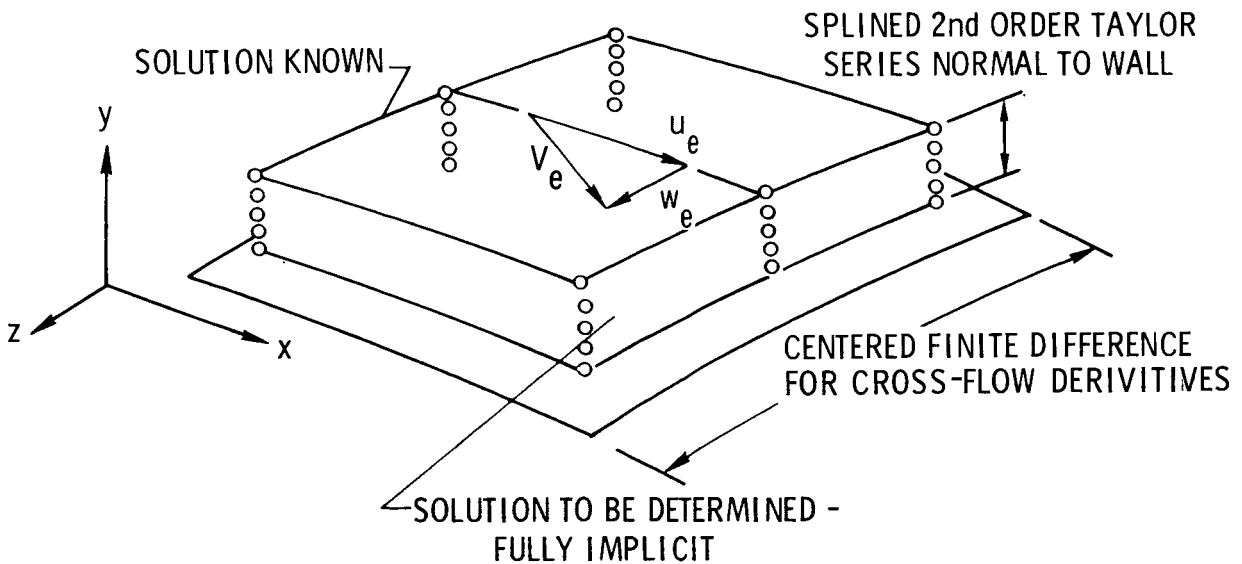


Figure 59.- Mesh point network for integral-matrix procedure.

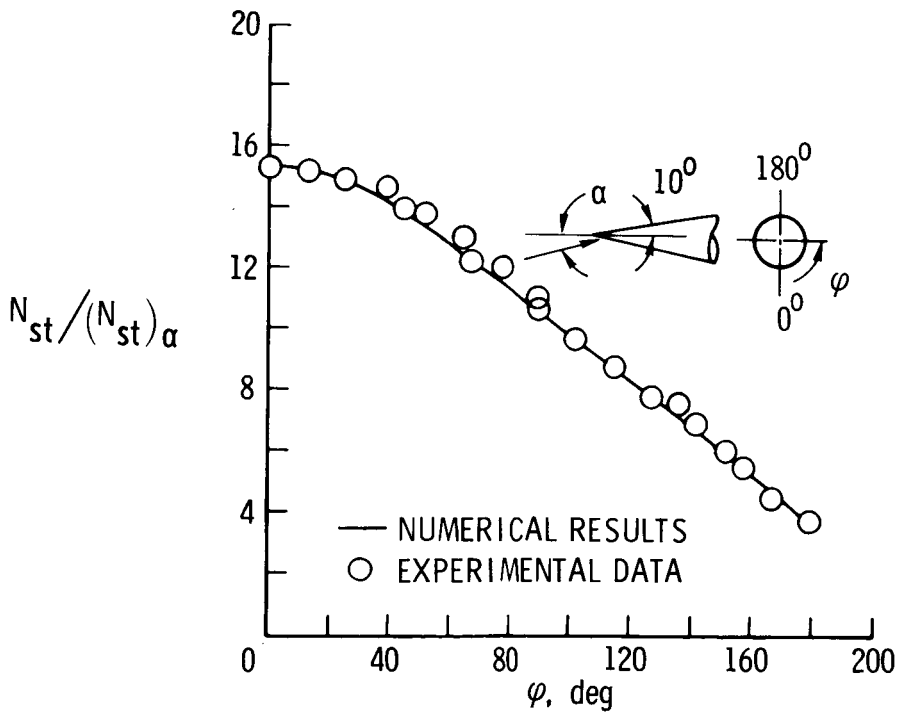


Figure 60.- Comparison of numerical results with surface heating data (from ref. 292) for a cone at angle of attack in hypersonic flow. $M_{\infty} = 7.95$; $\gamma = 7.95$; $\alpha = 4^{\circ}$.